Bastian Kremser, BSc

Establishing a Rieske non-heme iron oxygenase purification system for biotransformations *in vitro*

MASTER'S THESIS

to achieve the university degree of

Diplom-Ingenieur

Master's degree programme:

Biotechnology

submitted to

Graz University of Technology

Supervisors

Dr. Sandy Schmidt

Prof. Dr. Robert Kourist

Institute for Molecular Biotechnology

Graz, January 2021

AFFIDAVIT

I declare that I have authored this thesis independently, that I have not used other than the declared sources/resources, and that I have explicitly indicated all material which has been quoted either literally or by content from the sources used. The text document uploaded to TUGRAZonline is identical to the present master's thesis.

Graz, 25.01.2021

_____

Signature

Acknowledgments

First of all, I would like to thank Prof. Dr. Robert Kourist for giving me the opportunity to be part of his research group, where I was able to expand my professional knowledge and my understanding of modern research.

Secondly, I want to thank my thesis advisor Dr. Sandy Schmidt for allowing me to work as one of her master students, to share her professional knowledge and to guarantee smooth supervision, both at the IMBT Graz and eventually remotely from Groningen.

Furthermore, I want to thank all colleagues of Prof. Dr. Kourist's work group, since really every single one has provided useful information and helped me during my work. Special thanks to my topic-related group members Feyza Özgen and Michael Runda, who gave me the most valuable tips during all my experiments and were always there to support me at any time of day. I also got big help from Selina Pieber, Elif Erdem, Anna Schwaiger, Hanna Büchsenschütz, Leen Assil Companioni, Ivana Drienovska, Andrea Nigl, Yue Sun, Kristin Bauer and Kay Novak.

I would further like to thank Maria Schabhüttl and Simone Scharl for guaranteeing such smooth working conditions at any time in the lab! Additionally, I want to thank Andrea Chánique for spending so many hours at the Äkta with me, and special thanks to Leonie Strolz for all the help in the laboratory. I would also like to thank Elia Calderini for sharing the bench with me while taking things so easy.

Regarding support outside of university, I would like to greatly thank my flatmates Anna Lagger, Daniel Preston and Thomas Walcher for supporting me whenever they could, which was basically 24/7.

Last but not least, I would like to sincerely thank my grandparents, parents and my sister, who always believed in my ambitions and have been more than supportive in every way.

List of abbreviations

c.o.:	codon-optimized
CDO:	cumene dioxygenase from *Pseudomonas fluorescens* IP01
CFL:	sterile-filtered cell-free lysate
ddH_2O:	distilled water (A. dest.)
des.-SPB:	desalting sodium phosphate buffer
DO:	dioxygenase
ee:	enantiomeric excess
elu.-SPB:	elution sodium phosphate buffer
EC:	enzyme commission
equi.-SPB:	equilibration sodium phosphate buffer
EV-CFL:	empty vector cell-free lysate
EVC:	empty vector control
FAD:	flavin adenine dinucleotide
Fd:	ferredoxin
FdR:	ferredoxin-reductase of the CDO
FdR^x:	CDO ferredoxin-reductase containing a non-sense base deletion
Fe-S:	iron-sulfur
FMN:	flavin mononucleotide
GC-FID:	gas chromatograph with flame ionization detector
GC-MS:	gas chromatograph-mass spectrometry
His:	histidin
IPTG:	isopropyl β-D-1-thiogalactopyranoside
kan:	kanamycin
LB:	*Lysogeny* broth
MO:	monooxygenase
MW:	molecular weight
MWCO:	molecular weight cut-off
NAD(P)H:	nicotinamide adenine dinucleotide (phosphate)
NDO:	naphthalene dioxygenase from *Pseudomonas sp.* 9816-4
O_2:	molecular oxygen
ONC:	overnight culture
Oxy:	oxygenase or (in multi component systems) terminal oxygenase component
Oxy(2xHis):	CDO Oxy with His tagged CumA1 and CumA2, respectively
Oxy(1xHis):	CDO Oxy with His tagged CumA1 only and CumA2
PCR:	polymerase chain reaction
Pol.:	polymerase
Red:	reductase
RO:	Rieske non-heme iron dioxygenase
ROS:	radical oxygen species
RT:	room temperature
SOC:	Super Optimal Broth
SP:	sodium phosphate
SPB:	sodium phosphate buffer
TB:	Terrific Broth
WT:	wild type

Abstract

Rieske non-heme iron oxygenases (ROs) catalyze multiple chemo-, regio- and stereoselective oxyfunctionalization reactions, including hydroxylations, oxidative cyclizations, and dealkylations. The broad substrate spectrum of ROs comprises alkenes and arenes that are typically converted to the corresponding mono- or dihydroxylated products, which are difficult to obtain when performed by classical chemical synthesis. ROs are multicomponent systems, in which the belonging flavin (FMN/FAD) dependent reductases (Reds) require the costly cofactors NAD(P)H. Among ROs, there is either two or three component systems, of which in both cases initially a Red oxidizes NAD(P)H. In three component systems single electrons are then transferred to a soluble ferredoxin (Fd) and eventually shuttled to the terminal oxygenase component (Oxy) for catalysis. In two component systems the Red can directly transfer electrons from NAD(P)H to the Oxy. Due to this complex electron transport chain, practically applied ROs are often utilized in *in vivo* biocatalysis. Furthermore, utilization of whole-cell systems offers an easy to use cofactor recycling approach for the regeneration of NAD(P)H. However, *in vitro* studies of this electron transport chain have only been published for certain ROs. In this study, the three-component RO cumene dioxygenase (CDO) from *Pseudomonas fluorescens* IP01 was purified and the electron transport chain was investigated. Therefore, a purification protocol for the single CDO components was established. During *in vitro* biotransformations with indene, the successful monohydroxylation to 1-indenol with a conversion of 24 % could be achieved using NADH, additional empty vector cell-free lysate (EV-CFL) and a surplus of CDO Red (FdR) and Fd over the Oxy at an Oxy:Fd:FdR ratio of 1:14.5:4.7 µM without cofactor recycling. During investigation of the electron transport chain, it was shown that oxyfunctionalization exclusively occurs when all three CDO components are present, but does not occur, when either only Fd, or both Fd and FdR are absent. Interestingly, oxyfunctionalization was also demonstrated to occur upon addition of EV-CFL to purified Oxy and Fd in absence of FdR, indicating interchangeability of the FdR with a cellular *E. coli* Red. Finally, the cofactor preference of the FdR was observed to be NADPH. However, the highest conversion during biotransformations was accomplished using NADH. Hence, further experiments, including implementation of cofactor recycling, need to be carried out in order to finally determine the cofactor preference of the FdR.

Zusammenfassung

Rieske nicht-Häm Eisen Oxygenasen (ROs) katalysieren chemo-, regio- und stereselektive Oxyfunktionalysierungsreaktionen, wie z.B. Hydroxylierungen, oxydative Cyclisierungen, oder Dealkylierungen. Das breite Substratspektrum von ROs umfasst Alkene und Arene, die typischerweise zu den korrespondierenden mono- oder dihydroxylierten Produkten katalysiert werden, welche durch chemische Synthese schwer zu erhalten sind. ROs sind Multikomponentensysteme, bei welchen die zugehörigen Flavin (FAD/FMN) abhängigen Reduktasen (Reds) die teuren Cofaktoren NAD(P)H benötigen. Unter ROs existieren zwei- oder drei-Komponenten Systeme, in denen zunächst eine Red NAD(P)H oxidiert. In drei-Komponenten Systemen werden einzelne Elektronen dann auf ein lösliches Ferredoxin (Fd) übertragen, von wo aus diese schließlich auf die terminale Oxygenase (Oxy) für die Oxyfunktionalysierung transferiert werden. In zwei-Komponenten Systemen kann die Red Elektronen direkt an die Oxy übertragen. Aufgrund dieser komplexen Elektronentransportkette sind Beispiele praktischer Anwendungen von ROs oft auf *in vivo* Biokatalyse beschränkt. Außerdem bietet die Ganzzellbiokatalyse ein leicht zu implementierendes Cofaktor Regenerations System für NAD(P)H. *In vitro* Studien über die Elektronentransportkette sind zudem nur auf bestimmte ROs beschränkt. In dieser Arbeit wurde die drei-Komponenten RO Cumene Dioxygenase (CDO) von *Pseudomonas fluorescens* IP01 aufgereinigt und die Elektronentransportkette untersucht. Dafür wurde ein Aufreinigungsprotokoll für die einzelnen CDO Komponenten etabliert. Während *in vitro* Biotransformationen mit Indene, NADH, Leervektor Zell-freiem Lysat (EV-CFL) und einem Überschuss an CDO Red (FdR) und Fd zur Oxy im Verhältnis Oxy:Fd:FdR von 1:14.5:4.7 µM konnte die erfolgreiche Monohydroxylierung zu 1-Indenol bei 24 % Produktbildung ohne Cofaktor Regeneration erzielt werden. Die Untersuchung der Elektronentransportkette zeigte, dass Oxyfunktionalisierung ausschließlich stattfindet, wenn alle drei CDO Komponenten beteiligt sind, nicht jedoch, wenn entweder nur Fd, oder Fd und FdR in der Reaktion fehlen. Oxyfunktionalisierung ohne FdR konnte jedoch bei Zugabe von EV-CFL zu aufgereinigten Oxy und Fd beobachtet werden, was auf die Austauschbarkeit der FdR mit einer *E. coli* Red schließen lässt. Schließlich wurde die Cofaktor Präferenz der FdR mit NADPH beobachtet, wobei die höchste Produktausbeute der Biotransformationen mit NADH erzielt wurde.

Weitere Experimente, inklusive der Implementation eines Cofaktor Recycling Systems, sind daher nötig, um die Cofaktor Präferenz der FdR endgültig zu bestimmen.

Table of contents

1 Introduction

1.1 Oxidoreductases as biocatalysts

A short glance at literature about oxidation reactions using conventional chemical catalysts is sufficient to become aware of the limitations implied, which range from the expense of oxidizing reagents to the limitation of control and thus predictability of the obtained product structures. The growing need of hydroxy- and oxy- compounds in the pharmaceutical, chemical and food industry has led to the discovery of interesting novel oxidoreductases as an alternative to conventional chemical synthesis.[1,2] The potential of enzymes to catalyze highly regio-, chemo- and enantioselective reactions under relatively mild conditions has especially drawn interest in the pharmaceutical industry. In 2010, it was reported that chiral compounds made up 70 % of active substances in pharmaceutical products.[3] Biocatalysts have proven their capability of being considerable alternatives to conventional catalysts, since they are able to catalyze a wide range of (difficult) chemical reactions under relatively environmentally friendly and cost-effective operating conditions, in the fields of bioremediation, medicine and pharmaceuticals. Additionally, research in the fields of protein engineering by e.g. directed evolution or rational design has led to an enhanced versatility of recombinant enzymes in biocatalysis.[4] Furthermore, the term "green chemistry" has been defined as the "design of chemical products and processes to reduce or eliminate the use and generation of hazardous substances".[5] Certain metrics of green chemistry performance, like raw material efficiency (RME), atom economy or E-factor have been established to develop novel reactions with the simultaneous reduction of waste, optimization of solvent usage, minimization of energy input, material usage, as well as cost efficiency and finally safety concerns.[2]

A particularly interesting group of enzymes are oxidoreductases, which are capable of catalyzing oxidation reactions of a compound, either a reducing agent or an electron donor, at the expense of the simultaneous reduction of another, either an oxidizing agent or an electron acceptor, according to the scheme $A^- + B \rightarrow A + B^-$. They are classified in the enzyme commission primary class as class 1 (EC 1.-) and make up almost one third of all enzymatic activities listed in the BRaunschweig ENzyme Database (BRENDA).[6] Among several

representants within the class of oxidoreductases, there is oxidases, peroxidases and oxygenases, for which oxygen atoms serve as the electron acceptor, whereas in the case of dehydrogenases, which remove hydrogen from their substrates, no active oxygen intermediates are implicated.[1]

Enzymes, which directly incorporate molecular oxygen (O_2) into their substrates are referred to as 'oxygenases'. The fact that O_2 is a readily and ubiquitously available oxygen source and the relatively mild reaction conditions needed for these enzymatic reactions make them especially considerable as sustainable catalysts.[7] Particularly, enzymatically catalyzed oxygenation reactions are becoming more important, as the direct oxyfunctionalization of (non-activated) organic substrates still remains a difficult task in classical chemical synthesis. On the one hand, many industrially applied catalytic oxidation processes have been developed using O_2, where simple raw materials (e.g. alkanes, alkenes or aromatics) are converted into valuable (intermediate) products, like aldehydes, alcohols or carboxylic acids, but the therein used catalysts often only have a narrow substrate range covering only few organic compounds. Moreover, conventional chemical synthesis comes along with the lack of regio- or enantiospecificity. On the other hand, these highly selective oxygenation reactions can be catalyzed using biocatalysts, wherein among oxidoreductases, three subclasses for enzymatic oxygen-transfer from O_2 can be distinguished (figure 1): **Monooxygenases** (MOs) only incorporate one oxygen atom from O_2 into the substrate, whereby the second oxygen atom is reduced to water (H_2O) using typically NAD(P)H as cofactor (figure 2 A). **Dioxygenases** (DOs) are able to catalyze the simultaneous incorporation of both oxygen atoms from O_2 into a substrate (figure 2 B), where unstable and highly reactive peroxo species are formed, which are immediately reduced (enzymatically or non-enzymatically), yielding the more stable (di)hydroxy products. Finally, **oxidases** mainly transfer electrons to O_2, which usually yields hydrogen peroxide (H_2O_2) or H_2O as byproducts.[8]
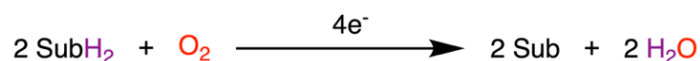
Figure 1 General scheme for reactions catalyzed by monooxygenases, dioxygenases and oxidases. Donor = NAD(P)H.

Regarding MOs, incorporation of one oxygen atom of O_2 into the substrate is mediated via the formation of activated oxygen-transferring species by either transition metal containing cofactors (Fe or Cu), or heteroaromatic systems (pteridine or flavin). Most of the iron (Fe) dependent MOs belong to the Cytochrome P-450 type, in which the Fe species is coordinated via a heme moiety and a cysteine residue. Depending on the enzyme, single electrons from NAD(P)H for the reduction of this Fe (resulting in a change from a ferrous Fe^{2+} to a ferric Fe^{3+} state) are transferred either via a flavin, an iron-sulfur (Fe-S) ferredoxin (Fd) or a cytochrome b_5.[8]
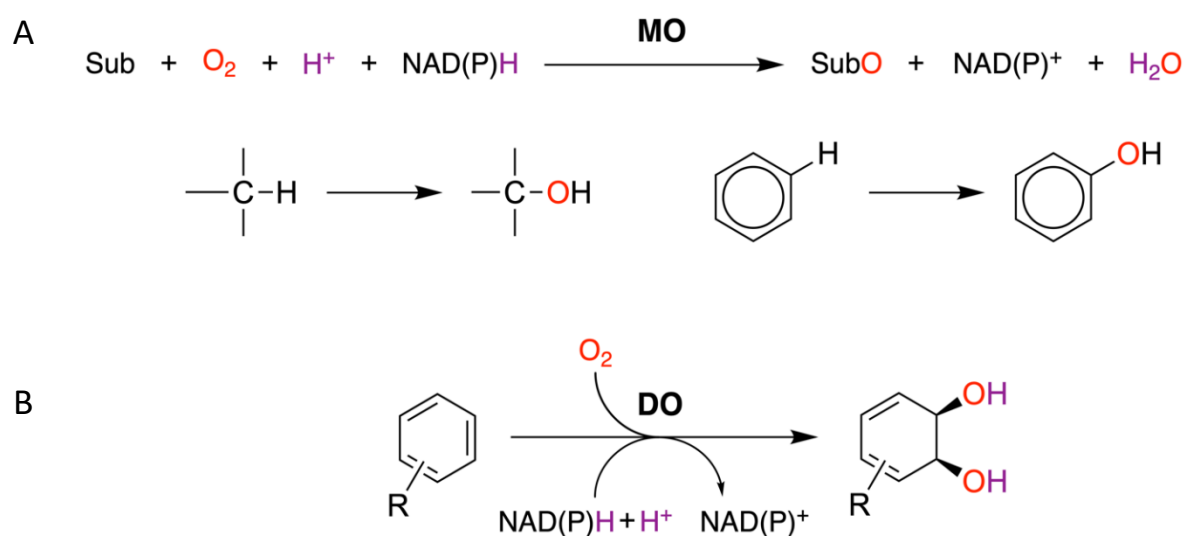
Figure 2 (A) General scheme of a MO catalyzed reaction. With alkane substrates (left) alcohols are formed, whereas with aromatic substrates (right) phenols are obtained.[8] (B) DO catalyzed reaction exemplified from a RO. R = aryl or alkyl.[23]

Iron-dependent **Dioxygenases** (DOs) catalyze the simultaneous incorporation of both molecular oxygen atoms into their products (figure 2 B). Two major enzyme classes can be distinguished: heme-dependent iron-sulfur plant DOs and Rieske non-heme iron-sulfur DOs (ROs),[9] whereof the latter show higher redox potential and the majority is NADH dependent.[1] For ROs there is growing interest for biotechnological applications due to their ability to perform a wide range of challenging stereo- and enantiospecific oxidative transformations (like hydroxylations, oxidative cyclizations, and dealkylations) that have been proven difficult in synthetic organic chemistry.[10] These transformations are performed on a broad range of aromatic and even alkene compounds and thus go way beyond the natural substrates of the corresponding host bacterium.[11] Especially the enantioselective dihydroxylation of arenes, which is a common initial step within the microbial degradation of aromatic substrates catalyzed by ROs,[12] has gained interest due to the broad spectrum of reactions and products. In naturally occurring microbial systems containing ROs, the resulting diol products are often

3

further metabolized. However, knock-out mutants of e.g. *P. putida* have been developed, in which the *cis*-dihydroxylated products accumulate and have been operated at commercial scale.[1]

ROs are two or three component systems consisting of a reductase (Red), capable of oxidizing NAD(P)H, a Rieske ferredoxin (Fd) (only in three component systems) and an oxygenase (Oxy) that performs oxyfunctionalization of the substrate using molecular oxygen.[10,12,13] This complex electron transfer chain distinguishes ROs from many flavin-dependent MOs that directly obtain electrons from NAD(P)H. The fact that ROs require reducing equivalents provided by NAD(P)H contributes to one limitation of practical applicability of these enzymes, because these expensive cofactors need to be regenerated in order to be cost-effective eventually. That is why most synthetic RO applications rely on recombinant whole-cell biocatalysts.[14] Moreover, the multi-component character of ROs brings along challenging difficulties for *in vitro* catalysis due to non-covalent linkage between the single components. Furthermore, ROs have been reported to be of rather unstable character, once isolated from the cells.[15] Thus, direct application of isolated ROs has been hampered by enzyme instability, oxygen sensitivity of the 2-iron-2-sulfur ([2Fe-2S]) centers, and the expensive cofactors requirements.[10]

1.2 Rieske non-heme iron dioxygenases (ROs)

Rieske non-heme iron dioxygenases (ROs) are the only known enzymes capable of performing the stereoselective formation of vicinal *cis*-diol products in on step.[10] ROs are capable of transforming a variety of aromatic compounds and can be seen as the non-heme analogues of cytochrome P450 MOs. Particularly, the enzymatically catalyzed stereoselective asymmetric dihydroxylation of alkenes to chiral products has drawn attention to these enzymes due to the ease of further processing of the thereby formed chiral diol intermediate products into valuable endproducts for the chemical and pharmaceutical industry.[14] These chiral oxyfunctionalized compounds can therein serve as chiral ligands, synthons or auxiliaries for e.g. pharmaceutical or agrochemical products. Moreover, ROs serve as an alternative for conventional asymmetric dihydroxylations using toxic metal catalysts and furthermore come with a broad substrate scope, capable of converting over 300 substrates.[16] Gibson et al.'s work with *Pseudomonas putida* in 1968 firstly identified ROs as arene-dihydroxylating enzymes,

wherein the formation of a *cis*-benzene glycol intermediate was observed during benzene bioconversion to catechol.[17] ROs are of particular interest for large-scale biosynthesis of arene compounds, because of their broad versatility. A prominent example for the striving for a more environmentally friendly and milder synthesis approach using a RO as biocatalyst would be the production of the small aromatic dye indigo by using the naphthalene DO from *Pseudomonas sp.* 9816-4 (NDO) recombinantly expressed in *E. coli*. The aromatic dye indigo is applied during cotton fabric dyeing and can eventually be obtained within an engineered tryptophan pathway by the dihydroxylation of indole to *cis*-indole-2,3-dihydrodiol, followed by spontaneous dehydration. Its chemical synthesis on the other hand, is accompanied by side-product formation of carcinogens. Hence, application of the NDO and bioengineering of *E. coli* expression strains for the large-scale production is desired. However, even though the process showed substantial technical feasibility, the low cost of chemical synthesis of indigo overseas still surpasses the biological indigo production in the United States and more adaptations will be required to implement this process at industrial scale.[13] The NDO has also been shown to perform a monohydroxylation reaction when utilizing the substrate fluorene,[18] and has furthermore been shown to accept over different 100 substrates.[19]

A prominent example for the commercial interest of ROs is the synthesis of precursors for the production of the HIV protease inhibitor Indinavir (Crixivan®) from indene: both *cis*-(1*S*,2*R*)-indandiol and *trans*-(1*R*,2*R*)-indandiol are precursors for (-)-*cis*(1*S*,2*R*)-1-aminoindan-2-ol, a key chiral synthon in Indinavir synthesis. Biotransformations with isolates of indene toxicity-resistant *Rhodococcus sp.* strains MB 5655 and MA 7205 yielded 2 g/l *cis*-(1*S*,2*R*)-indandiol (*ee ≥ 99 %*) *and* 1.4 g/l *trans*-(1*R*,2*R*)-indandiol (*ee ≥ 98 %*).[20] The reaction was patented in 1997 by Merck & Co., Inc.[21] It was firstly demonstrated in 1987 that indene could be enzymatically converted to 1-indenol and *cis*-1,2-indandiol by the toluene DO from *P. putida* F39/D. Despite the thereby achieved *ee* of 32 % for *cis*-(1*S*,2*R*)-indandiol (the desired enantiomer for Crixivan® synthesis), still 39 % of monohydroxylated 1-indenol was produced.[22] However, due to difficulties among yields and optical purity of enzymatically yielded *cis*-(1*S*,2*R*)-indandiol, Indinavir is to date still produced entirely by organic chemistry.[13] Thus, the search for engineering strategies with regard to future implementation of biological catalysts is still ongoing.

In 2015, Gally et al. were able to modulate the regio- and stereoselectivity of the CDO from *P. fluorescens* IP01 via site-directed mutagenesis of one single amino acid within the active site towards several substrates, including styrene, vinylcyclohexane and indene. During *in vivo* bioconversions of indene, mono- and di-hydroxylated product was obtained with both the CDO WT and the CDO mutant M232A at ~80 % total product formation. Within the CDO mutant M232A a methionine was substituted with an alanine residue within the catalytic site located in the large α-subunit (CumA1) of the Oxy, which is of the heterohexameric $α_3β_3$-type. However, this single amino acid substitution led to the formation of enantiocomplementary catalysts during the oxyfunctionalization of indene. With the WT CDO, an enantiomeric excess (*ee*) of 10 % for *(R)*-1-indenol and an *ee* of 38 % for *cis*-(1*S*,2*R*)-indandiol was observed (figure 3 A), whereat a reversed selectivity could be achieved using the CDO mutant M232A, yielding an *ee* of 87 % for *(S)*-1-indenol and an *ee* of 54 % for *cis*-(1*R*,2*S*)-indandiol (figure 3 B).[23] Despite the fact that *cis*-(1*S*,2*R*)-indandiol is the desired chiral synthon for Crixivan®, this site-directed incorporation of different sized amino acids and thus resulting reversed selectivity still shows the immense potential of engineering this enzyme class towards the desired features.
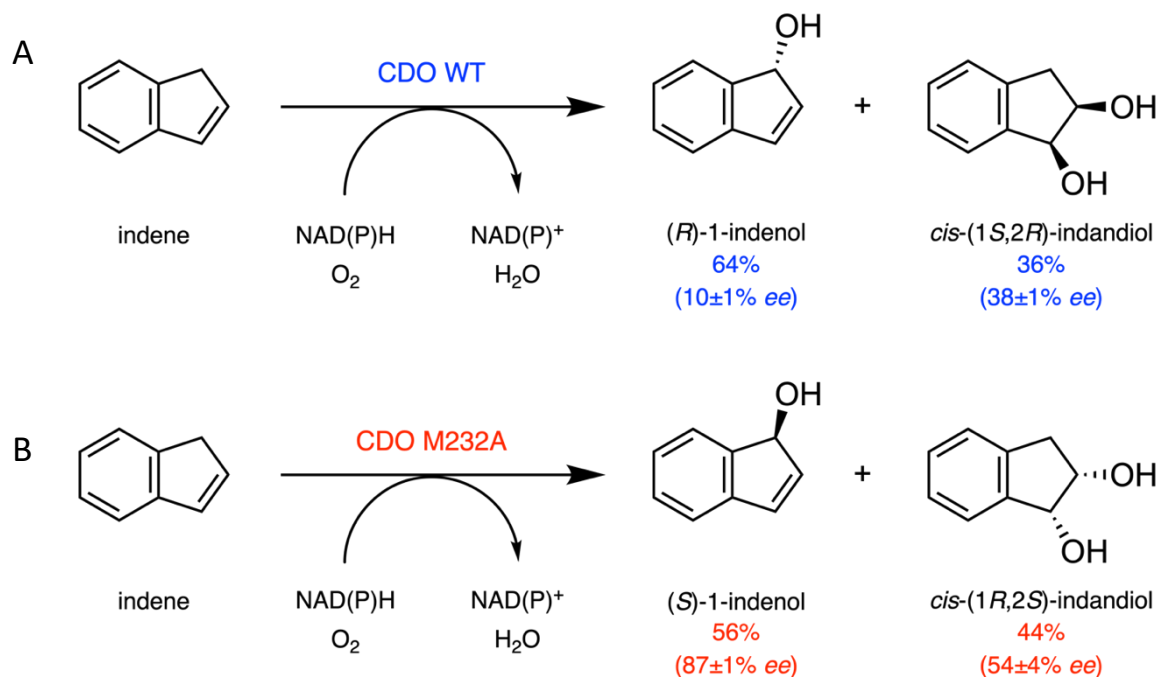

Figure 3 (A) Model reaction of oxyfunctionalization of indene by the CDO WT. (B) Model reaction of oxyfunctionalization of indene using the CDO variant M232A. Both reactions were proposed by Gally et al. from *in vivo* bioconversion of indene to 1-indenol and 1,2-indandiol.[23]

1.2.1 Classification of ROs

Various different characteristic features have been used for the classification of ROs since the early 1990s.[24–28] Ferrarro et al. described a classification scheme based on the components into Class IA, IB, IIA, IIB and III, as well as based on the four RO families: Naphthalene, Toluene/Biphenyl, Benzoate and Phthalate. The former classification is based on the number of electron transfer components and contained flavins, as well as the type of iron-sulfur clusters (table 1). Thereof, all mentioned five classes share the characteristic Rieske-type [2Fe-2S] cluster and the catalytic mononuclear iron in their Oxy component. Class IA and IB cover two component systems, which contain a reductase (Red) and an Oxy, of which the Red of both classes contains a plant-type [2Fe-2S] cluster, but the flavin in the Red of class IA is a FMN, whereas of class IB is a FAD. Class IIA, IIB and III represent three component ROs. Thereof, IIA and IIB contain an additional Fd as a third component, harboring either a plant-type (IIA) or a Rieske-type (IIB) [2Fe-2S] cluster, both accompanied with a FAD dependent Red. Finally, class III ROs comprise a FAD dependent Red with a Rieske-type [2Fe-2S] cluster and a Rieske-type [2Fe-2S] Fd.[12] Prominent ROs of Class IIB include the RO system cumene dioxygenase (CDO) from *Pseudomonas fluorescens* IP01, which was used in this work, biphenyl 2,3 DO (BPDO) from *Sphingobium yanoikuyae* B1, as well as carbazole 1,9a DO from *Nocardioides aromaticivorans* IC177.

Table 1 Classification scheme based on RO components, as described by Ferraro et al.[12]

System	Class	Reductase	Ferredoxin	Oxygenase	Model Enzyme
2-component	IA	FMN, [2Fe-2S]$_P$	none	[2Fe-2S]$_R$, Fe	Phtalate dioxygenase
	IB	FAD, [2Fe-2S]$_P$	none	[2Fe-2S]$_R$, Fe	Benzoate dioxygenase
3-component	IIA	FAD	[2Fe-2S]$_P$	[2Fe-2S]$_R$, Fe	Pyrazon dioxygenase
	IIB	FAD	[2Fe-2S]$_R$	[2Fe-2S]$_R$, Fe	Cumene dioxygenase
	III	FAD, [2Fe-2S]$_R$	[2Fe-2S]$_R$	[2Fe-2S]$_R$, Fe	Naphtalene dioxygenase

$_P$ plant/adrenodoxin-type iron-sulfur cluster, $_R$ Rieske-type iron-sulfur cluster

Historically, ROs have been grouped based on their components, in which the classification was proposed according to the type of Fe-S cluster contained in the Red, the presence and type of flavin (FMN or FAD), as well as, if the system includes a Fd, the type of therein contained Fe-S cluster.[24,25] Batie et al. grouped ROs into three Classes (IA, IB, IIA, IIB and III) according to the number of proteins involved in the electron transport chain, as well the presence and nature of contained flavins and the type of [2Fe-2S] clusters.[24] Another classification of ROs relies on their native substrate specificities and phylogenetic trees.[27,29] Werlen et al. proposed during homology studies that genes and gene products of the

chlorobenzene DO from *Pseudomonas sp.* P51 belong to the same subclass of aromatic DOs that also includes the toluene and benzene DO. After comparison of several amino acid sequences of the catalytic Oxy α-subunits, four DO families (Naphthalene, Toluene/Benzene, Biphenyl, and Benzoate/Toluate) were identified in total.[27] Nam et al. proposed a classification scheme based on amino acid homologies between the Oxy α-subunits while proposing difficulties among characterization of newly identified ring-hydroxylating Oxys due to limitations of Batie et al.'s classification scheme.[26] Also in 2000, Gibson and Parales claimed that the then prevailing classification of aromatic hydrocarbon DOs, which belong to the large family of aromatic-ring-hydroxylating DOs, did not distinguish between MOs and DOs. Thereby, all family members of aromatic-ring-hydroxylating DOs either comprise an Oxy together with one or two electron transport proteins. However, also MOs were considered part of this family, as e.g. the 2-oxo-1,2-dihydroquinoine MO and benzoate DO were both classified in Class IB due to their common trait of only containing one iron-sulfur flavin Red together with the Oxy. To counteract this confusion, they suggested to change in the classification, in this sense to consider the ROs as the superfamily, and to designate MOs and DOs for unambiguous systems, based on the native substrates and the amino acid sequences of the Oxy α-subunits.[29]

1.2.2   Structure of ROs – the electron transport chain

The fact that ROs are two or three component systems implicates that electron transfer between the single components occurs via a complex transfer chain (as exemplified using the CDO in figure 4 A). There is usually a Red component that can oxidize an electron donor, like NAD(P)H, which can then transfer single electrons either directly (in two component systems) or via a Rieske Fd (in three component systems) to the Oxy, which eventually catalyzes the substrate di-hydroxylation.[12,14] Electrons are obtained via oxidation of NAD(P)H by the Red, wherein they are passed to the contained flavin cofactor (FMN or FAD), from which single electrons are further transferred on to a [2Fe-2S] center, either located within the Red itself or (in three component systems) located within a separate Fd component. Eventually, single electrons are passed on to a Rieske [2Fe-2S] center contained in the Oxy component, wherefrom electrons are handed on to a catalytic mononuclear iron (Fe) center, where interaction with O_2 and the substrate takes place.[13] Because both of the electrons from either NADH or NADPH need to be transferred as a hydride in a simultaneous fashion, whereas Fe can only undergo single electron reactions, a suitable Red that can act as a two to one electron

8

switch is required for this transition.[24] For this reason, Reds of two component systems contain both a flavin, as well as a [2Fe-2S] center. Protein-bound Fe-S clusters belong to one of the most common prosthetic groups in biological systems.[30] Initially, these groups were discovered within electron transfer enzymes involved in photosynthesis and respiration and existed among the first ever biological catalysts. The reason of their ubiquity lies in the fact that Fe-S clusters can delocalize the electron density between the Fe and S atoms.[31] Several iron-sulfur clusters exist in nature, including the three most common types [2Fe–2S], [3Fe–4S], [4Fe–4S], and hybrid or mixed metal types, which are categorized based on their atomic content.[12] The cluster types [2Fe–2S], [3Fe–4S], [4Fe–4S] are associated with electron transfer and can be found in Fds, whereas the coupled electron/proton transfer catalyzed by Rieske proteins is accomplished by therein contained [2Fe–2S] clusters.[31] Among the latter cluster type, two general types are known, differing in their coordinating amino acid residues: the Rieske-type [2Fe2S] cluster, in which one of the two Fe atoms (Fe_1) is incorporated via two histidine (His) residues, whereas the other Fe atom (Fe_2) is stabilized via two cysteine (Cys) residues and the plant-/adrenodoxin-type [2Fe2S] cluster, which is solely coordinated to the protein by four Cys residues. Upon reduction of the Rieske-type [2Fe2S] cluster, only the His-coordinated Fe_1 atom changes to a ferrous oxidation state, whereas the Cys-coordinated Fe_2 atom remains in a ferric state. Therefore, only one electron can be stored on a Fd upon reduction by the Red and thus, two Fds are necessary to shuttle two electron equivalents from NAD(P)H for eventual dioxygenation of the substrate by the Oxy.[12]

The terminal Oxy component of ROs is responsible for the oxyfunctionalization of the substrate and has been shown, depending on the RO class (table 1), to either consist of two separate proteins, namely a large catalytic α-subunit and a smaller β-subunit of the hetero-multimeric $α_nβ_n$-type, or solely an α-subunit of the homo-multimeric $α_n$ type.[14] Structures of RO Oxy that have been determined to date all indicate either homo-trimeric $α_3$ or hetero-hexameric $α_3β_3$-structures, which are reminiscent of the shape of a mushroom. The β-subunit had been assumed to have structural purpose only in ROs like the NDO from *Pseudomonas sp.* 9816-4 (NDO_{9816-4} Oxy), but other reports suggest that the β-subunit may affect the substrate selectivity.[12] The well-studied model of the NDO Oxy_{9816-4}, which was the first RO Oxy with a solved crystal structure,[32] is of the hetero-hexameric $α_3β_3$-type, and the crystal structure of

the CDO Oxy from *P. fluorescens* IP01 that was used in this work was determined by Dong et al. to have the same quaternary arrangement.[33]
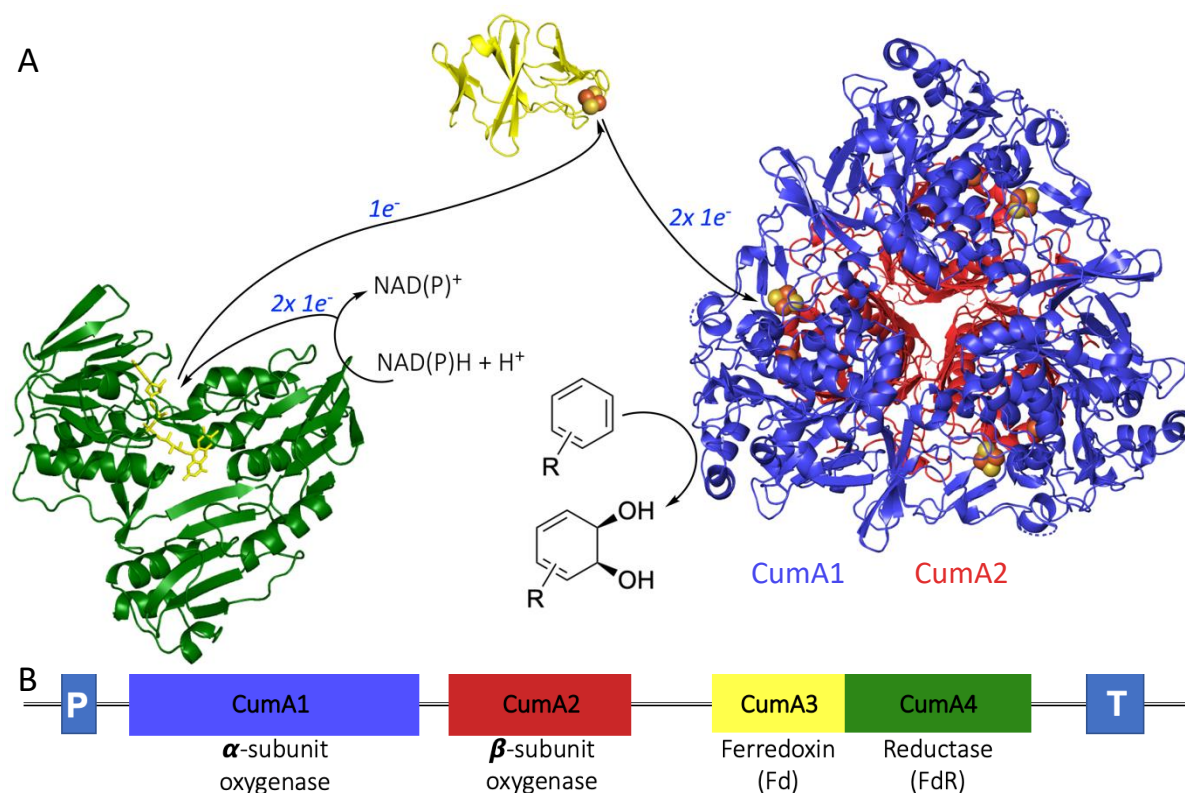
Figure 4 (A) Electron transfer chain of a RO from NAD(P)H along a reductase (FdR) and a ferredoxin (Fd) to the terminal oxygenase (Oxy) component exemplified using the CDO from *P. fluorescens* IP01, adapted from Ferraro et al. and Dong et al.[12,33] (B) RO operon harboring the genes of the four subunits exemplified for the CDO; *P promoter, T terminator*.[14]

1.2.3 Catalytic mechanism

Electrons from NAD(P)H are gated to the Oxy either by a Fd (in three component systems) or directly via a Red (in two component systems). Within the Oxy α-subunit, the Rieske [2Fe-2S] cluster accepts the electrons and hands them on to the mononuclear iron for catalysis. The structure and catalytic mechanism has extensively been studied using the NDO_{9816-4} Oxy, which to date serves as a model enzyme for three component ROs.[32,34,35] The NDO_{9816-4} Oxy is of the $α_3β_3$-type and has demonstrated that the distance between the mononuclear Fe and the Rieske [2Fe-2S] cluster of two neighboring α-subunits is only ~12 Å, whereas the mononuclear Fe and the Rieske [2Fe-2S] cluster within one catalytic α-subunit are ~44 Å apart (as exemplified using the CDO Oxy in figure 5, left).[36] This suggests electron transfer to occur rather between adjacent α-subunits than within a single α-subunit in an intramolecular way.[10] The connection for the electron transfer between the Rieske [2Fe-2S] center and the mononuclear Fe of a neighboring α-subunit is governed by an aspartate (Asp) residue that

10

bridges two histidine residues via hydrogen bonds.[10,12,33] Dong et al. determined the CDO Oxy crystal structure by means of molecular replacement using the crystal structure of the NDO$_{9816-4}$ Oxy,[32] wherein the ligation between the non-heme mononuclear Fe and the Rieske [2Fe-2S] center within the very same α-subunit and bridging of these centers between neighboring α-subunits via hydrogen bonds of the single amino acid residue of the CDO Oxy (Asp231) was similar to the structure of the NDO$_{9816-4}$ Oxy (Asp205).[33]
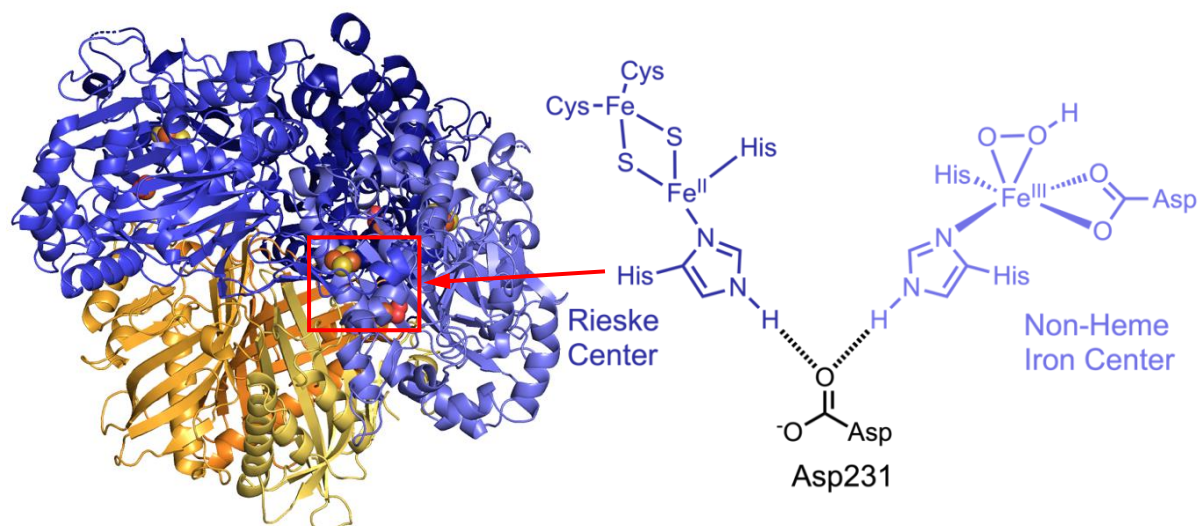
Figure 5 Left: structure of the α$_3$β$_3$-quaternary structure of the CDO Oxy. The single smaller β-subunits (CumA2) are shown in different yellow/orange colors, whereas those of the catalytic α-subunits (CumA1) are shown in different blue/purple colors. The Rieske [2Fe-2S] clusters are depicted as orange/yellow spheres and the catalytic non-heme Fe center atom with bound O$_2$ is represented by orange/red spheres. Electron transfer from the Rieske center to the catalytic non-heme iron center occurs between two adjacent α-subunits, as highlighted in the red rectangle. Visualized using PyMOL and adapted from Dong et al.[33] Right: molecular structure of the Rieske center, the catalytic non-heme Fe center and the connecting Asp 231 residue (aspartate bridge) of the CDO Oxy. Visualized using ChemDraw and adapted from Barry and Challis.[10]

The active site consisting of the mononuclear Fe, which many non-heme iron-dependent enzymes have in common, is coordinated by three amino acids, namely the "2-His-1-carboxylate triad" (figure 5, right) that consists of two His residues together with either an aspartate or glutamate residue ligand of flexible character that is further coordinated by one or two water molecules.[10] The carboxylate residue is assumed to be bidentately coordinated to the Fe, but also monodentate structures have been reported,[36] as e.g. in the case of CDO Oxy.[33] Studies of the 2-oxoquinoline 8 MO from *P. putida* propose that the one-electron reduction of the [2Fe-2S] cluster leads to the protonation of the Rieske center-belonging His that is part of the 2-His-1-carboxylate triad, which can thus act as a hydrogen bond donor within this bridge. This results in a conformational change upon reduction of the [2Fe-2S] cluster, where the movement of the bridging Asp towards the His residue leads to a change

11

within the coordination geometry at the catalytic non-heme Fe center and further promotes binding of O_2.[10]

The reaction mechanism involved in RO-catalyzed reactions is not fully understood due to difficulties in gaining spectroscopic insights of the catalytic mononuclear iron, because of limited spectroscopic accessibility in the presence of the Rieske center.[14] However, the 2-His-1-carboxylate triad of the NDO_{9816-4} Oxy was shown to point the face of the catalytic mononuclear Fe towards the large hydrophobic active site.[12] The active site of the NDO_{9816-4} Oxy was also shown to undergo a change of the ferrous Fe coordination geometry upon binding of naphthalene, resulting in a five-coordinate square pyramid. The NDO Oxy thereby presumably follows an ordered mechanism, whereat reduction of the [2Fe-2S] center and binding of the substrate naphthalene to the active site Fe is necessary for the binding of O_2 to the active site Fe. Thus, activation of O_2 without naphthalene, which might lead to oxidative inactivation of the Oxy, would thereby be prevented by such ordered mechanism.[10]

Current understanding of the catalytic mechanism of the NDO indicate two possible cycles, which differ in the oxidation states, either being Fe(IV) or Fe(V), that the catalytic iron goes through during O_2 activation.[10,37] Both mechanisms start with the binding of naphthalene to the active site, followed by elimination of a water from the resting state octahedral ferrous complex, in which the Fe is coordinated by one Asp and two His residues, as well as two water molecules. In one possible reaction cycle, binding of O_2 leads to formation of a five-coordinate complex, which, upon transfer of one electron from the Rieske [2Fe-2S] cluster, yields a ferric peroxide complex that, after protonation and elimation of water, leaves behind a bidentate hydroperoxide complex. Subsequent coupled O-O bond cleave and naphthalene oxidation leads to a Fe(IV)=O complex together with a hydroxynaphthalene radical intermediate, which further reacts to a ferric alkoxyhydroxynaphthalene complex. During the second proposed mechanism, the mentioned O-O bond of the bidentate hydroperoxide complex is cleaved prior to naphthalene oxidation, resulting in a Fe(V)=O(OH) complex that further reacts with naphthalene and thereby forms the mentioned ferric alkoxyhydroxynaphthalene complex. From this step on, both catalytic cycles are followed by the transfer of a second electron from the Rieske [2Fe-2S] cluster, resulting in the formation of a ferrous alkoxyhydroxynaphthalene complex, which upon protonation leads to release of the dihydroxylated product and regeneration of the resting state of the octahedral ferrous complex.[10] However, Ferraro et al.

claimed that no higher order oxidation state than the Fe(III) within the formed Fe(III)-(hydro)peroxo complex is required for a concerted mechanism, which eventually leads to substrate *cis*-dihydroxylation.[12]

1.2.4   Stability and effect of varying ratios of Oxy, Fd and FdR

Regarding the stability of single RO components, several differences between the RO Oxy and the reductive partners Fd and Red have been found in literature.[38,39] Especially Fd was shown to be of rather unstable character, once isolated from cell extracts.[39] It was therefore demonstrated that a molar excess of the redox partners Fd and also Red over the Oxy has beneficial effects on the activity of the Oxy.[40,41] In 1994, Tan et al. demonstrated during the investigation of the benzene DO from *P. putida* ML2 (NCIB 12190), that addition of purified Fd or Red significantly stimulated benzene bioconversion *in vitro* upon adding these purified components to CFL of *P. putida* harboring Oxy, Fd and Red. An exponential increase in activity of the Oxy was achieved after adding 10 µg purified Fd to CFE, which led to an activity of 20 nmol/min, and the addition of 50 µg purified Fd to CFE resulted in an increase of activity to 65 nmol/min. In comparison, when only purified Red was added, a less significant influence was noted. Furthermore, the addition of purified Oxy did not significantly alter the Oxy activity.[40] Moreover, molar excess of the Fd over the Oxy has been described beneficial for the Oxy activity during *in vitro* bioconversions for the NDO.[42] In 2017, Halder et al. showed that during *in vitro* conversion of 2 mM naphthalene to 1,2-naphthalendihydrodiol catalyzed by the NDO, at equal Oxy concentrations the increase of Oxy:Fd:FdR from 1:12:3 µM to 1:20:5 µM led to a more than 2-fold increase from 0.64 ± 0.06mM to 1.48 ± 0.02 mM product formation.[41] Hence, especially the latter result of *in vitro* bioconversions using a three-component RO (NDO) and the therein described varied ratios between the Oxy and the redox partners, which resulted in increased Oxy activity, seem to be a considerable approach for other three-component ROs.

1.3 Cumene dioxygenase from *P. fluorescens* IP01 (CDO)

A prominent RO is the cumene dioxygenase (CDO) from *Pseudomonas fluorescens* IP01, which belongs to class IIB and is a three component system.[12,14] The aromatic hydrocarbon cumene is a very important petrochemical commodity in the production of aceton and phenol. Cumene is industrially synthesized via the alkylation of benzene with propylene.[43] In 1995,

Aoki et al. were able to isolate and identify the strain *Pseudomonas fluorescens* IP01 from soil because of its capability to grow in minimal media containing cumene as sole carbon source. The genes responsible for the initial enzymatic arene-oxyfunctionalization were designated *cumA1*, *cumA2*, *cumA3* and *cumA4* and the enzymatic system was claimed to be a three-component system, namely "cumene dioxygenase" (CDO).[44] The Oxy was reported to be of the heterohexameric $\alpha_3\beta_3$-quaternary structure, where *cumA1* encodes for a large catalytic α-subunit (CumA1) and *cumA2* encodes for the smaller β-subunit (CumA2). Furthermore, *cumA3* encodes for a ferredoxin (Fd) and the *cumA4* gene encodes for a ferredoxin-reductase (FdR). The FdR harbors a FAD, whereas the Fd contains a Rieske-type [2Fe-2S] cluster. In this multicomponent CDO system, electrons from NAD(P)H are obtained by the FdR and Fd acts as an electron shuttle that transfers single electrons to the Oxy for catalysis.[10,12,14]

The substrate specificity of the CDO was investigated during *in vivo* studies by Aoki et al. Out of 24 substrates, *P. fluorescens* IP01 was shown to be able to grow on 8, including cumene, toluene, propylbenzene, and butylbenzene. However, co-oxidation was observed in total on 18 substrates, including styrene and biphenyl. Interestingly, for recombinant *E. coli* JM109 harboring the CDO system, the same 18 substrates were initially oxidized and further converted into *meta*-cleavage compounds.[44] Takami et al. showed that both *P. fluorescens* IP01 and recombinant *E. coli* JM109 harboring the CDO are capable of degrading several chlorinated compounds, e.g. trichloroethylene up to 90 % and 75 %, respectively.[45] Dong et al. solved the crystal structure of the CDO Oxy by means of molecular replacement using the solved crystal structure of the NDO Oxy, wherein the CDO was reported to exhibit high amino acid sequence identity to the biphenyl DO (BphDO) from *Burkhorderia cepacia* LB400 (with 74 % and 59 % for the α- and β-subunit, respectively) and to the BphDO from *Burkorderia sp.* RHA1 (BphDO$_{RHA1}$) (67 % for the α-subunit).[33] Overlays of several RO Oxy α- and β-subunit structures (carbazole DO from *Pseudomonas resinovorans* CA10, nitrobenzene DO from *Comamonas sp.* JS765, BphDO$_{RHA1}$, 2-oxoquinoline MO from *P. putida* 86, as well as CDO and NDO), were compared by Ferraro et al., wherein the N-terminal parts of the α-subunits were highly conserved in the region that contains the Rieske cluster-binding domain and showed more structural variability close to the catalytic mononuclear iron-binding site. Moreover, the structures of the corresponding β-subunits were shown to be highly conserved, even though they show low sequence homology.[12]

14

In 2015, Gally et al. were able to modulate the regio- and stereoselectivity of the CDO by incorporating different sized amino acids via site-directed mutagenesis of one single position within the active site towards several substrates, including styrene, vinylcyclohexane and indene, but also towards the non-arene olefine substrate myrcene. During *in vivo* bioconversions of e.g. indene with *E. coli* JM109, mono- and di-hydroxylated product was obtained at ~80 % total product formation with both the CDO WT (figure 3 A) and a CDO mutant (M232A) (figure 3 B). The mutation M232A is located within the catalytic site located in the large α-subunit (CumA1) of the Oxy. However, this single amino acid substitution led to the formation of enantio-complementary catalysts for the oxyfunctionalization of indene (figure 3).[23] Only recently, Özgen et al. demonstrated the first practical application of a photoinduced RO system *in vivo* using the CDO. This system is based on light-harvesting complexes, namely photosensitizers, (e.g. eosin Y, 5(6)-carboxyeosin or rose bengal) in combination with a sacrificial electron donor (e.g. EDTA, MOPS or MES). Hence, it is a natural cofactor-independent system that does not require the use of NAD(P)H or regeneration systems thereof. During these *in vivo* bioconversions using the CDO M232A variant harbored by *E. coli* JM109 with e.g. the substrate indene, 83 % product formation could be observed, which is approximately the same amount of detected product from Gally et al.'s studies,[23] which are based on conventional *in vivo* biotransformations. However, the diastereomeric ratios, as well as the distributions between mono- and dihydroxylated products differed significantly dependent on the combination of the used photosensitizers and electron donors.[46]

1.4 Uncoupling of enzyme activity by H_2O_2 production

For both ROs and P450 MOs an undesired effect called "uncoupling", in which electrons from NAD(P)H are wasted in side reactions, has been described in presence of substrates with non-productive binding modes for the active site.[47,48] However, besides the native productive cycles that ROs and P450 MOs undergo during oxyfunctionalization, the formation of the intermediate Fe(III)-hydroperoxo complex can also take place directly using H_2O_2 via the so-called "peroxide-shunt", thus obviating the necessity of electron sources like NAD(P)H.[8,49,50]

Using the example of MOs, stoichiometric amounts of reducing equivalents are required in order to perform selective introduction of electrophilic oxygen species obtained by reductive

activation of molecular O_2 at the active site. The electron equivalents are naturally provided by NAD(P)H. However, these electron equivalents can also unfavorably be wasted in side reactions, which in turn leads to the diversion of the reducing power from the target substrate towards undesired reductions. Thereby, O_2 is known to be a strong reducing equivalent sink for which it is a common cause for futile reduction reactions. Thereby caused formation of reactive oxygen species (ROS) is considered to be the greatest issue in uncoupling. Hence, the bulk of *in vitro* reaction schemes make use of ROS-converting enzymes, like superoxide dismutases or catalases. Furthermore, undesired diversion of the reducing power of electron equivalents during catalysis leads to an inefficient and high consumption of cofactors.[51]

Regarding ROs, Lee et al.'s studies of the NDO revealed that during benzene bioconversion uncoupling of substrate turnover and resulting H_2O_2 formation leads to both irreversible inhibition of benzene-dependent O_2 consumption and irreversible Oxy inactivation. This irreversible DO inactivation was proposed to be a Fenton-type reaction. Benzene has therein been shown to be a partial uncoupling substrate, which leads to the formation of *cis*-benzene 1,2-dihydrodiol and H_2O_2. During catalysis 40-50 % of the NDO-consumed O_2 was reduced to H_2O_2. However, inactivation of the NDO Oxy could be prevented completely by the presence of catalase.[48]

Interestingly, the formation of the intermediate Fe(III)-hydroperoxo complex during RO catalyzed oxyfunctionalization can also take place directly using H_2O_2, which is known as the "peroxide shunt" that can even be applied purposely. Wolfe et al. demonstrated the peroxide-shunt using the NDO Oxy with naphthalene (without Fd or Red), where the addition of H_2O_2 led to *cis*-hydroxylated product. However, after one turnover the peroxide shunt halted, which was not caused by enzyme inactivation, but was rather the result of the product not being released. The product release was shown to be dependent on the reduced Fe(II) oxidation state of the mononuclear Fe. During the peroxide-shunt, no additional electron source (like NADH) is available to reduce the mononuclear Fe to the Fe(II) oxidation state. Hence, after the peroxide-shunt, the product was trapped because the catalytic mononuclear iron was shown to be in the oxidized Fe(III) state, just like after single turnover.[49] Recent nuclear resonance vibrational spectroscopy studies of the benzoate 1,2 DO revealed that during the peroxide shunt reaction H_2O_2 reacted with the Fe(III) catalytic site and an oxidized Rieske cluster with

benzoate already bound, resulting in the correct *cis*-dihydroxylated product, which also arises from the native O_2 reaction, but at a much slower rate.[50]

1.5   Thesis Aim

During this work, the RO enzyme system cumene dioxygenase (CDO) from *P. fluorescens* IP01 was investigated *in vitro* using the substrate indene, based on *in vivo* studies of Gally and colleagues.[23] In this multicomponent CDO system, the FdR presumably oxidizes NAD(P)H and Fd acts as an electron shuttle that transfers single electrons to the Oxy for catalysis.[10,12,14] The amount of literature covering recombinant CDO *in vivo* is fairly limited.[23,44–46] Even less literature has been published regarding *in vitro* characterization of the CDO, which is also a barrier for potential practical application, since the feasibility of utilizing this RO for *in vitro* biocatalysis is uncertain. Hence, in order to gain a better understanding of this enzyme system, the aim of this current study was 1) to achieve sufficient expression of all CDO components, Oxy, Fd and FdR, in terms of solubility, as well as to govern the correct formation of the quaternary $\alpha_3\beta_3$-structure of the Oxy required for activity, 2) to establish a suitable purification protocol for the CDO, 3) to thereby obtain active CDO for *in vitro* biotransformations, 4) to determine the cofactor preference between NADH and NADPH during the investigation of the system's electron transport chain and finally 5) to examine the dependency of Fd and FdR, as well as EV-CFL during bioconversions. Therefore, several approaches were followed, including the comparison between suitable expression hosts *E. coli* BL21(DE3) and *E. coli* JM109(DE3), pET28a expression systems, expression constructs and finally purification systems for the Oxy, Fd and the FdR, respectively.

2 Materials and Methods

2.1 Devices & Chemicals

Standard laboratory equipment was used for the experimental approaches in this thesis (unless stated otherwise). All chemical compounds were obtained from Sigma-Aldrich Inc., Carl-Roth GmbH, Thermo Fisher Scientific or TCI Deutschland GmbH (unless stated otherwise). Used devices and chemicals are listed in table 2.

Table 2 List of devices or agents and manufacturers.

Application	Device	Model/Agent/Manufacturer
Cultivation, expression, biotransformations		
	Incubation shakers	Certomat® BS-1, (Sartorius; Göttingen, Germany); Multitron Standard (INFORS HT; Bottmingen, Switzerland)
	20 mL air-tight sealed glass vials	Screw neck 24- 400 (Macherey-Nagel; Düren, Germany)
Centrifugation		
Cell harvest, enzyme purification	Refrigerated high-speed centrifuge Centrifugation tubes	Avanti^{TM} J-20 XP centrifuge with JA-10 and JA-25.50 Fixed-Angle Aluminum Rotor (Beckman Coulter; Brea, USA). Nalgene® 500 mL and 40 mL centrifuge tubes (Nalge Nunc International; Rochester, NY)
Enzyme purification, plasmid isolation, 2-phase extraction	Refrigerated table centrifuges	5810R and 5415R centrifuges (Eppendorf; Hamburg, Germany)
Physical cell disruption		
	Sonicator	Sonifier™ 250 equipped with a ½" Dia. Tapped Bio Horn and a Ultrasonics™ Sonifier™ Flat Tip (Branson Ultrasonics; Danbury, USA)
DNA amplification (PCR)		
	Thermocycler	GeneExplorer ADVANCED GE4852T thermocycler (Bio-Gener Technology Co., Ltd.; Hangzhou, China)
Enzyme purification		
Sterile-filtration	Syringe-filters	Filtropur S 0.2 sterile filter (pore size: 0.2 nm; SARSTEDT AG & Co. KG, Nümbrecht, Germany)
Enzyme entrapment	Purification column	Econo-Pac® Gravity Flow columns (Bio-Rad Laboratories, Inc.; Hercules, USA) with 2 mL HisPur™ Ni-NTA Resin (Thermo Fisher Scientific; Massachusetts, USA)
Desalting	Desalting column	PD-10 Desalting Columns (GE Healthcare; Chicago, USA)
Enzyme concentration	Ultra centrifugation unit	Amicon^{TM} Ultra Centrifugation Units (Merck Millipore; Massachusetts, USA) with a MWCO of 10,000 kDa
Purification at 4°C		
	Purification system	ÄKTA^{TM} pure 25 chromatography system, ÄKTA^{TM} pure sample pump and fraction collector F9-C (GE Healthcare; Chicago, USA)
Enzyme entrapment	Purification column	HisTrap^{TM} Fast Flow crude 5 mL column prepacked with precharged Ni Sepharose® 6 Fast Flow (GE Healthcare; Chicago, USA)

Fraction collection	96-well plate	96 well Whatman® UNIPLATE microplates (Merck Millipore; Massachusetts, USA)
SDS- and NativePAGE		
	Chamber	XCell *SureLock* TM Mini-Cell (Invitrogen™, Thermo Fisher Scientific; Massachusetts, USA).
DNA visualization		
	Imaging device	G:BOX (Syngene; Cambridge, UK)
Physical DNA transformation		
	Electroporator	MicroPulser Electroporator (Bio-Rad Laboratories; Hercules, USA).
Analytic devices		
Quantitative/qualitative compound analysis	GC-FID	For specifications, see section 2.5.2, table 15 and section 2.5.4, table 19.
Qualitative compound analysis	GC-MS	For specifications, see section 2.5.3, table 16.
Optical density measurement (cell density)	Photometer	6131 BioPhotometer (Eppendorf; Hamburg, Germany)
Photometric NAD(P)H measurement	Spectrophotometer	Cary Series UV-Vis Spectrophotometer (Agilent Technologies, Inc.; Santa Clara, USA)

2.1.1 Enzymes

All used commercial enzymes, respective applications and suppliers are listed in table 3.

Table 3 List of used commercially available enzymes.

Enzyme	Application	Manufacturer
Lysozyme (≥35,000 FIPU/mg)	Enzymatic cell disruption	Carl Roth GmbH; Karlsruhe, Germany
DNase (2,000 U/mL)	Enzymatic cell disruption	New England Biolabs; Ipswich, USA
PfuPlus! DNA Polymerase (2.5 U/µL)	DNA amplification	EURx; Gdańsk, Poland
Phusion and DreamTaq DNA Polymerase	DNA amplification	Thermo Fisher Scientific; Massachusetts, USA

2.1.2 Chemicals

All used chemicals for the preparation of liquid and solid cultivation medium, antibiotic and inducing agent stock solutions, compounds utilized for the preparation of storage and buffer solutions, as well as chemicals used during agarose gel electrophoresis and sample preparation for GC analysis are summarized in table 4 including the suppliers.

Table 4 Chemicals used for cultivation, expression, storage and buffers.

Application	Chemical	Supplier
Cultivation, expression		
Antibiotic	Kanamycin sulphate	
Inducing agent	IPTG (≥99 % pur.)	
Lysogeny broth (LB) medium	LB broth (Lennox)	Carl Roth GmbH; Karlsruhe, Germany
Terrific Broth (TB) medium	Yeast extract	
	Tryptone/Peptone	
	$K_2HPO_4 \cdot 3H_2O$ (≥99 % pur.)	
	KH_2PO_4 (≥98 % pur.)	

Super Optimal Broth (SOC) medium	KCl (≥99,5 % pur.)	
	$MgCl_2$ (≥98.5 % pur., anhydrous)	
	$MgSO_4$ (≥99 % pur., anh.)	
	Glucose monohydrate	
LB agar (solid cultivation medium)	Agar-Agar (Kobe I)	
Aqueous glycerol stock solution	Glycerol (SOLVAGREEN®, ≥98 % pur., anh.)	
Long time storage of devices		
Aqueous ethanol storage solution	Ethanol (ROTIPURAN® ≥98 % pur.)	Carl Roth GmbH; Karlsruhe, Germany
Buffer solutions for enzyme purification and biotransformations		
Buffers	$Na_2HPO_4x2H_2O$ (≥98 % pur.)	
	$Na_2HPO_4x2H_2O$ (≥98 % pur.)	Carl Roth GmbH; Karlsruhe, Germany
	NaCl (≥99.5 % pur.)	
	NaOH (≥98 %)	
	H_3PO_4 (≥85 %)	
Agarose gel electrophoresis		
TAE buffer	Tris (PUFFERAN® ≥99.3 %)	Carl Roth GmbH; Karlsruhe, Germany
Agarose gels	LabQ Standard agarose LE	LabConsulting; Vienna, Austria
DNA intercalating dye	GelGreen® Nucleic Acid Gel Stain (20,000X)	Biotium; Fremont, USA
Sample preparation (GC analysis)		
Organic solvent	Dichloromethane (DCM) (≥99.8 pur.)	Chem-Lab NV; Zedelgem, Belgium
Internal standard	Acetophenone (≥99.5 %)	Sigma-Aldrich; St. Louis, USA

2.1.3 Chemicals for cell cultivation and protein expression

Antibiotics: Kanamycin-stock solution, β(kan-stock) = 40 g/L

2 g kanamycin sulphate were dissolved in 50 mL ddH_2O, filtered using a Filtropur S 0.2 sterile filter and portioned to 1.5 mL aliquots for long term storage at -20°C.

Inducing agent: IPTG-stock solution, c(IPTG-stock) = 1 M

For a 1 M IPTG-stock solution 11.915 g IPTG were dissolved in 50 mL ddH_2O and filtered using a Filtropur S 0.2 sterile and portioned to 1.5 mL aliquots for long term storage at -20°C.

Liquid cultivation media:

Lysogeny broth (LB) medium

20 g ready-to-use LB Broth powder were dissolved in 1 L ddH_2O to a final concentration of 20 g/L using a 1 L glass bottle and autoclaved.

Final concentrations: β(tryptone) = 10 g L^{-1}; β(yeast extract) = 5 g L^{-1}; β(NaCl) = 5 g L^{-1}

Terrific Broth (TB) medium

24 g yeast extract, 12 g tryptone/peptone and 5 g glycerol were dissolved in 900 mL ddH$_2$O using a 1 L glass bottle and autoclaved.

A 10x TB salt stock was created by dissolving 164.4 g K$_2$HPO$_4$*3H$_2$O and 23.2 g KH$_2$PO$_4$ in 1 L ddH$_2$O within a 1 L glass flask upon autoclaving.

100 mL of 10x TB salt stock were then added to 900 mL TB medium. Both solutions were autoclaved separately and mixed only shortly before using.

Final concentrations: β(yeast extract) = 24 g L^{-1}; β(tryptone/peptone) = 12 g L^{-1}; β(glycerol) = 5 g L^{-1}; β(K$_2$HPO$_4$) = 12.55 g L^{-1}; β(KH$_2$PO$_4$) = 2.32 g L^{-1}

Super Optimal Broth (SOC) medium

A 10x SOC medium stock was created by dissolving 2 g KCl, 20 g MgCl$_2$, 20 g MgSO$_4$ and 40 g glucose monohydrate in 1 L ddH$_2$O within a 1 L glass flask upon autoclaving.

100 mL of 10x SOC stock were then added to 900 mL autoclaved ddH$_2$O.

Final concentrations: β(KCl) = 0.2 g L^{-1}; β(MgCl$_2$) = 2 g L^{-1}; β(MgSO$_4$) = 2 g L^{-1}; β(glucose monohydrate) = 4 g L^{-1}

Solid cultivation media:

LB agar with kanamycin

20 g ready-to-use LB Broth powder and 15 g Agar-Agar were dissolved in 1 L ddH$_2$O in a 2 L glass flask upon autoclavation. Then the LB agar was cooled down to 60°C and 1 mL of 40 mg/mL kanamycin stock solution was added shortly before pouring the mixture into polystyrene Petri dishes, which were then stored at 4°C.

Final concentrations: β(tryptone) = 10 g L^{-1}; β(yeast extract) = 5 g L^{-1}; β(NaCl) = 5 g L^{-1}; agar-agar = 15 g L^{-1}; β(kanamycin = 40 mg L^{-1})

2.1.4 Solutions for longtime storage of bacterial culture-stocks

Aqueous glycerol stock solution, w(glycerol) = 60 %

60 g glycerol were dissolved in 40 mL ddH$_2$O and autoclaved.

2.1.5 Chemicals for longtime storage of devices

Aqueous ethanol storage solution, ϕ(ethanol) = 20 %

For the long-term storage of Ni-NTA Purification Columns, PD-10 Desalting Columns and Amicon^{TM} Ultra Centrifugation Units at 4°C an aqueous ethanol storage solution was prepared by adding 20 mL ethanol to 80 mL ddH$_2$O in a 100 mL shot bottle.

2.1.6 Chemicals for enzyme purification and in vitro biotransformations

Ni-bead solution for the entrapment of His-tagged enzymes

For enzyme purifications carried out at room temperature 2 mL HisPur^{TM} Ni-NTA Resin were used to bind the enzymes to Econo-Pac® Gravity Flow columns.

Buffer solutions for enzyme purification at both RT as well as at 4°C and biotransformations

The following buffer solutions were used for cell washing, resuspension of cell debris, purification and desalting of enzymes as well as for *in vitro* biotransformations. The compounds and supplier companies are listed in table 4 (see section 2.1.2) and the exact concentrations are shown in table 5. The used buffers were prepared as followed: All compounds were weighed in a 1 L glass flask, then the flask was filled with 800 mL ddH$_2$O. The pH was subsequently adjusted to 7.2 using NaOH or H$_3$PO$_4$ and then the volume was increased to 1 L.

Table 5 Used buffer solutions for enzyme purifications and biotransformations.

	Purification buffers (RT)		
Compounds	*equi.-SPB 1*	*elu.-SPB 1*	*des.-SPB 1*
NaH$_2$PO$_4$ x 1H$_2$O	100 mM	100 mM	100 mM
Na$_2$HPO$_4$ x 2H$_2$O	100 mM	100 mM	100 mM
NaCl	300 mM	300 mM	-
Glycerol	10 %	10 %	-
Imidazol	30 mM	400 mM	-
	Purification buffers (4°C, ÄKTA^{TM} pure)		
Compounds	*equi.-SPB 2*	*elu.-SPB 2*	*des.-SPB 2*
NaH$_2$PO$_4$ x 1H$_2$O	25 mM	25 mM	25 mM
Na$_2$HPO$_4$ x 2H$_2$O	25 mM	25 mM	25 mM
NaCl	300 mM	300 mM	-
Glycerol	10 %	10 %	-
Imidazol	30 mM	400 mM	-
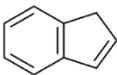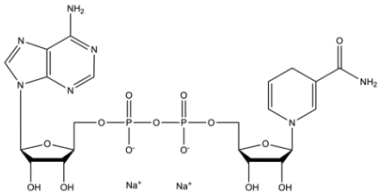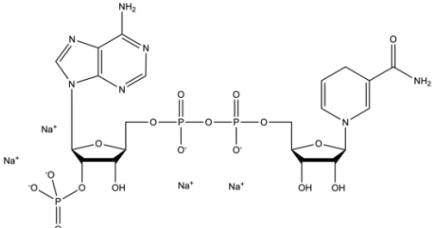
Aqueous glycerol buffer solution for biotransformations, w(glycerol) = 20 %

For the preparation of biotransformations, aliquots of 67 μL concentrated purified enzymes were added to 33 μL 60 % glycerol stock solution and stored at -20°C. $w_{(glycerol)}$ = 20 %.

Substrates and products from biotransformations

The used substrate, as well as cofactors and obtained products from *in vitro* biotransformations by the CDO enzymes are summarized in table 6.

Table 6 Chemical structures, supplier and Cas numbers of the used substrate, cofactors and obtained products from biotransformations.

Substrate	Structure	Purity	Supplier	Cas Nr.
Indene		≥99 %	Sigma-Aldrich	95-13-6
1-indanone		≥99 %	Sigma-Aldrich	83-33-0
1-indenol		-	not available as a pure product	56631-57-3
NADH-Na$_2$		≥94 %	Carl Roth	606-68-8
NADPH-Na$_4$		≥95 %	Carl Roth	2646-71-1

2.1.7 Chemicals for SDS-PAGE

All SDS-PAGE and Native-PAGE experiments were carried out using material and agents obtained by Invitrogen™, Thermo Fisher Scientific (Massachusetts, USA) as listed in table 7. All buffers were diluted to a final (1X) concentration with ddH_2O from stock solutions.

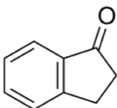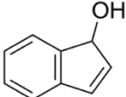**Table 7** Materials and chemicals used for SDS-PAGE and Native-PAGE experiments.

	SDS-PAGE
Gels	10- or 15-well NuPAGE™ 4-12 % Bis-Tris Protein gels
Sample buffer	NuPAGE™ LDS Sample Buffer (4X)
Reducing agent	NuPAGE™ Sample Reducing Agent (10X)
Protein ladder standard	PageRuler™ Prestained Protein Ladder (10 to 180 kDa)
Running buffer	NuPAGE™ MES SDS Running Buffer (20X)

Native -PAGE	
Gels	10-well NuPAGE™ 3-8 % Tris-Acetate Protein Gels (1.0 mm)
Sample buffer	Novex™ Tris-Glycine Native Sample Buffer (2X)
Protein ladder standard	NativeMark™ Unstained Protein Standard (20 to 1,200 kDa)
Running buffer	Novex™ Tris-Glycine Native Running Buffer (10X)

2.1.8   Staining and destaining solutions for protein visualization

Proteins separated via SDS- and Native-PAGE were stained using staining solution containing Coomassie blue and later destained with a destaining solution, as listed in table 8.

Table 8 Staining and destaining solution used during protein visualization for both SDS- and Native-PAGE gels.

Coomassie staining solution		Destaining solution	
1 g	Coomassie Brilliant R-250	100 mL	Glacial acetic acid (conc.)
100 mL	Glacial acetic acid (conc.)	300 mL	Ethanol
300 mL	Ethanol	600 mL	dH_2O
600 mL	dH_2O		

2.1.9   Reagents for agarose gel electrophoresis

TAE buffer

1 L 50X TAE buffer was prepared as a stock by dissolving 242 g tris, 100 mL 0.5 M EDTA stock solution (pH = 8.0) and 57.1 mL acetic acid and 842.9 mL ddH_2O.

Agarose gels

For the preparation of 1 % agarose gels, 1 g LabQ Standard agarose was dissolved in 100 mL 1X TAE buffer.

DNA intercalating dye

GelGreen® Nucleic Acid Gel Stain (20,000X) was added to a polymerizing agarose gel upon cooling.

2.1.10 Chemicals used during GC sample preparation

During the extraction of the substrate indene, the expected products 1-indanone and 1-indenol, dichloromethane (DCM) was used as the organic solvent, containing 2 mM acetophenone, which served as the internal standard.

2.2 Microbiological Methods

2.2.1 Bacterial host strains

The used *E. coli* host strains utilized during this work are listed in table 9.

Table 9 Bacterial host strains, respective genotypes and supplier companies.

Strain	Genotype	Supplier
JM109(DE3)	*end*A1, *rec*A1, *gyr*A96, *thi, hsd*R17 (r_k^-, m_k^+), *rel*A1, *sup*E44, λ–, Δ(*lac-pro*AB), [F′, *tra*D36, *pro*AB, *lacI*qZΔM15], lDE3	Promega (Madison, USA)
BL21(DE3)	F– *omp*T *hsdS*$_B$ (r_B–, m_B–) *gal dcm* (DE3)	Thermo Fisher Scientific (Waltham, USA)
TOP10 F′	F′ [*lacI*q, *Tn*10(Tet^R)] *mcr*A Δ(*mrr-hsd*RMS-*mcr*BC) φ80*lacZ*ΔM15 Δ*lac*X74 *rec*A1 *ara*D139 Δ(*ara-leu*)7697 *gal*U *gal*K *rps*L(Str^R) *end*A1 *nup*G	Thermo Fisher Scientific (Waltham, USA)

2.2.2 Overnight culture preparation

Overnight cultures (ONC) were prepared using 50 mL LB medium, 50 µL kanamycin (final concentration: [β(kanamycin) = 40 mg L^{-1}] and the respective cell amount in a 300 mL baffled Erlenmeyer flask. For plasmid isolations 5-10 mL LB medium were used for the inoculation in a 50 mL Greiner tube. The *E. coli* cells used for the inoculation were either taken from glycerol stock solutions (stored at -80°C or at -20°C) or from agar plates. The ONC were incubated for 17-20 h, shaking at 130 rpm at 37°C.

2.2.3 Main culture preparation

The main cultures were prepared using 400 mL TB medium, 400 µL kanamycin (final concentration: [β(kanamycin) = 40 mg L^{-1}] and the respective amount of ONC to inoculate to an OD$_{600}$ of 0.1 in a 2 L baffled Erlenmeyer flask.

2.2.4 Glycerol stock preparation

Bacterial glycerol stocks were prepared by adding 1 mL of ONC to 1mL autoclaved aqueous glycerol solution w(glycerol) = 60 % in a 2mL Bio-One Cryo tube for long time storage at -80°C and -20°C.

2.3 Molecular Biological Methods

2.3.1 Vector constructs in silico

Any *in silico* DNA-visualization, primer design as well as any DNA sequence for the creation of the plasmids harboring the CDO genes (via Gibson® Assembly) were carried out using the software Genious Prime (Biomatters Ltd.; Auckland, New Zealand) and Benchling (Benchling; San Francisco, USA).

A list of all mentioned plasmids containing native (*P. fluorescens* IP01) and *E. coli* codon-optimized (c.o.) CDO genes is shown in table 10. The pET28a(+) vector constructs contain *E. coli* codon-optimized variants of the single CDO genes *cumA1* (CDO α-subunit), *cumA2* (CDO β-subunit), *cumA3* (CDO ferredoxin) and *cumA4* (CDO ferredoxin reductase). The constructs harboring only one of the CDO genes, respectively, were kindly supplied by Peter Wied and were used for several cloning approaches and further experiments in this thesis. The c.o. synthetic genes had been ordered by Peter Wied from GeneArt (Thermo Fisher Scientific, Regensburg, Germany) and codon-optimized using the company-own algorithm.

pET28a(+) vectors are commonly used strong expression vectors, wherein the gene of interest is cloned under the control of the strong T7 promoter and thus can be induced upon the addition of IPTG, given that the used host cell contains a genomic T7 RNA polymerase, like in this thesis *E. coli* JM109(DE3) or BL21(DE3).

Table 10 All plasmid constructs mentioned or used in this work, the harbored c.o. CDO genes and the contained resistance marker genes. (×) The construct pFdR(N-His)× contained a base deletion at position 277 bp (277_278del), resulting in a nonsense mutation.

Construct[a]	Name	Genes	Resistance gene	Length (bp)
1	pCumA1(N-His)	*cumA1*	*KanR*	6724
2	pCumA2(N-His)	*cumA2*	*KanR*	5950
3	pFd(N-His)	*cumA3*	*KanR*	5367
4	pFdR(N-His)×	*cumA4*×	*KanR*	6606
5	pFdR(N-His)	*cumA4*	*KanR*	6607
6	pOxy(1xHis)	*cumA1, cumA2*	*KanR*	7327
7	pOxy(2xHis)	*cumA1, cumA2*	*KanR*	7474
8[a]	pOxy(1xHis)*	*cumA1, cumA2*	*KanR*	7327
9[a]	pOxy(2xHis)*	*cumA1, cumA2*	*KanR*	7474

[a] the *cumA1* gene on construct 8 and 9 contains a C-terminal 16 bp WT sequence remaining after the Gibson® assembly. The resulting amino acid-sequence is identical to the c.o. construct 6 and 7.

2.3.2 Plasmid DNA isolation

Plasmid DNA was isolated using the GeneJET Plasmid Miniprep Kit (Thermo Scientific™, Thermo Fisher Scientific; Massachusetts, USA) and the provided protocol, except for minor changes: the initial centrifugation step was carried out for 12 min. During the wash step, the empty column was centrifuged for 2 min. Finally, for the elution 50 µL of prewarmed ddH$_2$O (60°C) were used.

2.3.3 Agarose gel electrophoresis

Agarose gel electrophoresis was carried out in order to separate DNA molecules according to differing molecule lengths for either validation or separation purposes. Therefore, a respective amount of LabQ Standard agarose LE was dissolved in 1X TAE buffer to achieve a final concentration of 1 % and the mixture was heated using a microwave until the agarose had dissolved completely. Then a respective amount of GelGreen® Nucleic Acid Gel Stain (20,000X) was added to the hand warm polymerizing agarose gel before pouring it into an electrophoresis chamber and cooling. The DNA containing samples, respectively a DNA standard ladder were subsequently loaded to the pockets.

The agarose gel electrophoresis was carried out at 100 V, max. 400 mA for 30-45 min, depending on the purpose of the respective experiment.

2.3.4 Agarose gel extraction

In order to obtain certain DNA molecules upon separation via agarose gel electrophoresis, the agarose gels were visualized using a G:BOX. The respective DNA bands were cut out under UV light using a scalpel. Subsequently, the contained DNA was extracted from the agarose gel pieces using the GeneJET Gel Extraction Kit (Thermo Scientific™, Thermo Fisher Scientific; Massachusetts, USA) and the provided protocol, except for minor changes: after adding the binding buffer, the gel mixture was incubated at 60°C for 10 min. The washing step was carried out two times. At the elution step, 50 µL of prewarmed ddH$_2$O (65°C) were added to the column centre, followed by an incubation step for 3 min at 60°C before centrifuging for 2 min to obtain the elution fraction.

2.3.5 Polymerase Chain Reaction (PCR)

All DNA fragments required for Gibson assembly® of the two different pET28a(+) co-expression constructs harboring the CumA1 and CumA2 genes were amplified via a classical Polymerase Chain Reaction (PCR). Usually, a gradient PCR with six different annealing temperatures was carried out for the initial reaction, respectively. The annealing temperature was determined using the calculators provided by the respective manufacturers. Either *Pfu*! Plus DNA Polymerase, DreamTaq or Phusion DNA Polymerase were used for the PCR. The conditions for every PCR carried out in this thesis are listed in tables 22-25 in the appendix, section 6.2.

2.3.6 Gibson Assembly® - Cloning of Oxy co-expression constructs

The CDO Oxy. co-expression constructs pOxy(2xHis) and pOxy(1xHis) were created via Gibson assembly®.[52] Therefore, the CumA2 gene with N-terminal His tag ('pre-insert 1' and further 'insert 1') and without His tag (insert 2) were amplified via PCR using pCumA2(N-His) as template, whereas the pET28a(+) vector backbone containing the CumA1 gene with N-terminal His tag, pCumA1(N-His), was also amplified and thereby linearized via PCR. All PCR reactions were carried out according to tables 22-25 in the appendix, section 6.2.

The uncleaned PCR products were treated with *Dpn*I as depicted in table 11 in order to digest residual parental plasmids.

Table 11 *Dpn*I reaction conditions.

*Dpn*I reaction compounds		*Dpn*I digest	temperature	time
1.0 µL	10x CutSmart buffer	incubation	37℃	2 h
1.0 µL	*Dpn*I (10 U)	Inactivation	80℃	20 min
8µL	PCR product (uncleaned)	store	10℃	∞

The Gibson assembly® was carried out as follows:

15 µL Gibson assembly® mix were taken from -20°C on ice for 15 min. Then 5 µL of a 3:1 mixture (molar ratio) of insert:vector were added , followed by a 1 h incubation at 50°C. Then chemically competent *E. coli* TOP10 F' cells were transformed with 5 µL of the Gibson assembly® mix containing the ligated DNA strands and were then incubated over night on LB-kan agar plates. Colonies were then picked for evaluation of successful Gibson assembly® events via colony PCR and eventually confirmed via Sanger Sequencing performed by Microsynth AG (Balgach, Switzerland).

28

2.3.7 Colony PCR

In order to evaluate successful Gibson assembly® results of the CDO Oxy co-expression constructs pOxy(2xHis) and pOxy(1xHis), the respective fragments contained on the plasmids of picked colonies were amplified via colony PCR. Therefore, after transformation with the ligated DNA constructs and incubating over night at 37°C, several colonies (only half of the cell material per colony, respectively) were picked from an LB-kan agarose plate with a pipette tip and dissolved in 20 µL ddH$_2$O in a 1.5 mL Eppendorf tube. This very pipette tip was then used to streak out the respective clone on a fresh LB-kan agarose plate (master plate), which was again incubated, to have enough cell material in case of a successful ligation event in the plasmid of this very clone. The 20 µL cell suspension was then incubated for 20 min at 95°C to denaturate proteins and break up the cell wall, followed by a centrifugation step at 16,100 g (5415R centrifuge, Eppendorf, Hamburg, Germany) for 1 min to obtain the dissolved plasmid DNA in the supernatant that served as the template in the colony PCR. DreamTaq DNA Polymerase (Thermo Fisher Scientific; Massachusetts, USA) was used for the reactions. The conditions for the colony PCR are listed in table 12.

Table 12 Compounds, respectively used volumina thereof and the PCR conditions for the colony PCR, which was used to determine successfully created Oxy. co-expression constructs via Gibson® assembly.

Colony PCR		PCR program	temperature	time
2.5 µL	10x DreamTaq buffer	initial denaturation	95°C	5 min
2.5 µL	dNTP mix, 2 mM each			
1.25 µL	Forward primer P9 [10 µM]	30 cycles:		
1.25 µL	Reverse primer P10 [10 µM]	denaturation	95°C	1 min
3.0 µL	Colony plasmid DNA	annealing	53°C	30 s
0.125 µL	DreamTaq DNA Pol. (0.625 U fin.)	Extension	72°C	3 min
14.375 µL	ddH$_2$O			
		final extension	72°C	4 min
25 µL	final volume	store	10°C	∞

2.3.8 QuikChange™ site-directed mutagenesis

Due to a base deletion at position 277 bp (277_278del) within the FdR gene on the vector pFdR(N-His)[x] (6606 bp), which led to a non-sense mutation (L94X) on the translational level, a QuikChange™ site-directed mutagenesis was carried out.

Therefore, a primer pair was designed that included one of the single missing nucleotides C or G, respectively. The reaction conditions are listed in table 13. Afterwards, the parental plasmids were degraded via *Dpn*I digestion (as described in table 11 of section 2.3.6). The primer sequences are listed in table 21 in the appendix, section 6.1.

Subsequently, electrocompetent *E. coli* TOP10 F' were transformed with the *Dpn*I-treated plasmid DNA in order to seal contained nicks derived and further to amplify the plasmids. Eventually, ONCs of 10 transformed *E. coli* TOP10 F' colonies were prepared using 10 mL LB medium containing 25 mg/L Cm. Contained plasmids were isolated the following day and sent for Sanger sequencing to confirm correct site-directed mutagenesis. Eventually, *E. coli* JM109(DE3) was transformed with the repaired FdR construct pFdR(N-His) (6607 bp), which is shown in figure 35 (right) in the appendix, section 6.4.

Table 13 Compounds, respective volumina and the cycling program used for the QuikChange™ site-directed mutagenesis of the non-sense mutation at the bp position 277 of the FdR gene in the construct pFdR(N-His)^x (6606 bp).

QuikChange™ reaction compounds		QuikChange™ program	temperature	time
5 µL	10x Pfu buffer	initial denaturation	95°C	5 min
1.25 µL	dNTP mix, 2 mM each			
0.5 µL	Fwd. primer (P13) [10 µM]	30 cycles:		
0.5 µL	Rev. primer (P14) [10 µM]	denaturation	95°C	1 min
1 µL	pFdR(N-His)^x (60 ng/µL.)	annealing (gradient)	55°C	1 min
0.125	PfuPlus! DNA Pol. (2.5 U/µL)	extension	72°C	8 min
36.5 µL	ddH$_2$O			
		final extension	72°C	7 min
25 µL	final volume	store	10°C	∞

2.3.9 Chemical transformation of E. coli cells

Each chemical transformation of *E. coli* cells in this thesis was carried out according to the following protocol (heat shock method):

The chemically competent cells (50 µL aliquots) were taken from -80°C and put on ice to thaw for 15 min. Then, 3-5 µL plasmid DNA were added to the cells and left on ice for 30 min to incubate. Subsequently, a heat shock at 42°C was carried out for 42 s followed by the addition of 450 µL prewarmed LB SOC medium (37°C). Afterwards, the transformed *E. coli* cells were incubated for 1 h at 37°C and 130 rpm. Then, 100 µL were plated on LB-kan agar plates, whereat the remaining 400 µL were centrifuged for 1 min at 5,900 *g* (5415R Eppendorf centrifuge), approximately 300 µL of the supernatant were discarded and the cell pellet was dissolved in the remaining 100 µL LB SOC medium upon plating on a separate agar plate. The LB-kan agar plates were incubated at 37°C overnight.

2.3.10 Electroporation of competent E. coli cells

Each electroporation of *E. coli* cells in this thesis was carried out according to the following protocol: the electro-competent cells (80 µL aliquots) were taken from -80°C and put on ice

to thaw for 15 min. Then, 1-3 µL plasmid DNA were added to the cells upon transferring the cells to a precooled electroporation cuvette. After incubation on ice for 1 min, the cuvette's electrodes were wiped dry and the cells were shocked using the preset EC2 program for bacteria on the MicroPulser Electroporator. Immediately after the shock, 700 µL prewarmed LB SOC medium (37°C) were added to the cells, which were then transferred to 1.5 mL Eppendorf tubes. Then, the transformed *E. coli* cells were incubated for 1 h at 37°C and 130 rpm. Subsequently, 100 µL were plated on LB-kan agar plates, whereat the remaining 680 µL were centrifuged for 1 min at 5,900 *g* (5415R Eppendorf centrifuge), approximately 580 µL of the supernatant were discarded and the cell pellet was dissolved in the remaining 100 µL LB SOC medium upon plating on a separate agar plate. The LB-kan agar plates were incubated at 37°C overnight.

2.3.11 DNA Sequencing

All DNA sequencing was carried out by Microsynth AG (Balgach, Switzerland) via Sanger. Therefore, respectively 12 µL purified plasmid DNA [40-100 ng/µL] and optionally 3 µL primer [10 µM] were added to a sterile 1.5 mL Eppendorf tube and shipped.

2.4 Biochemical Methods

2.4.1 Heterologous protein expression

Heterologous protein expression of the CDO enzymes was performed using *E. coli* BL21(DE3) and *E. coli* JM109(DE3). ONCs were incubated using 50 mL LB medium (kan [40 mg/L]) for 17-19 h at 37°C and 130 rpm. Onto inoculation of the main culture in 400 mL TB medium (kan [40 mg/L]) to an initial OD_{600} of 0.1 with the required amount of ONC, the main culture was further incubated at 37°C. Induction of the heterologous proteins was initiated at OD_{600} of 1 using 0.05 mM IPTG from whereon the expression of the respective CDO enzymes was carried out for 19 hours at 20°C.

2.4.2 Cell harvest

The *E. coli* cell cultures expressing the heterologous CDO enzymes were harvested after 19 h by transferring the 400 mL main culture into pre-weighed 500 mL Nalgene® centrifuge tubes, centrifugation at 3,583 *g* for 15 min at 4°C and discarding the supernatant. The remaining cell pellets were washed with 50 mL equi.-SPB 1 or 2 by vortexing and resuspending using a 5 mL

pipette (PIPETMAN®; Gilson Incorporated, Middleton, WI). The resuspended cells were then centrifuged at 3,583 g for 30 min at 4°C, the supernatant was discarded, and the wet cell weight was determined. Whenever possible, the cells were kept on ice during the whole procedure to minimize inactivation of heterologous expressed enzymes.

2.4.3 Cell disruption

After harvesting and washing, the cell pellets were again resuspended in 30 mL equi.-SPB 1 or 2 and transferred to 40 mL Nalgene® centrifuge tubes. A spatula tip of Lysozyme (≥35,000 FIPU/mg) and 30 µL DNase (2,000 U/mL) were added to the cell suspension followed by gentle shaking and 15 min incubation on ice. The cells were then transferred into metal tubes and disrupted via sonication using a Branson Sonifier 250 device. All sonication steps were carried out at 75 % duty cycle and with the output control set to 7.2. It was performed for 10-14 cycles of 15 s sonication and 10 s resting time, respectively. However, the sonication and resting time differed depending on the physical properties of the thereby obtained disrupted cell suspensions, the temperature of the sonication tube, which tends to heat quickly, and finally the activity of the contained enzymes. The sonicated cells were then transferred back to the 40 mL Nalgene® centrifuge tubes and centrifuged for 40 min at 53,343 g and 4°C. The thereby obtained cell-free lysate (CFL) was finally sterile-filtered (pore size: 0.2 nm). All steps were carried out on ice, whenever possible.

2.4.4 Sample preparation for expression studies

To obtain a useable and comparable amount of culture for the upcoming protein extraction using BugBuster^{TM} and further the determination of protein expression pattern via SDS-PAGE, samples of the *E. coli* main cultures were taken at different time points during the cultivations and for expression studies 7/OD$_{600}$ samples were taken. Samples taken between 2 h before induction up to 3.5 h after induction were transferred into pre-weighed 15 mL and 50 mL Greiner tubes, and centrifuged for 10 min at 4°C and 3,166 g (Eppendorf 5810R), whereas the samples taken at cell harvest were transferred into a pre-weighed 1.5 mL Eppendorf tube and centrifuged using the Eppendorf 5415R centrifuge for 10 min at 4°C and 3,300 g. After centrifugation, the supernatants were discarded and the remaining cell pellets were used for protein extraction.

2.4.5 Protein extraction

To evaluate protein expression patterns, cell disruption was carried out using BugBuster^{TM} reagent, for which Eppendorf tubes were pre-weighed. Additionally, one 1.5 mL Eppendorf tube was required for the soluble and insoluble fraction, respectively.

Soluble fraction: Per mg of obtained cell pellet 5 µL BugBuster^{TM} reagent were used to resuspend the cell pellet at room temperature (RT) by pipetting. The cell suspension was incubated on a shaking plate (Eppendorf Thermomixer comfort) at RT for 20 min at 45 rpm. The insoluble fraction was separated by centrifugation at 16,100 g for 20 min at 4°C (Eppendorf 5415R) and the supernatant (soluble fraction) was transferred into a new 1.5 mL Eppendorf tube.

Insoluble fraction: The obtained pellet of the final centrifugation step (Soluble fraction) was resuspended in the same amount of BugBuster^{TM} reagent as the original cell pellet. Then, the suspension was centrifuged at 16,100 g for 15 min at 4°C (Eppendorf 5415R) and the supernatant was subsequently discarded completely. The thereby obtained inclusion bodies were resuspended in 1⁄2 the original culture volume of 1:10 diluted BugBuster^{TM} reagent (with ddH$_2$O) and centrifuged again at 16,100 g for 15 min at 4°C (Eppendorf 5415R). The supernatant was discarded, and the final pellet was resuspended in the same amount of BugBuster^{TM} solution as the original cell pellet.

2.4.6 Protein separation via SDS-PAGE

SDS-PAGE was carried out to determine the amount of expressed proteins in the soluble and insoluble fractions, as well as the amount of protein during the enzyme purification steps in order to evaluate the efficiency of the purification conditions. All reagents used for SDS-PAGE are listed in table 7, section 2.1.7. For all SDS-PAGE experiments either 10-well or 15-well NuPAGE^{TM} 4-12 % Bis-Tris Protein gels were run in 1x NuPAGE™ MES SDS Running Buffer for 70 min at 100 V and 250 mA. 13 µL sample were mixed with 5 µL NuPAGE^{TM} LDS Sample Buffer (4x) and 2 µL NuPAGE Sample Reducing Agent (10x), incubated for 10 min at 70°C (Eppendorf Thermomixer comfort), cooled down 5 min at RT and centrifuged for 30 s at 4°C and 16,100 g (Eppendorf 5415R). Of this mixture, 15 µL were loaded onto a gel. As the standard ladder PageRuler^{TM} Prestained Protein Ladder, 10 to 180 kDa was used, whereof 4 µL were loaded, respectively. After running, the gels were stained using Coomassie® Blue Fast Stain for 1-4 h

and subsequently de-stained using SDS destaining solution (90 % H_2O, 10 % acetic acid) and afterwards ddH_2O overnight.

2.4.7 Enzyme purification at room temperature

Initially, all purification steps were carried out at RT, including desalting. Therefore, the sterile-filtered cell-free lysates (CFLs) were transferred to 50 mL Greiner tubes, whereat the volumina were note. Then, 20-40 mL sterile filtered cell lysate were transferred into Ni-beads-filled Econo-Pac® Gravity Flow columns, and the suspensions were incubated with rocking for 40 min on ice. The flowthrough (FT) was collected in 50 mL Falcon tubes. Afterwards, the resin was washed using 4 x 6 mL equi-SPB 1. Then, the enzymes were eluted using 3-4 x 2 mL elu.-SPB 1. The obtained fractions of all steps were collected in separate tubes, unless otherwise stated. Subsequently, 2.5 mL of the respective elution fractions were loaded onto GE Healthcare PD-10 Desalting Columns. When the volume had passed the column completely, the proteins were eluted using 3.5 mL des.-SPB 1. These two steps were carried out 3 times until an elution volume of approx. 10.5 mL was obtained. Subsequently, the desalted samples were transferred to Amicon™ Ultra Centrifugation Units and concentrated by centrifuging 25 min to 1 h at 2,424 *g* and 4°C (Eppendorf 5810R) to a final volume of 0.4-1.7 mL. Eventually, the purified enzymes were aliquoted to 100 µL with glycerol (20 % final) in 1.5 mL Eppendorf tubes for storage at -20°C. Per fraction mentioned above, 100 µL samples were taken for the determination of protein concentrations via a BCA assay and for the evaluation of the expression pattern using SDS-PAGE.

2.4.8 Enzyme purification at 4°C (ÄKTA™ pure 25)

Enzyme purification was eventually carried out at 4°C in order to preserve as much active enzymes as possible. Therefor, the ÄKTA™ pure 25 chromatography system equipped with a ÄKTA™ pure sample pump and fraction collector F9-C (GE Healthcare; Chicago, USA) was used. Before every run, the volume of available CFL for loading was set manually in the method settings of the UNICORN™ 7 software. Detailed method settings for the ÄKTA™ purifications of the CDO enzymes are listed in table 14. Fractions were eventually collected in 96 well Whatman® UNIPLATE microplates (Merck Millipore; Burlington, Massachusetts). Then, per enzyme 12-14 mL of the elution fractions from the 96 well microplates were pooled in 15 mL falcons. Subsequently, 2.5 mL of the pooled elution fractions were loaded onto GE Healthcare PD-10 Desalting Columns in a 4°C room. When the volume had passed the column completely,

the proteins were eluted using 3.5 mL des.-SPB 2. These two steps were carried out 4-5 times until an elution volume of approx. 14-17.5 mL was obtained. The desalted fractions were stored at 4°C overnight. The desalted samples were transferred to Amicon™ Ultra Centrifugation Units and concentrated by centrifuging 40 min to 1.5 h at 2,424 *g* and 4°C (Eppendorf 5810R) to a final volume of 0.4-1.3 mL. Eventually, the purified enzymes were aliquoted to 100 µL with glycerol (20 % final) in 1.5 mL Eppendorf tubes for storage at -20°C. Samples (100 µL) for SDS-PAGE and protein concentrations determination (BCA-assay) were taken for the following fractions during the purification: Flowthrough, Wash, Elution (start, intermediate, end), Desalted and Purified.

Table 14 ÄKTA™ pure 25 parameters for the CDO enzyme purifications at 4°C via the software UNICORN™ 7.

ÄKTA™ pure 25 parameters – Purification at 4°C	
Instrument	ÄKTA™ pure 25 (GE Healthcare; Chicago, USA)
Column	HisTrap™ FF crude, 5 mL column (GE Healthcare; Chicago, USA)
Column volume (CV)	5 mL
Pre column pressure limit	0.50 MPa
Delta column pressure limit	0.30 MPa
Wavelengths	
Oxy. (1x and 2x His):	UV1: 280 nm, UV2: 450 nm, UV3: -
Fd	UV1: 280 nm, UV2: 450 nm, UV3: 375 nm
FdR	UV1: 280 nm, UV2: 325 nm, UV3: 460 nm
Noise reduction UV	2.5 s (average time)
Injection valve	Manual load (ÄKTA™ pure sample pump - GE Healthcare; Chicago, USA)
Column position	1, Down flow
pH valve	pH cell and Flow restrictor: In-Line
Inlet A	A1 (Buffer: Equi.-SPB 2)
Inlet B	B1 (Buffer: Elu.-SPB 2)
System flow rate	5.0 mL/min
Fractionation	
Instrument	Fraction collector F9-C (GE Healthcare; Chicago, USA)
Fraction volume	2.0 mL (96 deep well plate)
Collected phases	Sample Application (Flowthrough), Column Wash, Elution
Phase: Equilibration	
Buffer	Equi.-SPB 2
Fill system	15 mL
Equilibration volume	1 CV
Injection valve	W1
Phase: Sample Application	
Instrument	ÄKTA™ pure sample pump (GE Healthcare; Chicago, USA)
Direct sample injection	Volume set manually
Phase: Column Wash	
Buffer	Equi.-SPB 2
Column wash volume	
Oxy. (1x and 2x His):	10 CV
Fd and FdR	14 CV
Phase: Elution	

Buffer	Elu.-SPB 2
Elution step gradient length	Single step gradient
Oxy. (1x and 2x His):	5 CV
Fd and FdR	10 CV
Phase: Final equilibration	
Buffer	Equi.-SPB 2
Fill system	15 mL
Equilibration volume	0 CV

CV: column volume.

2.4.9 Photometric NAD(P)H assay to determine the specific enzyme activity (FdR)

To determine the enzymatic activity and the cofactor preference of the purified FdR, the absorption of both NADH and NADPH was measured spectrophotometrically at 340 nm on the photometer Cary Series UV-Vis Spectrophotometer (Agilent Technologies, Inc.; Santa Clara, USA) (Extinction coefficient: 6.22 mM cm^{-1}; literature value) and analyzed using the software "Kinetics". Thereby, purified enzymes and/or EV-CFL were mixed with different substrates/co-substrates. Whenever Fd was added to the mixture together with the FdR, equimolar concentrations were aimed for. Prior to every measurement, sufficient mixing was achieved via pipetting up and down. Before each set of measurements, a blank solution with a total volume of 1 mL was pipetted into a 2.5 mL cuvette. Afterwards, 0.5-1 µL of a 250 mM NAD(P)H stock solution was added either to the blank solution or to a sample to be measured, respectively, to obtain an absorption around 1, in order to be in the linear range of the Beer-Lambert law. The measuring time differed between 2 and 20 min. The volumetric activity of the FdR was calculated based on the Beer-Lambert law (equation 1). Furthermore, the specific enzymatic activity of the FdR was calculated via dividing the volumetric activity by the determined protein concentration of the purified FdR, or the total protein concentration of the cell-free lysate of the FdR expressing culture, respectively.

Equation 1:
$$\frac{U}{mL} = \frac{\Delta A}{\Delta t} * \frac{V_{total}}{V_{sample} * \varepsilon * d}$$

- U/mL … conversion of one micromole of substrate per minute and mL [µmol min^{-1} mL^{-1}]
- $\Delta A/\Delta t$ … change of absorbance per min [min^{-1}]
- ε … molar extinction coefficient [mM cm$_{-1}$]
- d … thickness of cuvette [cm]
- V_{total} … total volume [µL]
- V_{sample} … sample volume applied [µL]

2.4.10 Biotransformations *in vitro*

In order to determine the conversion of indene by the CDO *in vitro*, biotransformation (BT) reactions were carried out using purified CDO components. All BTs were performed using 20 mL glass vials to ensure sufficient oxygen supply for the reaction and a total reaction volume of 1 mL. Thereby, firstly des.-SPB 1 or des.-SPB 2 were added to the vial. Subsequently, various combinations of purified enzymes, EV-CFL, cofactors (NADH/NADPH) and eventually pure indene were added while constantly keeping the mixture on ice. Indene was added last whilst shaking the vial by hand in order to avoid substrate inhibition of the enzymes. After all compounds had been added, the lid of the vial was closed and the reaction mixture was incubated for 24 h at 25°C and 130 rpm. The reaction was then either stored at -20°C or directly prepared for upcoming analysis via gas chromatography.

2.5 Analytics

2.5.1 Sample preparation for GC-MS and GC-FID analysis

A liquid/liquid extraction was carried out with finished biotransformation reactions to transfer the expected products into the organic phase. Therefore, 500 µL of reaction mixture were transferred into a 1.5 mL Eppendorf tube containing a spatula tip of NaCl and vortexed for 5 s. During this step, H_2O is pulled from the sample, due to the hygroscopic characteristics of NaCl. Subsequently, 500 µL DCM/acetophenone [2 mM] were added to the Eppendorf tube, followed by 10 s of vortexing. The mixture was then centrifuged for 2 min at 4°C and 16,100 g (Eppendorf 5415R). During this step two clearly separated phases, the aqueous phase (top) and the organic phase (bottom) form, separated by an interphase. Since both the substrate and the products will be found in the organic phase, it was carefully transferred to a fresh 1.5 mL Eppendorf tube containing a spatula tip of $MgSO_4$, followed by 4 s of vortexing and a centrifugation step for 10 min at 4°C and 16,100 g (Eppendorf 5415R). Finally, approximately 200 µL of this reaction mixture were added to an inlet of a 1 mL GC vial and used for GC-MS or GC-FID analysis. Additionally, per measurement 200 µL DCM/acetophenone [2 mM] and 200 µL DCM were added to separate GC vial inlets, respectively, which basically served as a blank and washing solution during the GC-MS/GC-FID measurements.

2.5.2 Qualitative analysis of products formed in indene bioconversions via chiral GC-FID

Products formed during biotransformations using indene as the substrate were qualitatively analyzed on a Shimadzu Nexis GC-2030 device equipped with an AOC-20i auto injector module (Shimadzu Europa GmbH; Duisburg, Germany) and a Hydrodex-β-6TBDM capillary column (Macherey-Nagel GmbH & Co. KG; Düren, Germany) for chiral analysis. The used parameters, as well as the applied method are listed in table 15.

Table 15 GC-FID parameters used for quantitative and qualitative analysis of organic compounds present after biotransformations.

Chiral GC-FID parameters – indene and 1-indenol detection	
Instrument	Nexis GC-2030 (Shimadzu Europa GmbH; Duisburg, Germany)
Column	Hydrodex-β-6TBDM (Macherey-Nagel; Düren, Germany)
Length	25 m, inner diameter: 0.25 mm, film thickness: 0.25 μM
Injection volume	1 μL
Injection temp.	230°C
Injection mode	Split
Flow control mode	velocity
Pressure	70.1 kPa
Total flow	85.8 mL / min
Column flow	0.82 mL / min
Linear velocity	25.4 cm / s
Purge flow	3 mL / min
Split ratio	100
Oven temp. program	5 min at 100°C, 15°C min^{-1} to 180°C, 5 min at 200°C, hold 5 min, 15°C min^{-1} to 230°C, hold 5 min
FID temperature	250°C
Compound retention times [min]	Indene 8 Acetophenone 9 1-indenol 12.8

2.5.3 Qualitative analysis of compounds from indene bioconversions via GC-MS

Qualitative detection of organic products formed during *in vitro* biotransformations of the substrate indene was achieved via GC-MS analysis. Presumably identified 1-indenol peaks from GC-FID analysis were therein validated via GC-MS analysis.

A Shimadzu GCMS type QP2010 device equipped with an inert capillary column type ZB-5MSi (Phenomenex®, Torrance, USA) was used with helium as carrier gas. Detailed parameters are listed in table 16.

Table 16 GC-MS parameters used for qualitative analysis of organic compounds present and validation of obtained 1-indenol after biotransformations.

GC-MS parameters – 1-indenol detection	
Instrument	GCMS-QP2010 SE (Shimadzu Europa GmbH; Duisburg, Germany)
Column	Zebron ZB-5MSi (Phenomenex ®; Torrance, USA)
Length	30 m, inner diameter: 0.25 mm, film thickness: 0.25 µM
Injection volume	1 µL
Injection temp.	250°C
Injection mode	Split
Flow control mode	linear velocity
Pressure	70.6 kPa
Total flow	14.8 mL / min
Column flow	1.17 mL / min
Linear velocity	39.5 cm / s
Purge flow	3 mL / min
Split ratio	9.1
Oven temp. program	4 min at 60°C, 10°C min^{-1} to 340°C, 4 min at 340°C
Compound retention times [min]	Indene 8.45
	Acetophenone 8.85
	1-indanone 12.5
	1-indenol 11.4
MS parameters	
Ion source temp.	250°C
Interface temp.	320°C
Mode:	Scan
Scan range	50 – 500 m / z

2.5.4 Quantification of 1-indanone and 1-indenol from indene bioconversions via GC-FID

Previous studies have revealed the CDO's capability of catalyzing the stereoselective monohydroxylation of indene to 1-indenol. The latter can further be react to 1-indanone, presumably due to a non-enzymatic isomerization reaction.[53,54] Therefore, these expected products from *in vitro* bioconversions catalyzed by the CDO were quantified via chiral and achiral GC-FID analysis. Since 1-indenol is not commercially available, a calibration curve was created solely with 1-indanone, which was then used to quantify 1-indenol via the corresponding response factor.

For the calibration curves of 1-indanone, seven dilutions within the range of 0.2-4 mM were created using des.-SPB 2. Subsequently, extraction was carried out as for every finished biotransformation sample (as described in section 2.5.1) in order to maintain equal extraction conditions and thus obtain comparable product concentrations.

The calibration curves for 1-indanone of both chiral and achiral GC-FID analysis are shown in figure 6, where the obtained integrated peak areas (IPA) are plotted on the y-axis against the

39

respective concentrations on the x-axes. The linear equations and the corresponding R^2 values are listed in table 17.

Table 17 Linear equations and R^2 values of the 1-indanone calibration curves measured on the achiral Zebron ZB-5 (Phenomenex Inc.; Torrance, USA) (y=283515x; R^2 = 1.0) and chiral Hydrodex-β-6TBDM column (Macherey-Nagel™, Düren, Germany) column (y=25051x; R^2 = 1.0). Both curves were established on a Nexis GC-2030 (Shimadzu Europa GmbH; Duisburg, Germany).

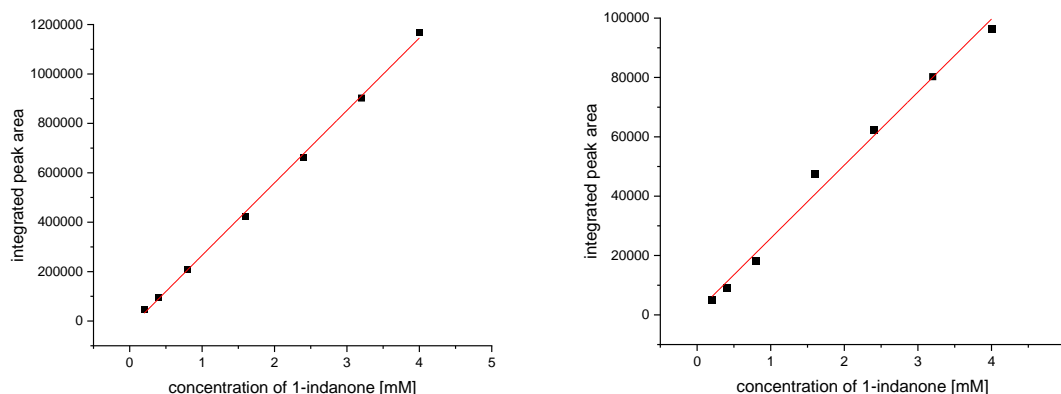| Compound	Linear equation	R^2	Column
1-indanone	y=283515x	1.0	Zebron ZB-5 (Phenomenex Inc.; Torrance, USA)
1-indanone	y=25051x	1.0	Hydrodex-β-6TBDM (Macherey-Nagel™, Düren, Germany)

Figure 6 1-indanone calibration curves measured on the achiral Zebron ZB-5 column (left) (Phenomenex Inc.; Torrance, USA) (y=283515x; R^2 = 1.0) and chiral Hydrodex-β-6TBDM column (right) (Macherey-Nagel™, Düren, Germany) (y=25051x; R^2 = 1.0). Both curves were established on a Nexis GC-2030 (Shimadzu Europa GmbH; Duisburg, Germany).

The product 1-indenol was quantified via a mathematical approach using the 1-indanone calibration curves obtained (**y=283515x** and **y=25051x**, figure 6). Thus, 1-indenol concentrations were determined using the corresponding response factors (RF) as well as the effective carbon numbers (ECN). To obtain the RF for 1-indenol, the ratio between the ECN of 1-indenol and 1-indanone was determined, as depicted in equation 2:

$$RF = \frac{RF_{(1\text{-indenol})}}{RF_{(1\text{-indanone})}}$$

A calibration curve for 1-indenol could be created considering the relative response factor (RRF) as well as the integrated peak areas (IPA). The RRF corresponds to the ratio of the response factor (RF) of the compound of interest (1-indenol) to the RF of the know substance (1-indanone), as shown in equation 3:

$$RF_{(1\text{-indenol})} = \frac{ECN_{(1\text{-indenol})}}{ECN_{(1\text{-indanone})}}$$

The ECN values obtained from literature and the thereof determined RF for both compounds are listed in table 18.

Table 18 Summarized values for ECN (effective carbon number) obtained from literature and determined RF (response factor) for 1-indanone and 1-indenol.

Compound	ECN	RF
1-indanone	9	1
1-indenol	8.35	0.93

Once the RF of 1-indenol was determined, the respective 1-indenol concentrations could be calculated according to equation 4:

$$c_{(1\text{-indenol, mM})} = \frac{IPA_{(1\text{-indenol})}}{IPA_{(1\text{-indanone})} * RRF} * c_{(1\text{indanone, mM})}$$

A Nexis GC-2030 device (Shimadzu Europa GmbH; Duisburg, Germany) equipped with a Zebron ZB-5 column (Phenomenex Inc.; Torrance, USA) was used with helium as carrier gas. Detailed parameters are listed in table 19.

Table 19 GC-FID parameters used for quantitative and qualitative analysis of organic compounds present after biotransformations.

Achiral GC-FID parameters – indene, 1-indanone and 1-indenol detection	
Instrument	Nexis GC-2030 (Shimadzu Europa GmbH; Duisburg, Germany)
Column	Zebron ZB-5 (Phenomenex Inc.; Torrance, USA)
Length	30 m, inner diameter: 0.32 mm, film thickness: 0.25 µM
Injection volume	1 µL
Injection temp.	240°C
Injection mode	Split
Flow control mode	Linear velocity
Pressure	37.2 kPa
Total flow	14.5 mL / min
Column flow	1.05 mL / min
Linear velocity	20.4 cm / s
Purge flow	3 mL / min
Split ratio	10
Oven temp. program	4 min at 60°C, 10°C min^{-1} to 320°C, 4 min at 320°C
FID temperature	320°C
Compound retention times [min]	Indene 10.3
	Acetophenone 10.75
	1-indenol 13.25
	1-indanone 14.35

3 Results

3.1 Gibson® assembly of Oxy co-expression constructs

The use of construct 1 and 2, which harbor the single α- or β-subunit genes of CumA1 or CumA2 only led to hardly detectable amounts of 1-indenol from indene conversion. Therefore, Oxy co-expression constructs 9 and 8 (namely pOxy(2xHis)* and pOxy(1xHis)*, see table 10 in section 2.3.1) were created via Gibson assembly®,[52] in order to govern successful formation of the $\alpha_3\beta_3$-hetero-hexamer *in vivo*. Therefore, the two inserts containing the *cumA2* gene with N-terminal His tag and without His tag, respectively, were amplified via PCR using construct 2 as template whereas the linearized vector of construct 1 containing the *cumA1* gene with N-terminal His tag, served as the backbone. The created Oxy co-expression constructs are shown in figure 7. A 16 bp long WT sequence on the *cumA1* gene harbored in constructs 8 and 9 was detected at a later stage during this work, wherefore the cloning was repeated to obtain completely c.o. Oxy co-expression constructs 7 and 6, namely pOxy(2xHis) and pOxy(1xHis).
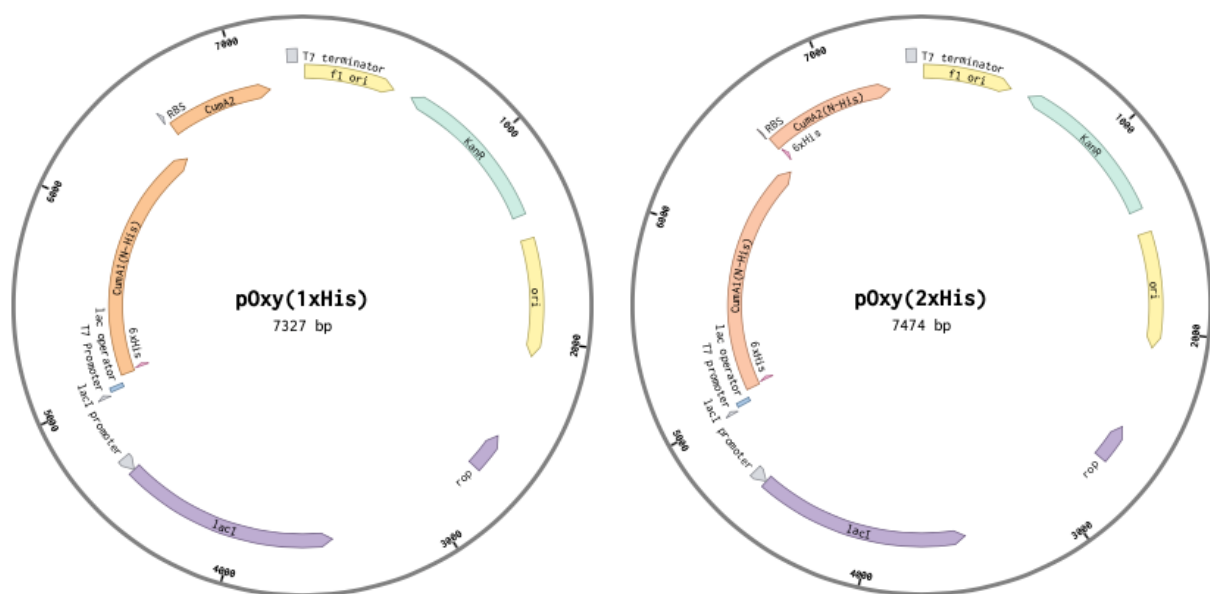

Figure 7 Oxy co-expression constructs pOxy(1xHis) (7327 bp, left) and pOxy(2xHis) (7474 bp, right) created by Gibson® assembly. Both constructs contain the for *E.coli* c.o. CDO genes *cumA1* and *cumA2*. *cumA1* is N-terminally His-tagged in both constructs, whereas *cumA2* carries a N-terminal His tag only on pOxy(2xHis). Both genes, *cumA1* and *cumA2* contain a RBS, which governs co-expression using only a single T7 promoter. The illustration was created using the software Benchling (San Francisco, USA).

3.2 Assembly confirmation: colony PCR

In order to evaluate successful Gibson assembly® results of the CDO Oxy co-expression constructs pOxy(2xHis) and pOxy(1xHis), the respective fragments contained on the plasmids of picked colonies were amplified via colony PCR. Therefore, after transformation with the ligated DNA constructs and incubating over night at 37°C, 40 colonies were picked for the insert amplification via colony PCR. The successfully amplified inserts of the N-His tagged *cumA2* gene (2432 bp) within pOxy(2xHis) and *cumA2* without N-His tag (2285 bp) within pOxy(1xHis) were observed at the expected heights, as shown in figure 8.
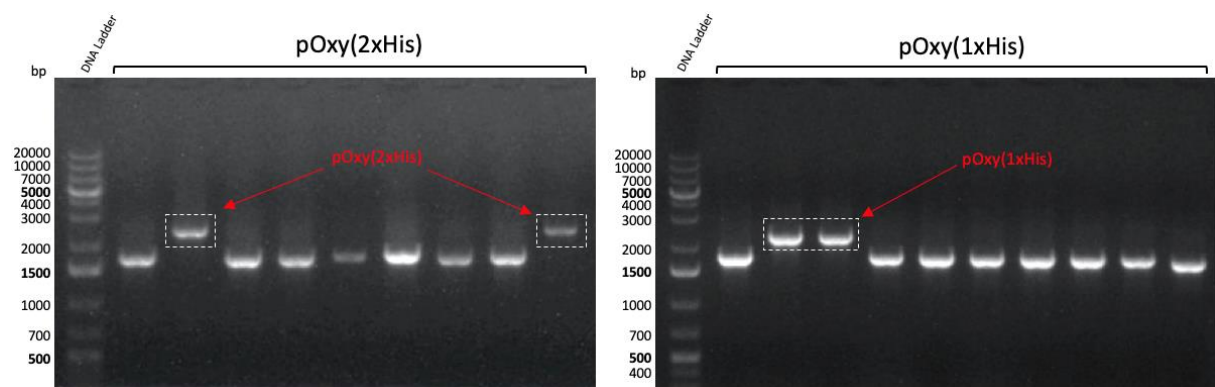
Figure 8 Agarose gel showing successful colony PCR amplifications of the plasmids pOxy(2xHis) (2432bp, left) and pOxy(1xHis) (2285bp, right), of which the respective clones were used for plasmid isolation and eventually verification was achieved via Sanger sequencing. DNA ladder: GeneRuler 1 kb Plus DNA Ladder (Thermo Scientific™; Massachusetts, USA).

3.3 QuikChange™ repair of pFdR(N-His)^x

Due to a base deletion at position 277 bp (277_278del) within the FdR gene (see sequencing result of figure 32 in the appendix, section 6.3) on the vector pFdR(N-His)^x (construct 4 as shown in table 10, section 2.3.1), which led to a non-sense mutation (L94X) on the translational level, a QuikChange™ site-directed mutagenesis was carried out. Therefore, a primer pair was designed that included one of the single missing nucleotides C or G, respectively (figure 33 in the appendix, section 6.3). Subsequently, electrocompetent *E. coli* TOP10 F' were transformed with the *Dpn*I-treated plasmid DNA in order to seal contained nicks and further to amplify the plasmids. Contained plasmids were sent for Sanger sequencing to confirm correct site-directed mutagenesis.

3.4 Initial expression studies with single CDO components

Initial heterologous protein expression was carried out with constructs harboring the single CDO components on construct 1-4 (table 10, section 2.3.1) expressed in *E. coli* BL21(DE3). The expression at 30°C using 2 mM IPTG (figure 9-12, left) was compared with expression at 20°C together with 0.05 mM IPTG (figure 9-12, right). The expected molecular weights of the single CDO components are listed in table 20.

Table 20 Molecular weights of the CDO genes *CumA1-4* and belonging His-tags (if contained)

Gene	Component	Molecular weight [kDa]	Tag
cumA1	Oxy α-subunit	55.84	6xHis
cumA2	Oxy β-subunit	26.99	6xHis
cumA2	Oxy β-subunit	21.62	-
cumA3	ferredoxin	15.34	6xHis
cumA4	ferredoxin reductase	47.95	6xHis

The CumA1 was clearly detected in the soluble and insoluble fractions (Figure 9, left: 30°C and 2 mM IPTG, right: 20°C and 0.05 mM IPTG). The bands at 55.84 kDa are visible under both expression conditions from t_{+1} on. However, by reducing both the expression temperature and IPTG concentration to 20°C and 0.05 mM, respectively, a successful shift from insolubly towards solubly expressed protein was achieved at t_{+1} and t_{+19}. The band of the CumA2 was also clearly visible at 26.99 kDa (Figure 10, left: 30°C and 2 mM IPTG, right: 20°C and 0.05 mM IPTG). The shift to the milder expression conditions showed similar effects as for the expression of the CumA1. However, the amount of expressed CumA2 in the soluble fraction could be increased to a greater extent at 20°C and 0.05 mM IPTG, especially at t_{+19}.
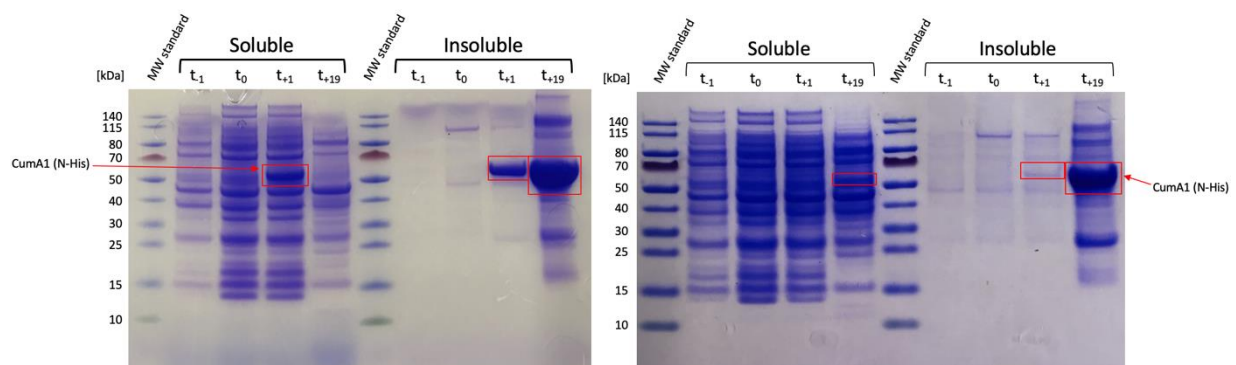

Figure 9 SDS-PAGE of CumA1 expression studies using *E. coli* BL21(DE3) at 30°C with 2 mM IPTG (left), and 20°C with 0.05 mM IPTG (right). t_{-1}, t_0, t_{+1} and t_{+19}: 1 hour before, at, 1 and 19 hours after induction. Protein standard: PageRuler™ Prestained Protein Ladder (10 to 180 kDa)
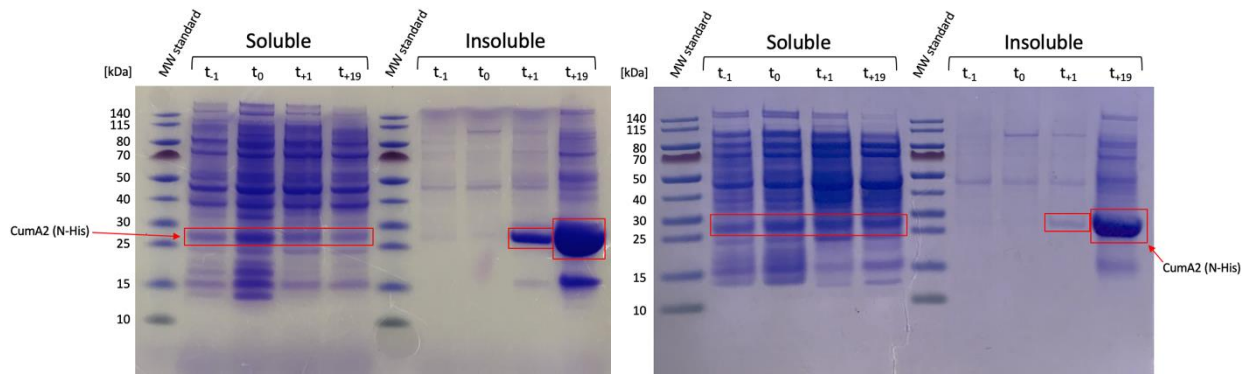
Figure 10 SDS-PAGE of CumA2 expression studies using *E. coli* BL21(DE3) at 30°C with 2 mM IPTG (left), and 20°C with 0.05 mM IPTG (right). t_{-1}, t_0, t_{+1} and t_{+19}: 1 hour before, at, 1 and 19 hours after induction. Protein standard: PageRuler™ Prestained Protein Ladder (10 to 180 kDa)

Fd (15.34 kDa) was distinctively observable under both expression conditions as well in the insoluble and soluble fraction. When using the initial expression temperature of 30°C together with 2 mM IPTG (Figure 11, left), at t_{+1} and t_{+19} Fd accounts for the two most strongly expressed enzymes within the insoluble fraction, while also being present in the corresponding fractions within the soluble fractions. By changing the expression conditions to 20°C and 0.05 mM IPTG (Figure 11, right), the majority of Fd was expressed in the soluble fraction. For the FdR no bands were detectable at the expected size of 47.95 kDa during these initial expression studies (figure 12). However, it was later revealed that the FdR gene within construct 4 contained a deletion (277_278del), leading to a non-sense mutation, which was repaired afterwards.
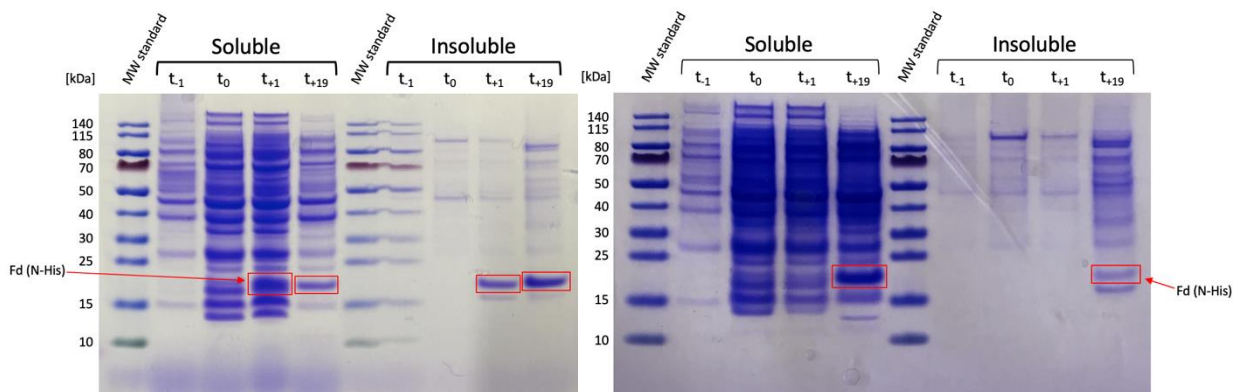

Figure 11 SDS-PAGE of Fd expression studies using *E. coli* BL21(DE3) at 30°C with 2 mM IPTG (left), and 20°C with 0.05 mM IPTG (right). t_{-1}, t_0, t_{+1} and t_{+19}: 1 hour before, at, 1 and 19 hours after induction. MW standard: PageRuler™ Prestained Protein Ladder (10 to 180 kDa)
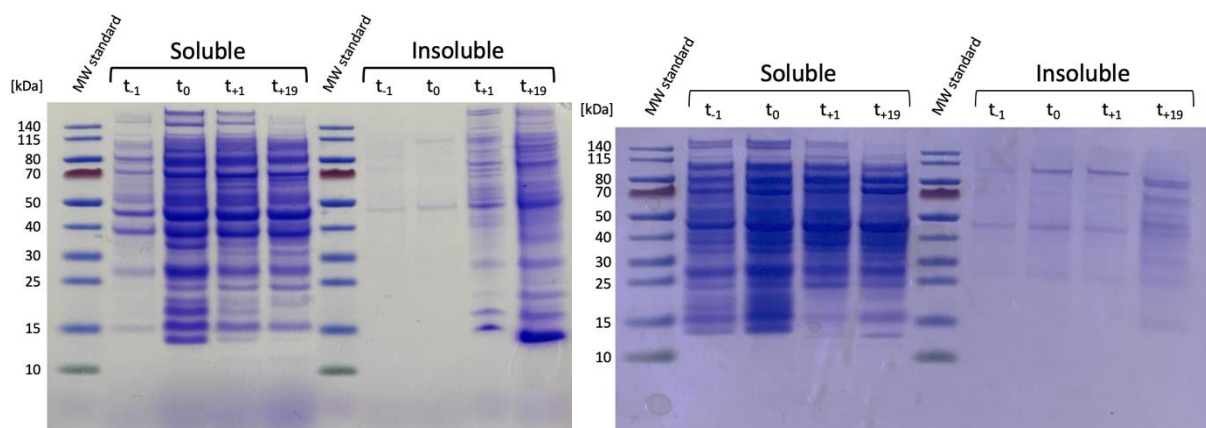
Figure 12 SDS-PAGE of FdR^x expression studies using *E. coli* BL21(DE3) at 30°C with 2 mM IPTG (left), and 20°C with 0.05 mM IPTG (right). No bands are visible at the expected MW of FdR (47.95 kDa) due to a base deletion, which was detected and repaired at a later time during this work. t_{-1}, t_0, t_{+1} and t_{+19}: 1 hour before, at, 1 and 19 hours after induction. MW standard: PageRuler™ Prestained Protein Ladder (10 to 180 kDa)

3.5 Oxy co-expression: *E. coli* BL21(DE3) vs. JM109(DE3)

E. coli BL21(DE3) was initially used for protein expression of the single CDO components. However, previous studies suggested the use of *E. coli* JM109 and JM109(DE3), respectively. In 2015, Gally and colleagues used *E. coli* JM109 cells expressing the CDO, and *E. coli* JM109(DE3) cells harboring the NDO to perform asymmetric dihydroxylations of olefins *in vivo*.[23] Therefore, the expression patterns of the constructs pOxy(2xHis) (figure 13) and pOxy(1xHis) (figure 14) (constructs 7 and 6, see table 10, section 2.3.1) were investigated for *E. coli* BL21(DE3) (figure 13 and 14, left) and *E. coli* JM109(DE3) (figure 13 and 14, right). For construct 7, both strains showed very similar expression of the CumA1 and CumA2, mainly being present in the insoluble fraction. The bands of the His tagged CumA2 (26.99 kDa) can be detected at all time points of the insoluble fractions. A band corresponding to the His-tagged CumA1 (55.84 kDa) only appears from t_{+2} of insoluble fractions on. Construct 6 on the other hand, where only the CumA1 carries a His tag, the CumA2 (21.62 kDa) is clearly stronger expressed in the soluble fractions for both strains. Eventually, *E. coli* JM109(DE3) was used for protein expression and purification, due to the slightly better expression of the His-tagged CumA1 in the soluble fraction at t_{+2} with both constructs.
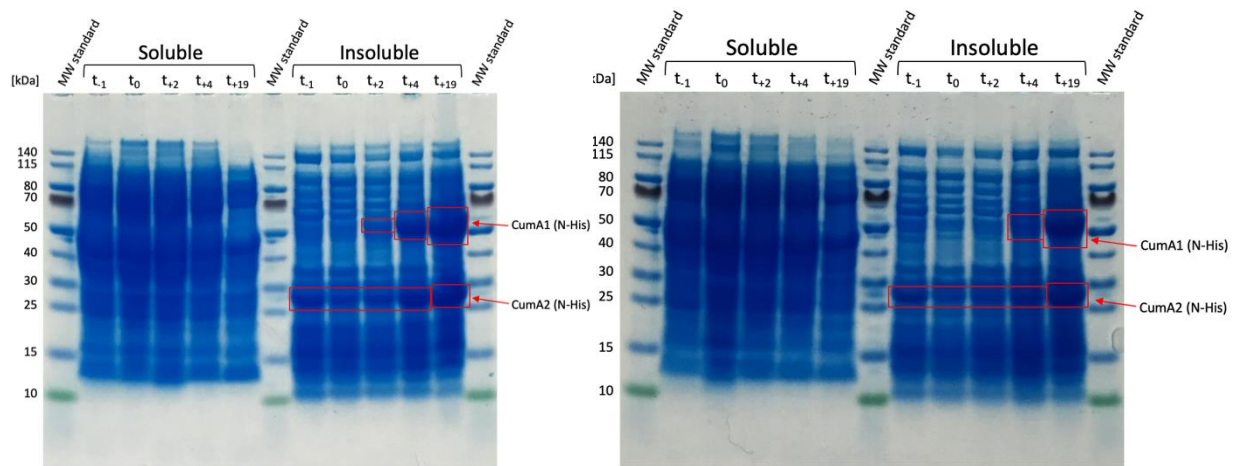
Figure 13 SDS-PAGE of Oxy co-expression construct pOxy(2xHis) at 20°C during comparison between expression hosts *E. coli* BL21(DE3) (left) and *E. coli* JM109(DE3) (right). t_{-1}, t_0, t_{+2}, t_{+4} and t_{+19}: 1 hour before, at, 2, 4 and 19 hours after induction. MW standard: PageRuler™ Prestained Protein Ladder (10 to 180 kDa).
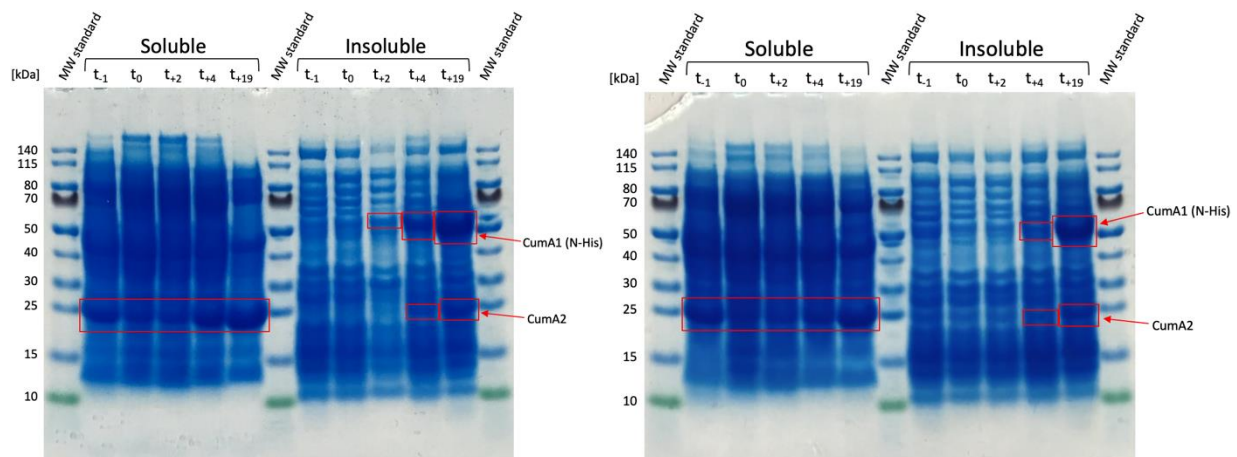

Figure 14 SDS-PAGE of Oxy co-expression construct pOxy(1xHis) at 20°C during comparison between expression hosts *E. coli* BL21(DE3) (left) and *E. coli* JM109(DE3) (right). t_{-1}, t_0, t_{+2}, t_{+4} and t_{+19}: 1 hour before, at, 2, 4 and 19 hours after induction. MW standard: PageRuler™ Prestained Protein Ladder (10 to 180 kDa).

3.6 Expression studies: Oxy, Fd and FdR in *E. coli* JM109(DE3)

The expression pattern of the final expression strain *E. coli* JM109(DE3) harboring either one of the Oxy co-expression constructs (constructs 6 and 7), Fd or the repaired FdR (Construct 3 and 5) was investigated (see table 10, section 2.3.1). Cell lysis was carried out using BugBuster®. For comparison purposes, also the expression pattern of the empty pET28a(+) vector was examined. The expected molecular weights of the single CDO subunits are listed in table 20, section 3.4.

Both Oxy co-expression constructs (constructs 7 and 6) showed leaky expression two hours before and at induction, which is a common observation for pET-derived vectors.[55] In the expression of pOxy(2xHis) (construct 7), the CumA1 is visibly expressed in all insoluble

47

fractions from two hours before (t$_{-2}$), up to 19 hours after (t$_{+19}$) induction, whereas the CumA2 is also expressed in the soluble fraction, clearly at least at t$_{-2}$ (as shown in figure 15, left). However, at t$_{+2}$ clear bands of the Oxy subunits can be detected only in the insoluble but not in the soluble fraction. The pOxy(1xHis) (construct 6) shows better solubility, where the band of the CumA1 is visible in the soluble fractions at all time points, whereas the band of the CumA2 is visible in the soluble fractions from t$_0$ to t$_{+19}$ (figure 15, right). The fact that construct 7 harbors two His-tags seems to promote inclusion body formation, which is reflected by the higher amount expressed in the insoluble fraction, especially at t$_{+19}$. Purification tags, like the His-tag, in combination with a strongly inducible pET28a system have shown to negatively affect the soluble folding of heterologous proteins in *E. coli*.[56] In comparison, when looking at the expression pattern of construct 6, which only contains one His tag in the N-terminal *cumA1* gene, at t$_{+19}$ there is clear bands visible for both Oxy subunits in the soluble fraction. Hence, this construct was favored as it seemed more suitable for purification and biotransformations.
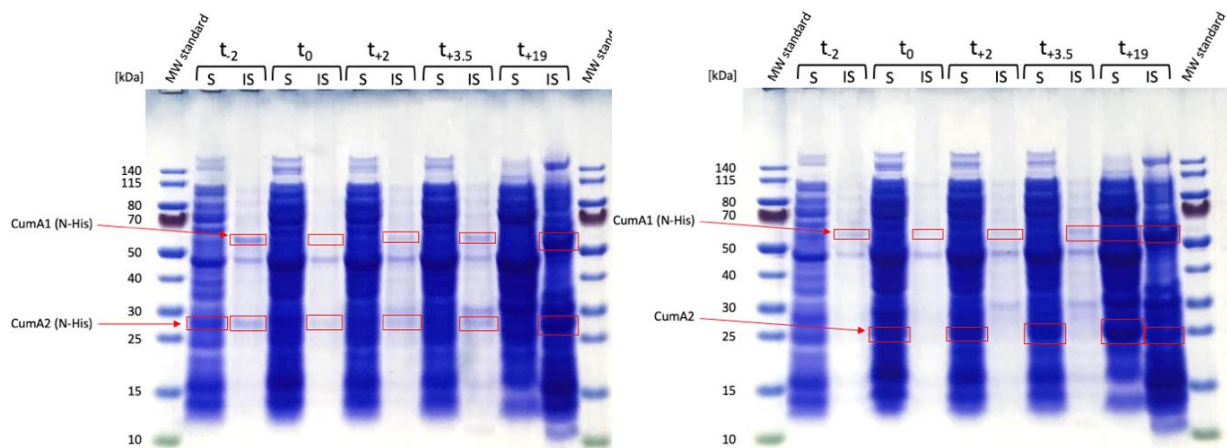

Figure 15 SDS-PAGE of Oxy co-expression constructs pOxy(2xHis) (left) and pOxy(1xHis) (right) expressed at 20°C using *E. coli* JM109(DE3). *t$_{-2}$, t$_0$, t$_{+2}$, t$_{+3.5}$* and *t$_{+19}$*: 2 hours before, at, 2, 3.5 and 19 hours after induction. MW standard: PageRuler™ Prestained Protein Ladder (10 to 180 kDa).

Fd (15.34 kDa) (construct 3) could already be detected in both the soluble and insoluble fraction at t$_{-2}$ (figure 16, left), indicating leaky transcription of the pET28a vector. Furthermore, at t$_0$ no band of Fd is present, which may be due to insufficient cell lysis. At t$_{+3.5}$ and t$_{+19}$ the band of Fd was detected, whereat the bulk enzyme seems to be expressed in the soluble fraction. FdR (47.95 kDa) (construct 5) is very strongly expressed in all fractions from t$_{-2}$ to t$_{+19}$ (figure 16, right). At t$_{+19}$ it seems at least half of the expressed FdR is present in the soluble

fraction. However, it would be worth to consider changing to a gentler expression system, e.g. pBAD derived vectors, in order to yield more soluble and active enzyme.
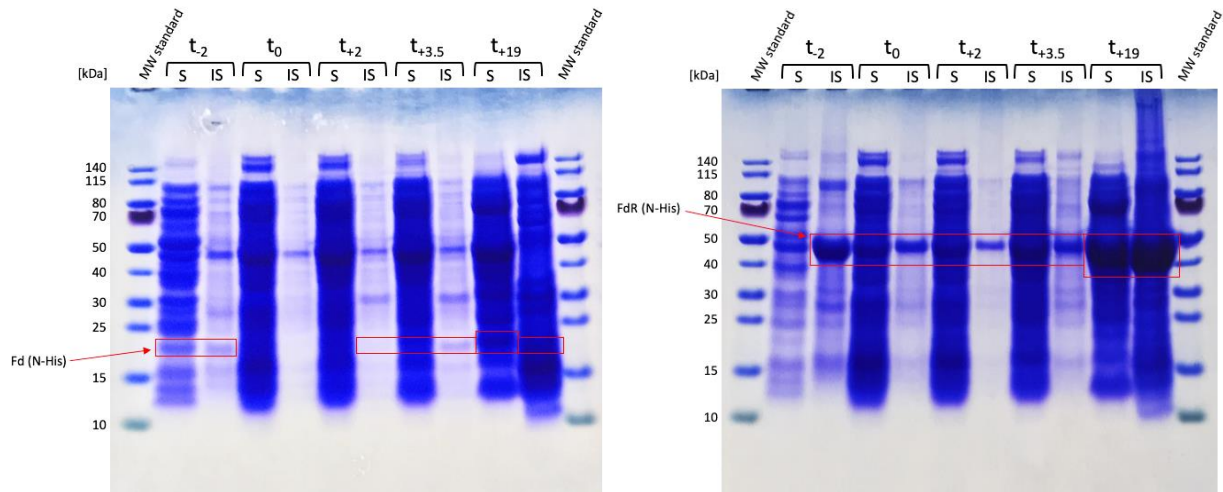

Figure 16 SDS-PAGE of Fd (construct 3) (left) and FdR (construct 5) (right) expressed at 20°C using *E. coli* JM109(DE3). *t*₋₂, *t₀*, *t₊₂*, *t₊₃.₅* and *t₊₁₉*: 2 hours before, at, 2, 3.5 and 19 hours after induction. MW standard: PageRuler™ Prestained Protein Ladder (10 to 180 kDa).

Expression studies were carried out for pET28a(+) empty vector lysate (figure 17) to be able to distinguish the CDO components from background protein of E. coli JM109(DE3).
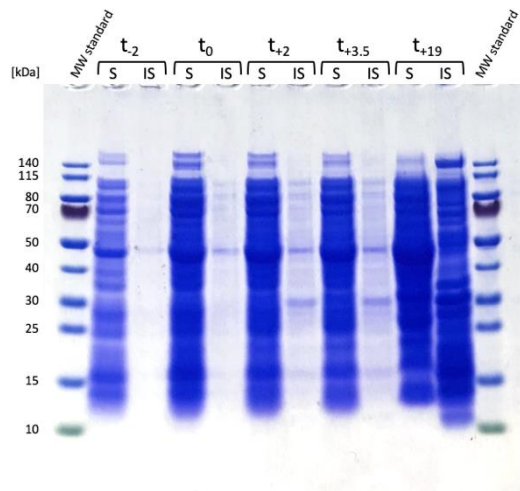

Figure 17 SDS-PAGE of pET28a empty vector cell-free lysate expressed at 20°C using *E. coli* JM109(DE3). *t*₋₂, *t₀*, *t₊₂*, *t₊₃.₅* and *t₊₁₉*: 2 hours before, at, 2, 3.5 and 19 hours after induction. MW standard: PageRuler™ Prestained Protein Ladder (10 to 180 kDa).

49

3.7 Initial purification studies at room temperature

Initial purification studies were carried out using Econo-Pac® Gravity Flow columns at room temperature (RT) with the constructs 1-4, harboring one of the four single CDO subunits, as well as Oxy co-expression constructs 9 and 8, namely pOxy(2xHis)* and pOxy(1xHis)*. Therefore, relevant fractions during the purifications were collected for CumA1, CumA2 (figure 18, left and right), Fd and FdR^x (figure 19, left and right) as well as Oxy(2xHis) and Oxy(1xHis) (figure 20, left and right). However, the final purified fractions of all CDO enzymes purified in this way still contained residual background proteins, wherefore following purifications were carried out using the ÄKTA^{TM} pure 25. The band of the CumA1 (figure 18, left) can be seen at 55.84 kDa in all fractions, except the third elution fraction, where the loading was not successful. The CumA2 (figure 18, right) was detected from the elution fractions on. However, in the unclean purified fraction the bulk expressed enzyme is not the CumA2. This is also the case for the purified Fd (15.34 kDa), where there is a band of background protein present at approximately 70 kDa (figure 19, left). No band of FdR (47.95 kDa; Figure 19, right) is present due to a deletion at position 277 bp (277_278del) within the gene of FdR^x on the vector pFdR(N-His)^x. The SDS-PAGE of both Oxy co-expression constructs (figure 20) revealed similar results, where the bands of CumA1 and CumA2 comprise the majority of the enzymes present from the first elution up to the purified fraction. The band of the CumA2 without His-tag (figure 20, right) can be seen at 21.62 kDa. Generally, all purifications carried out in this way did not yield sufficiently clean purified fractions.
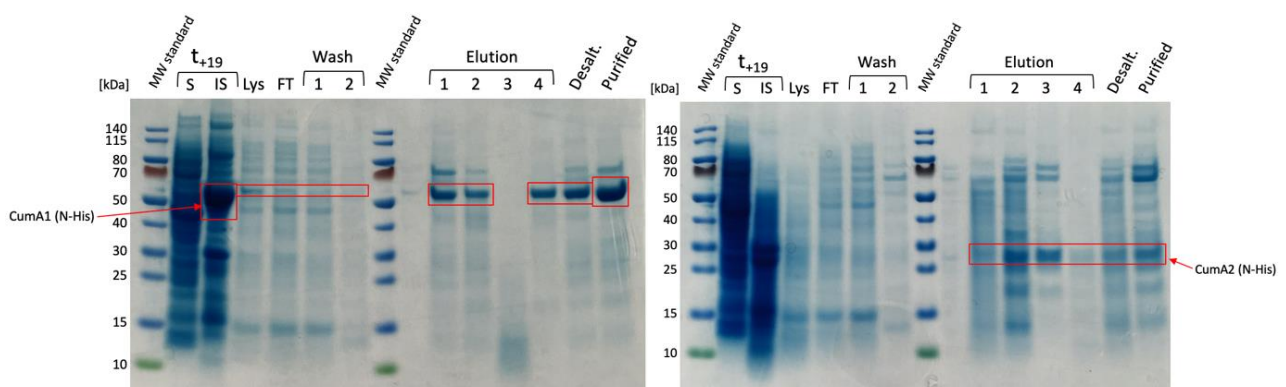

Figure 18 SDS-PAGE of initial purification studies at RT of CumA1 (construct 1) (left) and CumA2 (construct 2) (right) expressed at 20°C using *E. coli* BL21(DE3). *S* and *IS*: soluble and insoluble fraction; *Lys*: sterile-filtered cell-free lysate; *FT*: flowthrough; *Desalt.*: desalted pooled elution fractions; t_{+19}: 19 hours after induction. MW standard: PageRuler™ Prestained Protein Ladder (10 to 180 kDa).

Figure 19 SDS-PAGE of initial purification studies at RT of Fd (construct 3) (left) and FdR^x (construct 4) (right) expressed at 20°C using *E. coli* BL21(DE3). Right: no bands are visible at the expected size of FdR (47.95 kDa) due to a base deletion, which was detected and repaired at a later time during this work. *S* and *IS*: soluble and insoluble fraction; *Lys*: sterile-filtered cell-free lysate; *FT*: flowthrough; *Desalt.*: desalted pooled elution fractions; t_{+19}: 19 hours after induction. MW standard: PageRuler™ Prestained Protein Ladder (10 to 180 kDa).
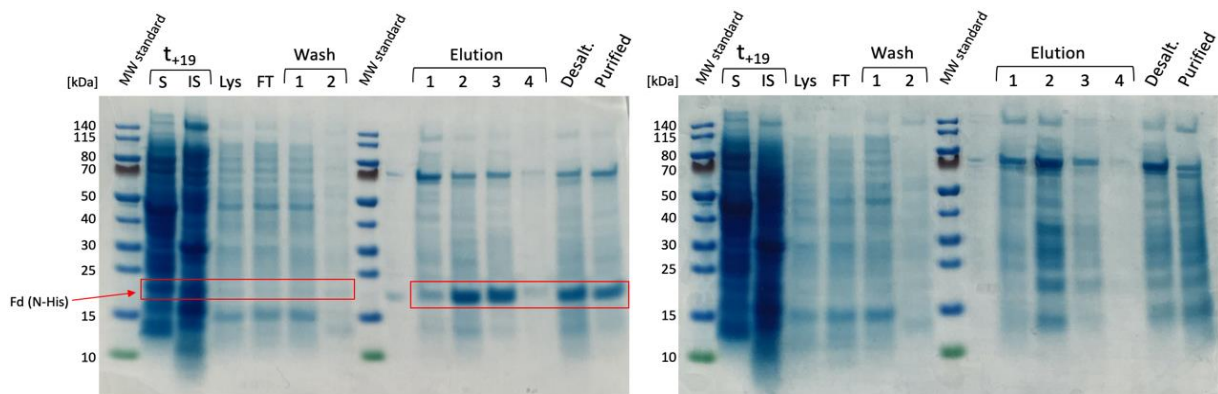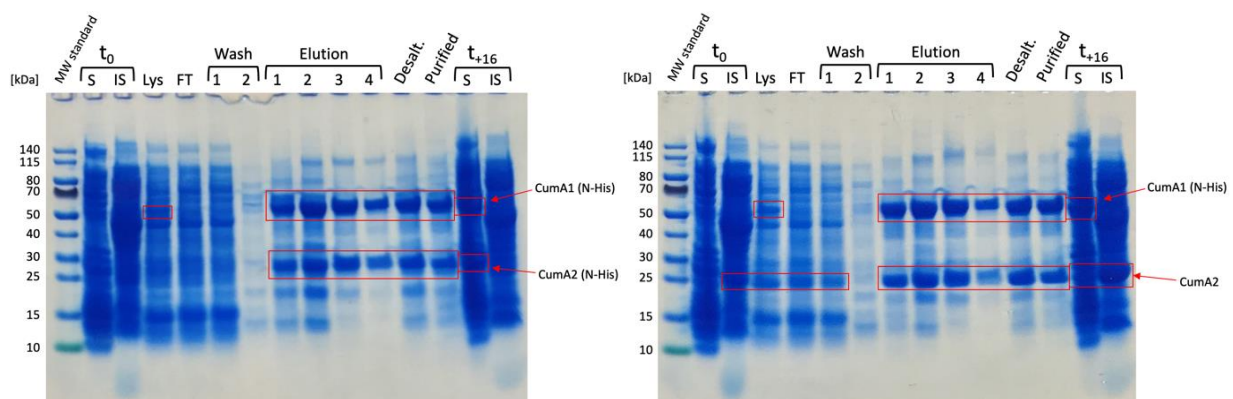

Figure 20 SDS-PAGE of initial purification studies at RT of Oxy co-expression constructs pOxy(2xHis)* (left) and pOxy(1xHis)* (right) expressed at 20°C using *E. coli* JM109(DE3). *S* and *IS*: soluble and insoluble fraction; *Lys*: sterile-filtered cell-free lysate; *FT*: flowthrough; *Desalt.*: desalted pooled elution fractions; t_0 and t_{+16}: at and 16 hours after induction; MW standard: PageRuler™ Prestained Protein Ladder (10 to 180 kDa).

3.8 Purification studies at 4°C (ÄKTA^{TM} pure)

Final purification studies were carried out completely at 4°C with the CDO Oxy co-expression constructs Oxy(2xHis) and Oxy(1xHis) (constructs 7 and 6), Fd and FdR (constructs 3 and 5) using the ÄKTA^{TM} pure 25, followed by desalting to preserve enzymatic activity. For Oxy construct 7 (figure 21, left), there are bands corresponding to the CumA1 and the CumA2 visible at 55.84 kDa and 26.99 kDa, respectively, within all fractions of the purifications, as well as in the insoluble fraction at t_0 and t_{+19}. The expression of the CumA1 is thereby significantly stronger. Construct 6 (figure 21, right) on the other hand clearly also shows bands of the CumA1 at 55.84 kDa and of the CumA2 without His tag at 21.62 kDa. However, compared to construct 7 the expression of both Oxy subunits seems to be stronger and furthermore, bands of both subunits are also visible in the soluble fraction at t_{+19}, wherein the amount of

51

expressed CumA2 is higher than of the CumA1, indicating construct 6, namely Oxy(1xHis), to be the more favorable construct in terms of folding properties and thus activity for biotransformations. However, the purified fractions of both constructs were not completely clean and showed some residual protein, but significantly improved in comparison with the respective fractions of the single CDO components during initial purifications at RT (section 3.7).
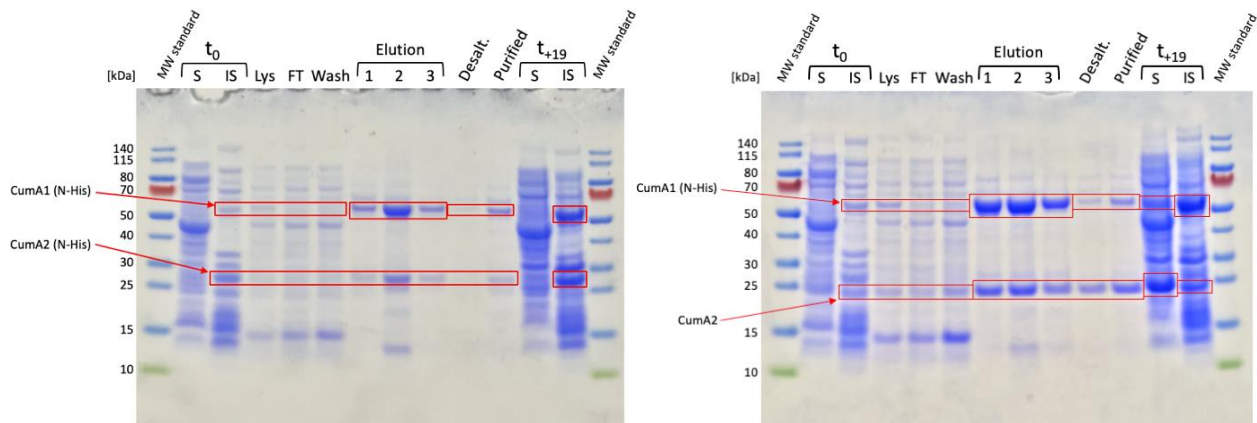

Figure 21 SDS-PAGE of final purification studies at 4°C using ÄKTA™ pure of Oxy co-expression constructs pOxy(2xHis) (left) and pOxy(1xHis) (right) expressed at 20°C using *E. coli* JM109(DE3). *S* and *IS*: soluble and insoluble fraction; *Lys*: sterile-filtered cell-free lysate; *FT*: flowthrough; *Desalt.*: desalted pooled elution fractions; t_0 and t_{+19}: at and 19 hours after induction. MW standard: PageRuler™ Prestained Protein Ladder (10 to 180 kDa).

For the purification of the Fd (15.34 kDa) using construct 3 (figure 22, left), the band of the Fd is present during all fractions except the wash fraction. However, the purified fraction still contains considerable amounts of background protein. At t_{+19}, most of Fd is expressed insolubly. FdR (47.95 kDa) seemed to be the most well expressed CDO enzyme, as it shows the strongest band present in all fractions during the purification (figure 22, right), whereat the purified fraction looks almost as clean as the respective fraction of the Oxy constructs (figure 21). At t_{+19}, the strongly expressed FdR seems to be equally distributed between the soluble and insoluble fractions.
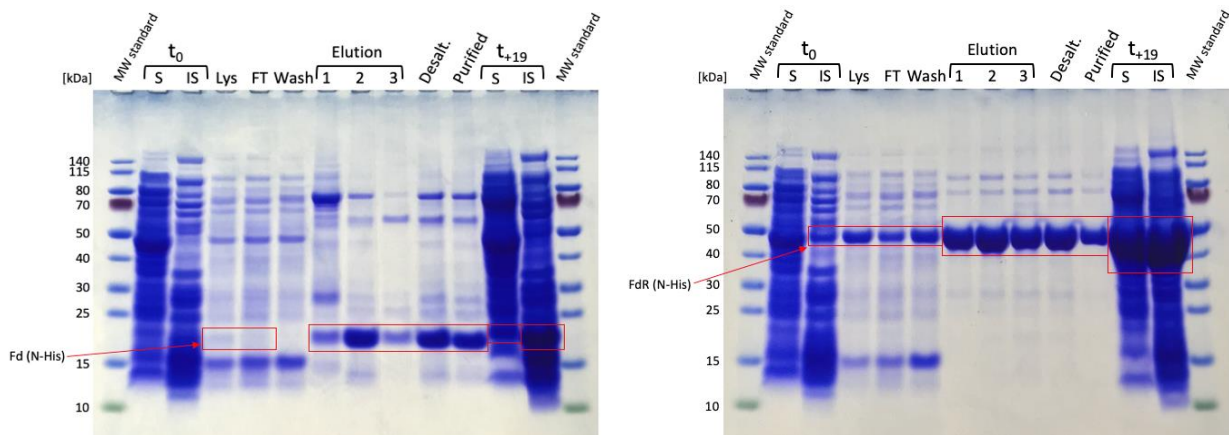
Figure 22 SDS-PAGE of final purification studies at 4°C using ÄKTA™ pure of Fd (construct 3) (left) and FdR (construct 5) (right) expressed at 20°C using *E. coli* JM109(DE3). *S* and *IS*: soluble and insoluble fraction; *Lys*: sterile-filtered cell-free lysate; *FT*: flowthrough; *Desalt.*: desalted pooled elution fractions; t_0 and t_{+19}: at and 19 hours after induction. MW standard: PageRuler™ Prestained Protein Ladder (10 to 180 kDa).

3.9 Native-PAGE: Validation of the Oxy $\alpha_3\beta_3$-hexamer formation

The formation of the CDO Oxy $\alpha_3\beta_3$-hexamer was investigated via a Native-PAGE (figure 23) using the purified Oxy stored at 4°C for 12 h after purification. Since significantly different expression patterns in terms of strength, as well as solubility, between the two Oxy co-expression constructs had been noticed, as described previously, the quaternary structure at native conditions was investigated for both Oxy constructs. For comparison purposes, 5 µg and 10 µg of purified Oxy were loaded, respectively. Interestingly, a faint band at the expected height is only visible for the Oxy(1xHis) (232.38 kDa). Furthermore, strong bands present at around 360 kDa can be observed comprising the majority of the contained enzyme within this sample, which could mean that either the single Oxy subunits or the α_3- or β_3-trimers had already precipitated. The Oxy(2xHis) on the other hand does not show a clear band at the expected height (249.49 kDa) but instead a smear of proteins is visible between around 600 and 400 kDa, again indicating precipitation among the Oxy subunits. Additionally, a significant amount of protein can be seen at the height of the buffer front, indicating the presence of the single α- or β-subunits (55.84 kDa and 21.62 kDa, respectively) that did not undergo folding of the heterohexamer. Furthermore, clear bands at 720 kDa are present for both Oxy constructs, which could again be the result of aggregated single α- or β-subunits. To further investigate the formation of the $\alpha_3\beta_3$-hexamer under native conditions, a size exclusion chromatography would need to be performed.
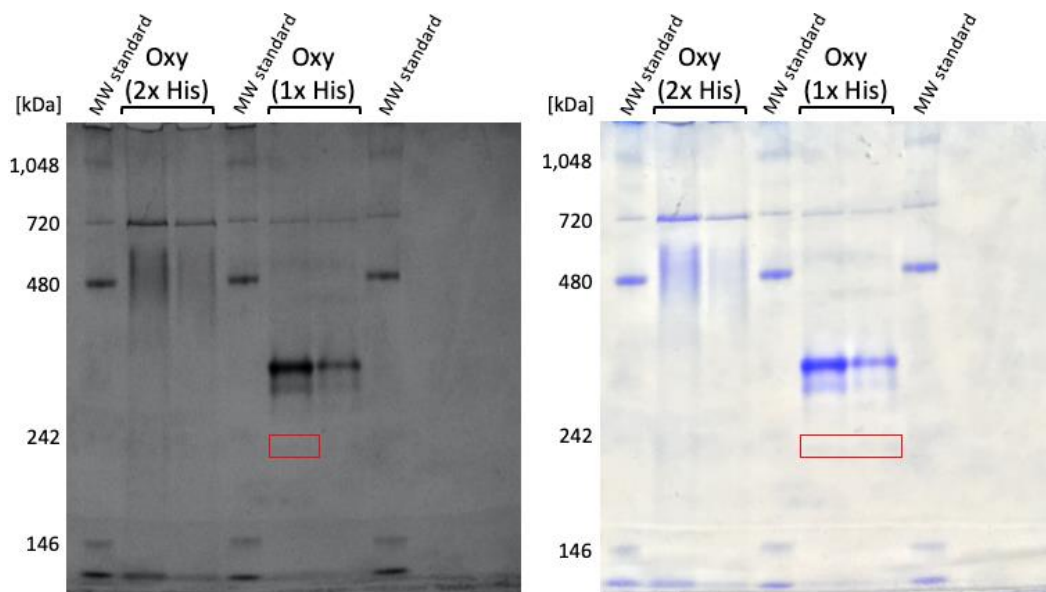
Figure 23 Native-PAGE of purified co-expression constructs pOxy(2xHis) (249.49 kDA) and pOxy(1xHis) (232.38 kDa) visualized via G:BOX (Syngene, Cambridge, UK) (left) and photographed on the bench (right). On the left lanes of both Oxy constructs 10 µg and on the right lanes 5 µg protein were loaded. Bands at the expected height are only slightly visible for the construct pOxy(1xHis) at 232.38 kDa, as highlighted in red. MW standard: NativeMark™ Unstained Protein Standard (1236, 1048, 720, 480, 242, 146, 66, 20 kDa) (Invitrogen™, Thermo Fisher Scientific; Massachusetts, USA).

3.10 NAD(P)H Assay – cofactor preference of purified FdR

To determine the enzymatic activity of the repaired FdR (construct 5, see table 10, section 2.3.1), the absorption of both NADH and NADPH was measured spectrophotometrically at 340 nm. Therefore, 10 µM of purified FdR and either 175 µM NADH or 150 µM NADPH were mixed in des.-SPB 2 and the absorbance was measured for 2 min in total, whereof the slope was being used to determine the enzymatic activity of the FdR. The obtained results (as depicted in figure 24) show the decrease in absorbance between 0 and 0.5 min in dependence of NADH and NADPH, respectively. Thereby, the graph of the NADPH containing reaction shows a greater decrease, thus also a more negative slope. This result indicates that the FdR preferably accepts NADPH, compared with NADH, as substrate.
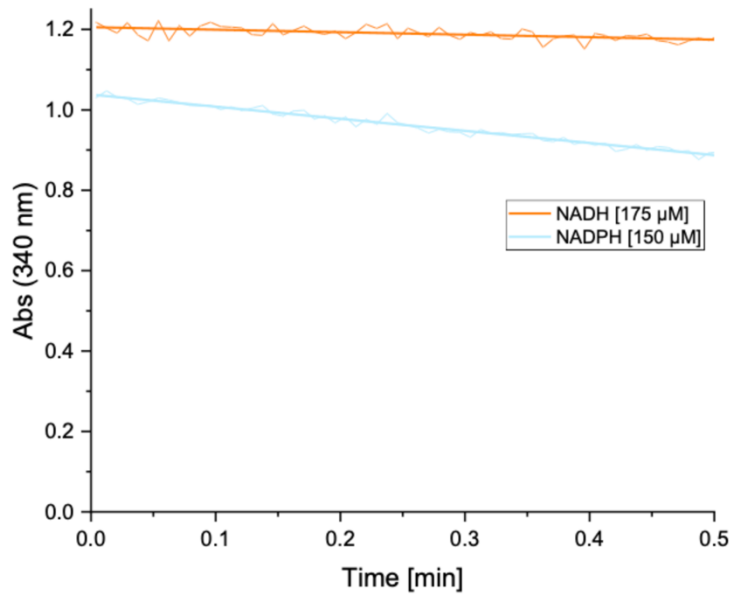
Figure 24 Measured absorbance of NADH (orange) and NADPH (blue) at 340 nm using purified FdR. Reaction conditions: 10 µM purified FdR, 175 µM NADH or 150 µM NADPH; buffer: des.-SPB 2 pH 7.2. Total reaction volume: 1 mL, measuring time: 2 min (initial 0.5 min are shown).

The obtained graphs (figure 24) were used for the calculation of the volumetric and specific activity of the FdR (figure 25, left and right). The volumetric activity using NADPH was determined with 0.47 U/mL, which is close to five times higher than 0.1 U/mL obtained when using NADH. Consequently, the specific activity of the same reactions was calculated at 0.1 U/mg using NADPH and 0.02 U/mg using NADH. Based on these results one could assume that the substrate preference of the FdR lies on the side of NADPH, however also NADH is oxidized, just to a smaller extent.
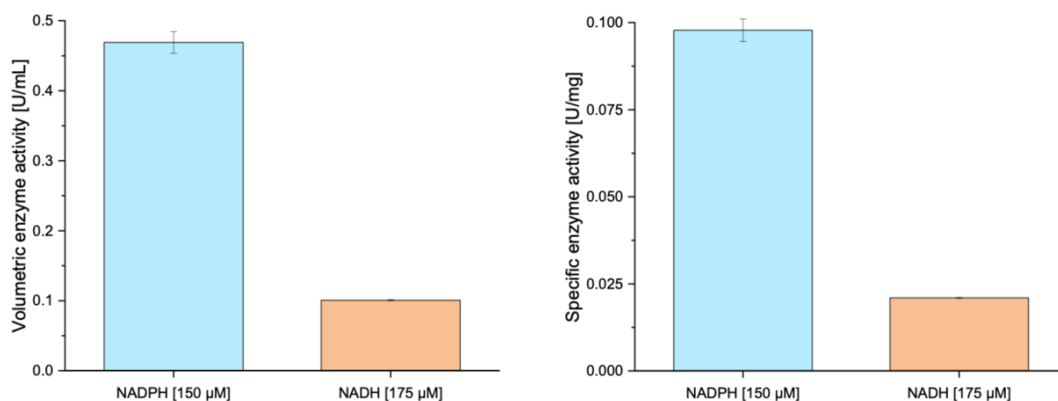
Figure 25 Determined volumetric (left) and specific (right) enzyme activities of the purified FdR using either NADH or NADPH, calculated from the measured absorbance at 340 nm (figure 24). Reaction conditions: 10 µM purified FdR, 175 µM NADH or 150 µM NADPH; buffer: des.-SPB 2 pH 7.2. Total reaction volume: 1 mL, measuring time: 2 min (initial 0-0.5 min were used for the calculation of the slope and further to determine volumetric and specific activities.

In order to consider the background activity of NAD(P)H consuming enzymatic reactions within the pET28a(+) EV-CFL, the volumetric activity was also determined photometrically using only respectively EV-CFL, EV-CFL with NADPH, or EV-CFL with NADH (figure 26). The volumetric enzyme activity was calculated at 0.2 (CFL), 0.27 (EV-CFL with NADPH) and 0.92 U/mL (CFL with NADH). Interestingly, compared to the volumetric activity of solely EV-CFL, the addition of NADPH leads to an increase of only approximately 0.07 U/mL, whereas the addition of NADH lead to an increase of 0.72 U/mL.
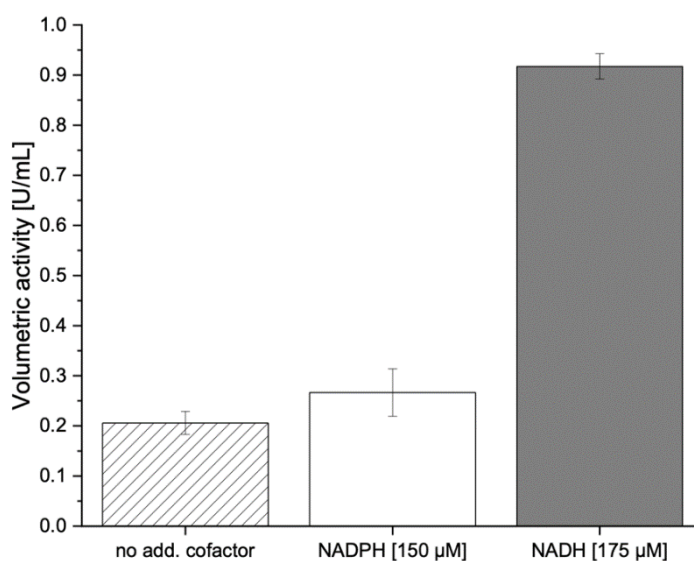

Figure 26 Determined volumetric enzyme activities of pET28a empty vector cell-free lysate (EV-CFL) with either no additional cofactor, NADH or NADPH calculated from the measured absorbance at 340 nm. Reaction conditions: 50 µL EV-CFL, 175 µM NADH or 150 µM NADPH; buffer: des.-SPB 2 pH 7.2. Total reaction volume: 1 mL, measuring time: 2 min (initial 0-0.5 min were used for the calculation of the slope and further to determine volumetric activities.

3.11 *In vitro* biotransformations: room temperature purified enzymes

Initial *in vitro* biotransformations were carried out using the single CDO subunits purified at RT, as described in section 2.4.7, with the constructs 1-4 harboring the single CDO subunits, respectively. A non-sense mutation contained on the gene of FdR[x] within construct 4 was discovered at a later stage during this thesis, consequently no FdR was present during these biotransformation experiments. However, using construct 1 and 2, which contain respectively one of the single Oxy α- or β-subunit genes *cumA1* or *cumA2*, only traces of 1-indenol after indene biotransformations *in vitro* were detected (data not shown). It was therefore continued using the Oxy co-expression construct 9 (Oxy(2xHis)[*]), harboring both *cumA1* and *cumA2* genes with N-terminal His tag.

With this construct the first successful *in vitro* conversion of indene to 1-indenol could be observed when using different ratios between Oxy, Fd and FdR[x] (Oxy:Fd:FdR[x]), based on literature showing that a molar excess of Fd over the Oxy components of other ROs systems *in vitro*, like the NDO,[37] or the benzene DO from *P. putida* ML2,[40] does not only result in increased Oxy activity, but is also the limiting bottleneck within the complex electron transport chain. Therefore, it was the initial goal to perform biotransformations with 5 mM indene and different ratios of Oxy:Fd:FdR[x] in the linear range of 1:1:1 to 1:8:8 (1 being equivalent to 0.25 mg/mL purified CDO component) at constant NADH concentration of 2 mM (figure 27). Interestingly, a linear increase of product starting from 21.8 µM (1:1:1) up to 0.29 mM (1:8:8) at constant Oxy concentration could be observed upon doubling only the concentration of Fd and FdR[x], respectively. At a ratio of 4:4:4, a product concentration of 0.8 mM could be observed. However, due to the non-sense mutation within the gene of FdR[x] harbored on the used construct 4, no active FdR was present at any time during this biotransformations.
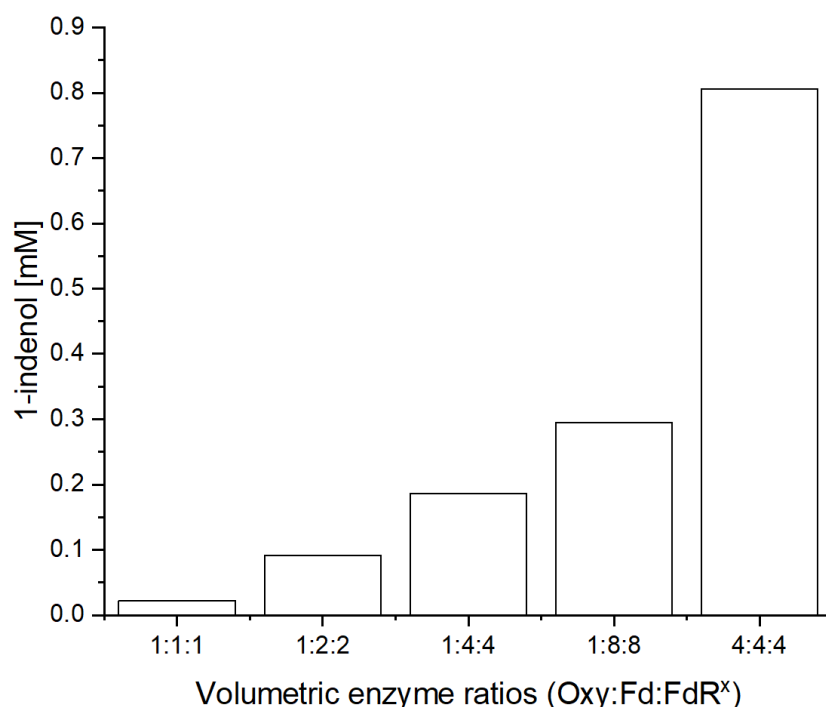
Figure 27 Obtained 1-indenol concentrations from quantification using chiral GC-FID after biotransformations with RT-purified Oxy (from co-expression construct 9), Fd and FdR[x] (from construct 3 and 4, respectively). The ratios 1:1:1 to 4:4:4 correspond to Oxy:Fd:FdR[x], 1 being equivalent to 0.25 mg/mL. No FdR was actually present due to a base deletion. Reaction conditions: 5 mM indene, 2 mM NADH, buffer: 100 mM des.-SPB 1, pH 7.2; total reaction volume: 1 mL, duration: 24 h at 120 rpm.

3.12 *In vitro* biotransformations: ÄKTA^{TM} purified enzymes (4°C)

The following biotransformations were carried out with purified CDO Oxy, Fd and the repaired FdR using construct 3, 5, 6 and 7 (see table 10, section 2.3.1). The purification was accomplished using the ÄKTA^{TM} pure 25 completely at 4°C. During *in vitro* conversions, 5 mM Indene served as the sole substrate and NADH or NADPH was added as cofactor also at a concentration of 5 mM, respectively (figure 28-31). During *in vivo* bioconversion studies of Gally et al.'s work with the WT CDO and the substrate indene, the products 1-indenol and 1,2-indandiol were observed in a ratio of 64:36 at 80 % total product formation (figure 3 A, section 1.2).[23] However, only traces of the expected product *cis*-1,2-indandiol (data not shown) were observed after *in vitro* biotransformation during this thesis. Furthermore, besides the mono-hydroxylated product 1-indenol, also traces of 1-indanone could be observed, presumably derived from an isomerization product of 1-indenol.[22]

3.12.1 Cofactor choice: NADH vs. NADPH

To investigate the cofactor preference during biotransformations, NADH and NADPH were compared respectively (figure 28), both at 5 mM, using equal mass concentrations of Oxy, Fd and FdR (1:1:1), as described previously. Interestingly, using NADH 30.3 µM 1-indenol and 0.9 µM 1-indanone were found, whereas with NADPH only 6 µM 1-indenol were obtained. Based on this result, the cofactor preference for the FdR would be on the site of NADH, as described by Dong et al.[33] However, further investigation would be required to determine the actual cofactor preference of the FdR.
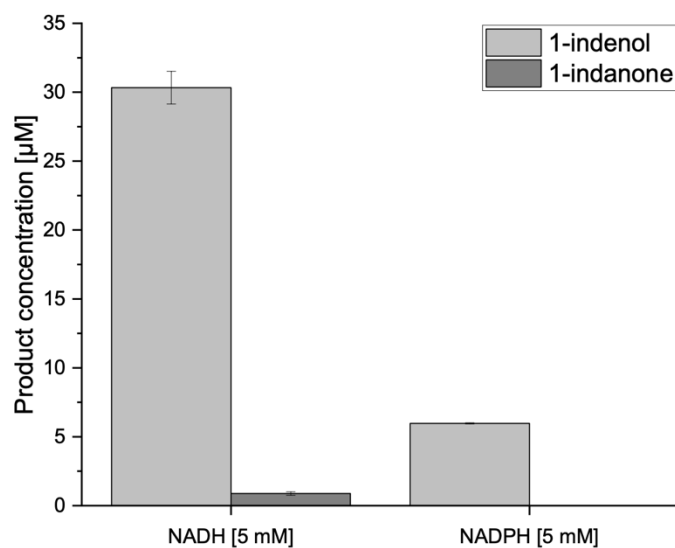
Figure 28 Obtained 1-indenol and 1-indanone concentrations after biotransformations with purified Oxy from co-expression construct 6, Fd and FdR (from construct 3 and 5, respectively) during cofactor comparison between NADH and NADPH from quantification using achiral GC-FID. Reaction conditions: 0.25 mg/mL Oxy, Fd and FdR, respectively, 5 mM indene, 5 mM NADH or NADPH, buffer: 50 mM des.-SPB 2, pH 7.2; total reaction volume: 1 mL, duration: 24 h at 120 rpm.

3.12.2 Comparison of Oxy co-expression constructs: Oxy(2xHis) vs. Oxy(1xHis)

Biotransformations with the Oxy constructs Oxy(2xHis) and Oxy(1xHis) (constructs 7 and 6), respectively, were carried out using different ratios of Oxy, Fd and FdR, 1:2:2 up to 1:8:8 (1 being equivalent to 0.25 mg/mL purified enzyme) (figure 29). Here, NADPH [5 mM] was used as cofactor due to the assumed substrate preference of the FdR towards NADPH, as described in section 3.10. Empty vector control (EVC) reactions were applied using EV-CFL. Overall, 1-indenol was the only detectable product. However, the obtained product concentrations were close to the detection limit of the GC-FID, thus detection of formed 1-indanone would not have been detected. No expected significant increase of product concentration could be observed upon increasing amounts of Fd and FdR. The Oxy(2xHis) shows an increase from 27.4 µM to 36.1 µM and 35.1 µM upon the doubling of the concentration of Fd and FdR to 1 mg/mL and 2 mg/mL, respectively. For the Oxy(1xHis), similar product concentrations (20.6 µM and 26.3 µM) were obtained for 0.5 mg/mL and 1 mg/mL Fd and FdR, respectively. Interestingly, the control reactions containing either only an Oxy construct with EV-CFL or only EV-CFL, did not lead to product formation. However, the obtained 1-indenol concentrations observed after the biotransformation from section 3.11 are significantly higher at equal Oxy and Fd concentrations and when using NADH as cofactor, e.g. at the enzyme ratio of 1:8 (Oxy:Fd), 0.29 mM product formation was observed, even though no active FdR was present. This indicates that either the cofactor preference of the FdR is on the side of NADH, or that

the NADPH concentration of 5 mM leads to substrate inhibition (figure 29). Even though product concentrations were observed to be a little higher with the Oxy(2xHis), all subsequent biotransformations were carried out using Oxy(1xHis) due to its more promising result from both the SDS-PAGE of the final purification and the Native-PAGE (section 3.8, figure 21 and section 3.9, figure 23).
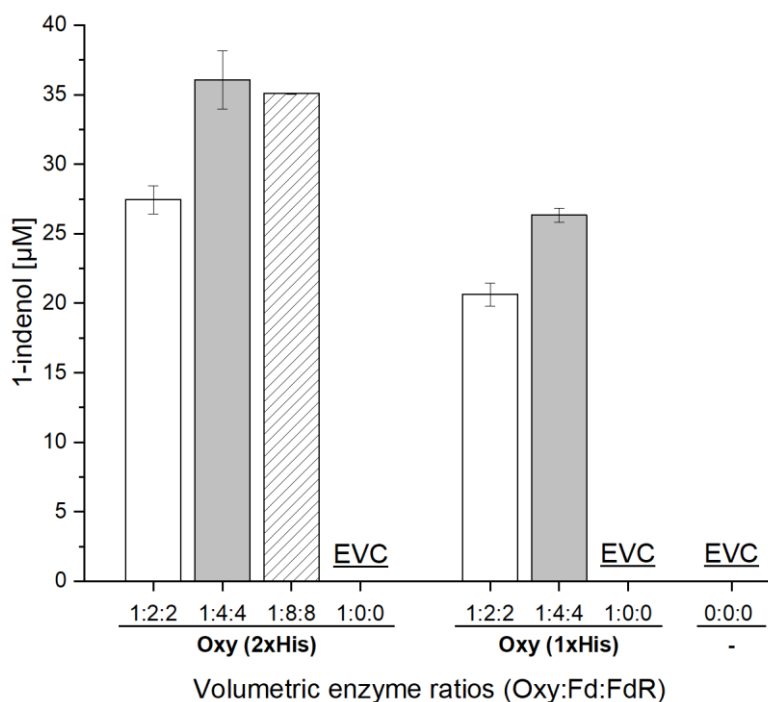

Figure 29 Obtained 1-indenol concentrations from quantification using achiral GC-FID after biotransformations with purified Oxy from co-expression constructs 7 and 6, Fd and FdR (from construct 3 and 5, respectively). The ratios 1:0:0 to 1:4:4 correspond to Oxy:Fd:FdR, 1 being equivalent to 0.25 mg/mL and 0 indicating the absence of a particular CDO component. Reaction conditions: 5 mM indene, 5 mM NADPH, buffer: 50 mM des.-SPB 2, pH 7.2; total reaction volume: 1 mL, duration: 24 h at 120 rpm. EVC: pET28a empty vector cell-free lysate.

3.12.3 Variation of volumetric ratios of Oxy, Fd and FdR

Further biotransformations with the Oxy(1xHis) were carried out with varying ratios of Oxy, Fd and FdR, as described previously, with 5 mM NADPH as cofactor, wherein enzyme ratios range from 1:1:1 to 1:8:8. Additionally, control reactions only containing the Oxy, or the Oxy with FdR were carried out (figure 30). No significant difference of product concentration can be observed from 1:1:1 (6 µM 1-indenol) to 1:2:2 (6.1 µM 1-indenol and 0.3 µM 1-indanone), as shown in figure 30. Also, a further increase of the ratios up to 1:8:8 only led to 10.7 µM 1-indenol and 0.6 µM 1-indanone formation, which does not reflect the expected changes of conversion when increasing the concentration of Fd. Interestingly, no 1-indenol was detected in the control reactions with only the Oxy present, which reinforces the theory that the Oxy

obtains the electrons via the Fd and thus no oxygenation of the substrate occurs without the Fd. Moreover, when both Oxy and FdR are present in the absence of Fd, also no conversion takes place, which further indicates that the electrons can apparently not be transferred from the FdR to the Oxy in a direct manner.

Figure 30 Obtained 1-indenol and 1-indanone concentrations from quantification using achiral GC-FID after biotransformations with purified Oxy from co-expression construct 6, Fd and FdR (from construct 3 and 5, respectively). The ratios 1:1:1 to 1:8:8 correspond to Oxy:Fd:FdR, 1 being equivalent to 0.25 mg/mL and 0 indicating the absence of a particular CDO component. Reaction conditions: 5 mM indene, 5 mM NADPH, buffer: 50 mM des.-SPB 2, pH 7.2; total reaction volume: 1 mL, duration: 24 h at 120 rpm.

3.12.4 Addition of empty-vector cell-free lysate to purified CDO enzymes

The activity of the purified Oxy, Fd and FdR in the ratio 1:1:1 was further investigated in presence of *E.* coli JM109(DE3) pET28a(+) EV-CFL and 5 mM NADH, whereat 200 μL EV-CFL were added per reaction (1 mL total volume) (figure 31). Surprisingly, hereby the highest conversion of 24.0 % 1-indenol and 0.04 % 1-indanone from 5 mM indene can be observed when all CDO components, EV-CFL and NADH were added to the reaction. Upon exclusion of the FdR, the conversion drops dramatically to only 3.2 % 1-indenol and 0.1 % 1-indanone formation, on the one hand highlighting the role of the FdR within the system, but on the other hand showing presumed interaction between a Red contained in the EV-CFL interacting with the CDO Fd. The latter is further supported by the absence of conversion at the reaction, where, besides the FdR, also the Fd is excluded, which again corroborates the belief that

electrons are shuttled from the FdR to the terminal Oxy via the Fd.[33] Furthermore, with all CDO components and EV-CFL present, but without additional NADH, still 2.4 % conversion to 1-indenol can be observed, presumably coming from remaining NADH within the EV-CFL. Finally, a control reaction with indene, NADH and EV-CFL was prepared, in order to see, whether the substrate underwent conversion catalyzed by cellular enzymes, which it apparently did not. Significant amounts of the substrate indene were still present in the reaction vials after biotransformations (data not shown), indicating that evaporation of the substrate was not the reason for the stop of conversion.
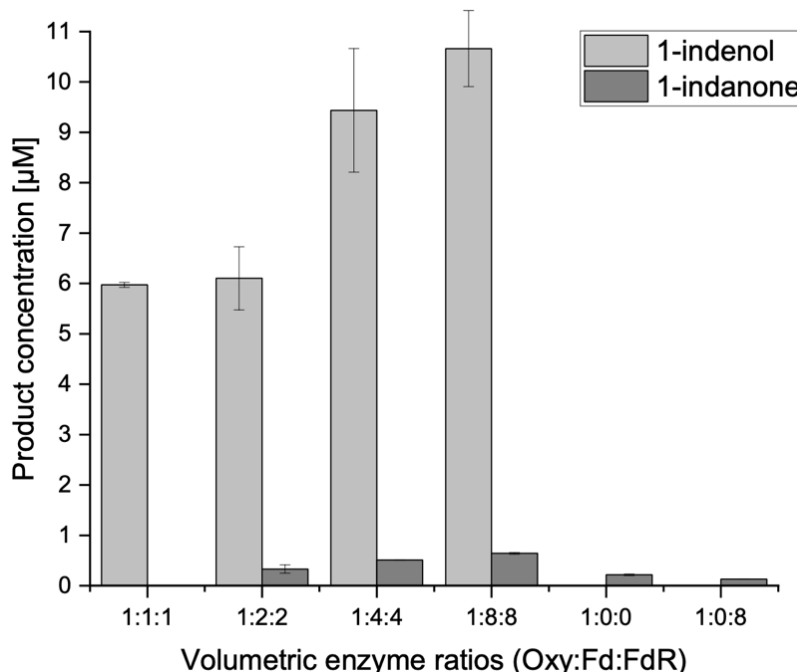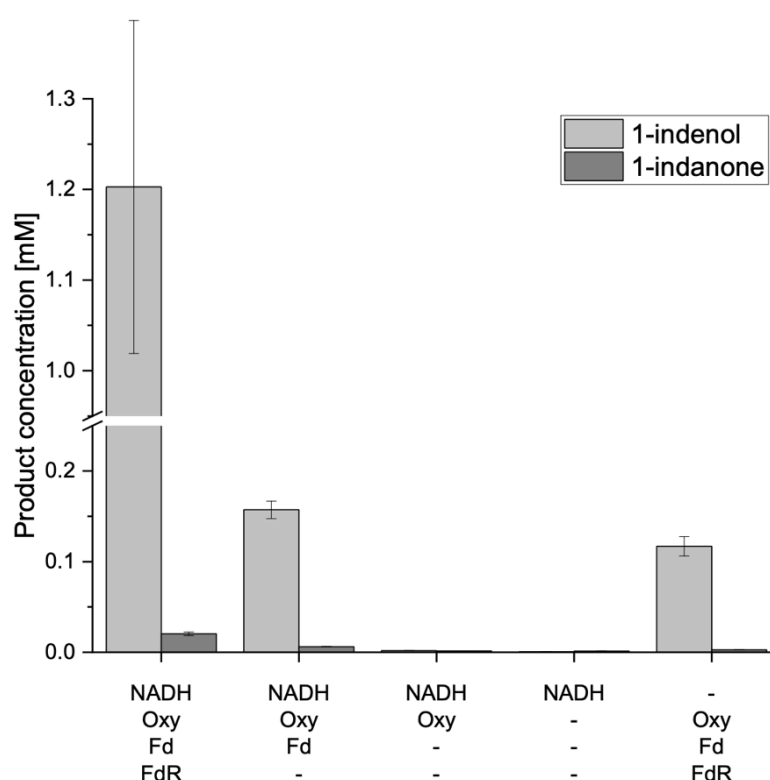

Figure 31 Obtained 1-indenol and 1-indanone concentrations from quantification using achiral GC-FID after biotransformations with purified Oxy from co-expression construct 6, Fd and FdR (from construct 3 and 5, respectively). "-": absence of a CDO component or NADH. Reaction conditions: 0.25 mg/mL Oxy, Fd and FdR, respectively, 5 mM indene, 5 mM NADH, 200 µL EV-CFL, buffer: 50 mM des.-SPB 2, pH 7.2; total reaction volume: 1 mL, duration: 24 h at 120 rpm.

4 Discussion

ROs are powerful biocatalysts and are to date the only known enzymes capable of catalyzing the stereoselective formation of vicinal *cis*-diols in one step.[10] In particular, the stereoselective asymmetric dihydroxylation of alkenes to chiral products has drawn attention to these enzymes due to the ease of further processing of the resulting chiral diol intermediate products into valuable endproducts for the chemical and pharmaceutical industry. However, the flavin (FMN/FAD) dependent reductases of ROs require NAD(P)H as cofactors.[12] Biotransformations with this enzyme class are performed using whole-cells,[7,14,57] partly due to the cost-effectivity of *in vivo* NAD(P)H cofactor regeneration.[14] The use of whole-cells is effective for several fermentative biotransformations, but often cannot be readily applied to heterologous multi-enzymatic cascades. Thereby, the reaction(s) of interest are often confounded with side activities of the cell accompanied with propagation, growth or other metabolic activities. Furthermore, toxic (intermediate-)substrates are often troublesome during *in vivo* approaches. Generally speaking, the successful *in vitro* implementation of enzymes in industrial processes can be a challenging task, as in many cases the costs related with the biocatalyst separation account for the bulk of the total production expenses. Furthermore, in multi-enzymatic processes (like in the case of ROs), these costs increase proportionally with the number of contributing enzymes, for which separate production and isolation is required.[58] *In vitro* studies on the other hand play an important role during the description and understanding of an enzyme system, where the purification of the enzyme(s) allows more precise characterization. Furthermore, several undesired effects that are accompanied with whole-cell approaches (such as impurities, multiple non-target enzymes competing for the same substrate, undesired further enzymatic transformations of the targeted products or the presence of different cofactors), can be avoided from any presumptions by *in vitro* studies.

Regarding the CDO, on the one hand, several *in vivo* studies with recombinant CDO have been published to date,[23,44–46,59] which either dealt with the natural substrate specificities, rational protein engineering or application of alternative cofactor regeneration systems for biocatalysis. On the other hand, however, to date no *in vitro* studies of the CDO system that deal with the electron transport chain, the cofactor preference or biotransformations have been published. The aim of this work was therefore the investigation of the CDO during *in*

vitro studies. *In vivo*, the conversion of indene catalyzed by the CDO results in a product ratio of 64:36 1-indenol to 1,2-indandiol with an overall conversion of 80 %,[23] which was thought to be obtained from this work's *in vitro* bioconversions as well. However, during this work only the monohydroxylated 1-indenol and the byproduct 1-indanone were observed. To date, no *in vitro* biotransformation studies of the CDO have been published, which makes direct comparison difficult.

Gally et al. successfully utilized all CDO WT genes encoded on one pUC19 vector during *in vivo* biotransformations using an IPTG concentration of 0.2 mM and 30°C expression temperature. However, overexpressed CDO bands were therein reported to be only hardly visible in SDS-PAGE.[23] During this work, the expression of the single c.o. CDO genes harbored on pET28a vectors was initially carried out under these very conditions as well. Strong bands of heterologously expressed CDO components were clearly visible, but to a greater extent within the insoluble fractions. Final expression conditions were therefore adapted to 50 µM IPTG concentration at 20°C expression temperature, leading to a shift towards more soluble expressed CDO enzymes (figure 15 and 16, section 3.6). Previous reports about only slightly visible Fd and FdR bands on SDS-PAGE gels were not confirmed here, as clear bands were obtained for both enzymes.[59–61]

The quaternary structure of the Oxy is of the $\alpha_3\beta_3$-hexamer type, containing three large CumA1 (α) and three small CumA2 (β) subunits, respectively. Since electrons, once shuttled to the Oxy from the Fd, are believed to be transferred from the Rieske [2Fe-2S] center of one α-subunit to the catalytic non-heme iron active site of a neighboring α-subunit,[33] the correct quaternary structure formation of the Oxy is required for oxyfunctionalization of the substrate. No product formation could be observed during biotransformations with the corresponding genes of CumA1 and CumA2 encoded on separate vectors (construct 1 and 2, see table 10, section 2.3.1), presumably because the formation of the $\alpha_3\beta_3$-hexamer was not successful *in vitro*. Hence, the Oxy co-expression constructs pOxy(2xHis) and pOxy(1xHis) (construct 7 and 6, see figure 7, section 3.1) were created in order to govern formation of the $\alpha_3\beta_3$-hexamer *in vivo*, which led to successful 1-indenol formation during biotransformations. Construct pOxy(2xHis), in which also the CumA2 is N-terminally His tagged, was created, because it was not clear, whether the quaternary structure of the Oxy would withstand the purification procedure and if both subunits would eventually remain in equimolar amounts

after the purification. During purification of the NDO Oxy, Halder and colleagues used a construct, where only the α-subunit carried a His tag, assuming that the interactions between the α- and the β-subunit would be sufficient for a collective purification of the $\alpha_3\beta_3$-hexamer.[41] Among the two Oxy co-expression constructs, the results of both the SDS-PAGE from the final purification at 4°C and the Native-PAGE favor construct pOxy(1xHis), since in the former, more enzyme was contained in the purified fraction (figure 21, section 3.8) and in the latter, a faint band could be detected at the expected height under native conditions only with this construct (figure 23, section 3.9). Comparison of the two Oxy co-expression constructs purified at 4°C during biotransformations with NADPH (figure 29, section 3.12.2) however did not lead to a significant difference in product formation.

Especially for CumA1 and the Fd, which both contain a Rieske-type 2Fe-2S cluster, obtaining sufficient amounts of soluble proteins was a challenging task. A literature search revealed that heterologous expression of enzymes containing Fe-S clusters has been reported to be troublesome.[62] Furthermore, CumA1 contains a disulfide bridge and was hence examined in *E. coli* SHuffle by Dong and colleagues.[33] However, expression of CumA1 using *E. coli* SHuffle was shown to not lead to increased amounts of soluble enzyme in comparison with *E. coli* BL21(DE3), but it has to be noted that also the growth rate of the first was thereby observed to be up to 2-fold decreased compared to the latter during studies of Wied et al.[59] It would be further worth to consider changing to a gentler expression system, which is not based on the T7 promoter, in order to yield more soluble and active enzyme. For example, the contained promoter P_{BAD} in pBAD-derived vectors allows tightly regulated induction using arabinose and thus rapidly turned on and off heterologous enzyme expression.[63] Hunold and colleagues successfully co-expressed several active *Phenylobacterium immobile* strain E belonging RO Oxys and Fd/Red in pBAD33 and pBAD18 systems, respectively using *E. coli* JW5510.[64] Overall, the expression of the CDO during this work was considered sufficient, since enough soluble and active CDO enzymes were expressed for initial successful *in vitro* biotransformations.

The cofactor preference between NADH and NADPH of the CDO, more precisely, of the FdR, to date is still subject of research. Dong et al. reported the electron equivalent source to be NADH.[33] However, in the course of the NAD(P)H assay during this work, the cofactor preference of the purified FdR was clearly on the side of NADPH (figure 24-26, section 3.10). Thereby, the specific activity with NADPH was determined five-fold higher (0.1 U/mg) than

compared to NADH (figure 25, section 3.10). Also, the background activity of NAD(P)H consuming enzymatic reactions within EV-CFL was determined spectrophotometrically (figure 26, section 3.10). Interestingly, compared to the volumetric activity of solely EV-CFL, the addition of NADPH lead to an increase of only approximately 0.07 U/mL, whereas the addition of NADH lead to an increase of 0.72 U/mL. During catabolism in chemoorganotrophic organisms primarily dissolved dehydrogenases catalyze the electron transfer to NAD^+, whereas reoxidation of NADH often occurs via the membrane-bound NADH-Ubichinon-Oxidoreductase (complex I) at the cytoplasmic membrane, where subsequently the oxidative phosphorylation takes place. NADPH on the other hand, supplies electrons for the biosynthesis during anabolism. *E. coli* uses the pentose phosphate pathway for NADPH regeneration, which operates simultaneously to glycolysis in the cytoplasm.[65] Therefore, $NADP^+$ reduction might still take place in the CFL, thereby recycling the NADPH that is then reduced by the FdR. Furthermore, a large number of NADH oxidizing enzymes should have been excluded from this assay simply due to the presumption that the membranes had been removed after cell disruption via centrifugation.

Interestingly, exactly contrary results to the photometrical NAD(P)H assay regarding the cofactor preference of the CDO were obtained during *in vitro* biotransformations with CDO enzymes purified at 4°C using 5 mM indene and either 5 mM NADH or NADPH (see section 3.12). Thereby, with NADH 30.3 µM 1-indenol were detected, whereas with NADPH only a fifth (6 µM) 1-indenol formation was observed (figure 28, section 3.12.1), which indicates that the cofactor preference of the FdR is on the side of NADH, as described by Dong and colleagues.[33] To a certain extent, the lower stability of NADPH *in vitro* compared to NADH might explain the reduced conversion of this work. Wu et al. compared the stability of NADH and NADPH at 41°C, wherein they found that the latter is generally less stable.[66] The half-life of NADPH at 19°C was thereby noted with 8 h, but at 41°C with only 1 h. Furthermore, they claimed that acidic pH had a dramatic effect on NADPH stability at the tested temperatures 19, 30 and 41°C, suggesting to not expose NAPDH to a pH below 7.4.[66] In order to further investigate the cofactor preference of the CDO system, implementation of a cofactor regeneration system *in situ* should be considered, which on the one hand would lower the required amounts of either NADH or NADPH in the reaction and on the other hand might lead to clear results after biotransformations in terms cofactor preference. For instance, the common enzymatic regeneration system of glucose and glucose dehydrogenase (GDH), which

66

accepts both NAD$^+$ and NADP$^+$, could be implemented to investigate and compare both cofactors during *in vitro* biotransformations at relatively low effort. This approach has the benefit that the equilibrium is shifted towards the product side, since the resulting gluconolactone from glucose oxidation undergoes spontaneous hydrolyzation to gluconic acid.[7]

Molar excess of the redox partner Fd over the Oxy has been described to be beneficial for Oxy activity during *in vitro* bioconversions for naphthalene DOs.[42] In 1994, Tan et al. showed during the investigation of benzene DO from *P. putida* ML2 (NCIB 12190) that addition of purified Fd or Red significantly stimulated benzene bioconversion *in vitro* upon adding these purified components to CFL of *P. putida* harboring Oxy, Fd and Red. An exponential increase in activity was observed, where addition of 10 µg purified Fd to CFL led to 20 nmol/min activity and the addition of 50 µg purified Fd to CFL led to an increase of activity to 65 nmol/min. In comparison, when only purified Red was added, a linear activity increase was observed, where the addition of 10 µg purified enzyme led up to 20 nmol/min activity. Hence, a less significant influence was noted for the Red in comparison to added Fd. It was furthermore shown that the addition of purified Oxy did not significantly affect enzyme activity.[40] Just in 2017, Halder et al. showed that during *in vitro* bioconversion of 2 mM naphthalene to 1,2-naphthalendihydrodiol using NDO, at equal Oxy concentrations the increase of Oxy:Fd:Red from 1:12:3 µM to 1:20:5 µM led to a more than 2-fold increase from 0.64 ± 0.06mM to 1.48 ± 0.02 mM product formation.[41] Therefore, it can be suspected that the Fd is also the bottleneck within the CDO electron transport system. Hence, in this work different ratios of Oxy:Fd:FdR were aimed at to investigate beneficial effects for the Oxy activity. However, instead of (equi-)molar comparability, ratios between mass concentration of 1:1:1-1:8:8, wherein 1 is equivalent to 25 mg/mL CDO component, were used for the sake of comparison. Therefore, a mass concentration ratio of 1:1:1 corresponds to the molar ratios 1:16:5.2 µM for Oxy(2xHis):Fd:FdR, and 1:14.5:4.7 µM for Oxy(1xHis):Fd:FdR, respectively.

The effect of these varying enzyme ratios during initial biotransformations of this work were investigated using the CDO components Oxy, Fd and FdR^x purified at RT. For clarification, these biotransformations (figure 27, section 3.11) did not contain active FdR at any due to non-sense base deletion and were the only biotransformations that contained this inactive FdR^x, since the deletion was repaired afterwards. However, despite lacking active FdR, with 5 mM indene,

2 mM NADH and an enzyme ratio of 1:8 between Oxy:Fd, 0.29 mM 1-indenol formation was observed. Under the same reaction conditions, but with an Oxy:Fd ratio of 4:4, even 0.8 mM 1-indenol formation was detected, accounting for 16 % product formation. In theory, per mole of dihydroxylated product formed from indene, one mole NAD(P)H would be required, which was not governed during these initial biotransformations. Hence, stoichiometric ratios between NADH and the substrate indene were not governed, which makes the comparison between the conversions of the CDO enzymes purified at RT and purified at 4°C difficult. Interestingly, the linear increase of product starting from 21.8 μM (1:1) up to 0.29 mM (1:8) at constant Oxy concentration could be observed upon doubling only the concentration of Fd. Since no FdR was actually present, the obtained results on the one hand suggest that an increase of purified Fd alone results in an increase of product, and on the other hand indicate that electrons shuffled to the Oxy are obtained by an *E. coli* own Red. However, the RT-purified enzymes in this work were not clean enough to exclude any residual cell-owned enzymes or residual NADH from the CFL for further assumptions, (see SDS-PAGE of figure 18-20, section 3.7).

Final biotransformations were carried out using CDO enzymes purified at 4°C with Oxy, Fd and the repaired FdR (see section 3.12). The concentration of NAD(P)H was increased to 5 mM. However, the thereby obtained 1-indenol concentrations were dramatically lower (μM, instead of mM), compared to any biotransformation with RT-purified CDO, despite there was no active FdR present during the latter. The mentioned findings of others regarding increased product formation upon increasing Fd and Red concentrations could not be confirmed here. Using NADPH, the variation of enzyme ratios between 1:1:1 and 1:8:8 only led to increasing product concentrations of 11 μM 1-indenol (figure 30, section 3.12.3). Furthermore, comparison of the two Oxy co-expression constructs with NADPH did not reveal significantly different 1-indenol formation (figure 29, section 3.12.2). However, the fact that no product was detected in control reactions containing only EV-CFL, or EV-CFL with additional Oxy (figure 29, section 3.12.2), on the one hand supports the hypothesis that the Fd is necessary for electron transfer to the Oxy and furthermore excludes potential side reactions with cellular enzymes and the substrate indene.

Surprisingly, the highest conversion of indene was observed with EV-CFL, 5 mM NADH as well as Oxy, Fd and the repaired FdR (purified at 4°C) in the ratio 1:1:1 (1:14.5:4.7 μM) (figure 31,

section 3.12.4). In this way 24 % 1-indenol and 0.04 % 1-indanone conversion was detected. Contrary results in literature, which describe that ROs contained in crude CFL are prone to inactivation,[15,67] lead to the assumption that the high activity in this work upon addition of EV-CFL might be the result of therein contained catalase. Hydrogen peroxide (H_2O_2) or other reduced oxygen species are known to be an undesired substrate analogue-dependent side product of ROs during uncoupling reactions.[48,68] Furthermore, H_2O_2 was shown to irreversibly inactivate the Oxy of NDO during bioconversion of its substrate analogue benzene. However, this inactivation could be prevented completely by the presence of catalase.[48] Wied et al. investigated the effect of adding catalase to *in vivo* light-driven biotransformations using the CDO variant M232A, which did not lead to increased product formation.[59] Nevertheless, the addition of catalase to *in vitro* CDO NAD(P)H-dependent biotransformations might lead to increased conversion and could as well be an explanation, why conversion with NADH and EV-CFL is dramatically higher (24 % conversion) (figure 31, section 3.12.4), than compared to the reaction containing the same compounds but without EV-CFL (30 µM 1-indenol (0.6 % conversion), figure 28, section 3.12.1).

Contrary results regarding the effect of CFL containing ROs were published by Catterall and Williams, who found that NDO containing crude CFE significantly lost activity under aerobic conditions, but could be reactivated by reducing agents, like dithioerythritol or sodium borohydride. They reported that after 24 h at 20°C 60-70 % and at 4°C about 30 % activity was lost. However, upon the addition of several reducing agents, dithioerythritol was found to reactivate activity after incubation under anaerobic conditions to a level of 45 % greater than what was obtained from the original CFL.[15] However, another study revealed that pyrazon DO contained in CFL would lose its activity completely after storage for 72 h at 4°C, whereas with the addition of 1,4-dithiothreitol an almost 90 % retainment of activity was achieved. However, the purified enzymes showed a relatively high stability upon storage at 4°C or deep-frozen. Moreover, a 2-fold increase in activity was reported after the addition of 1 mM ferrous iron (Fe^{2+}) to the CFE, and furthermore, addition thereof during dialysis prevented loss of enzyme activity in the course of purification. Noteworthy, the cause of Oxy inactivation was not the destruction of the Rieske [2Fe-2S] cluster, but rather dependent on the oxidation state of the mononuclear iron in the Oxy active site, of which the reduced form (Fe^{2+}) is more sensitive to H_2O_2 than the oxidized ferric form (Fe^{3+}).[67] However, the fact that firstly, the highest conversion of indene to 1-indenol observed during this work (24.0 %) is significantly

lower than what Gally and colleagues found in *in vivo* biotransformations with the CDO (1-indenol and *cis*-1,2-indandiol in the ratio 64:36 at 80% total product formation)[23] and secondly, that no dihydroxylated products could be detected during this work, the obvious assumption is that enzyme inactivation occurs at some point in the *in vitro* setup of this work. Furthermore, since during this work still significant amounts of indene could be detected after the biotransformations (data not shown), evaporation of the substrate can be excluded as a reason for the stop of conversion.

Finally, during control reactions wherein the FdR was excluded from the purified CDO enzymes with EV-CFL (figure 31, section 3.12.4), the activity does drop significantly to 3.2 % 1-indenol formation, but surprisingly still conversion takes place, indicating that reducing equivalents are supplied to the Fd via a Red present in the EV-CFL. A look at related literature revealed a study by Inoue and colleagues, who demonstrated strict specificities between Oxy and Fd but an interchangeability between Fd and Red during *in vitro* studies of the Class IIB RO carbazole 1,9a DO.[69] This would further be supported by the lack of conversion during the reaction, where also Fd was excluded, leaving behind the Oxy as the sole CDO component (figure 31, section 3.12.4). The hereby obtained results furthermore correlate with current understanding of the electron transport chain of three-component ROs.[10,12,33]

5 Conclusion

In summary, this study provides an initial proof-of-concept for the purification of active single Rieske non-heme iron oxygenase (RO) components for successful *in vitro* biotransformations of indene using the cumene dioxygenase (CDO) from *Pseudomonas fluorescens* IP01. Based on Gally et al.'s *in vivo* study of the CDO, where during indene biotransformations the products 1-indenol and 1,2-indandiol had been observed in the ratio 64:36 at 80 % total product formation, such ratio was expected for *in vitro* biotransformations in this work.[23] However, only the monohydroxylated 1-indenol could be observed in this study. Furthermore, the usage of *E. coli* c.o. CDO genes in combination with pET28a and the expression host *E. coli* JM109(DE3) were shown to yield sufficient expression results in terms of soluble enzyme amount. The cofactor preference of the purified FdR was preliminary determined photometrically to be on the side of NADPH, rather than NADH. However, during *in vitro* biotransformations, 1-indenol concentrations were observed at five-fold higher

concentrations with NADH, compared to NADPH. Published literature regarding the FdR's cofactor preference is fairly limited to the work of Dong et al. who reported it to be NADH.[33] ROs are known to be of rather unstable character,[15] and therefore, a purification protocol operated at 4°C was established. Since molar excess of the redox partner Fd over the Oxy has been reported to be beneficial for the Oxy activity,[41,42] a clear surplus of Fd and FdR was used during biotransformations of this work in the ratios of Oxy:Fd:FdR between 1:1:1 and 1:8:8 (1 being equivalent to 25 mg/mL CDO component) with 5 mM indene and 5 mM NADPH. However, only insignificant (µM) increase was detected upon increased concentrations of Fd and FdR. During subsequent investigation of the electron transport chain within this three-component system, exclusion of either Fd, or both Fd and FdR during *in vitro* biotransformations proved that their presence is essential for conversion and confirms current understanding of electron transfer among three-component ROs.[10,12,33] Upon exchanging the purified FdR with *E. coli* EV-CFL, however, conversion was observed, indicating interchangeability of the FdR with *E. coli* Reds, which has been reported for other ROs.[69] Interestingly, the highest 1-indenol yield of 24 % could be achieved with purified CDO Oxy, Fd and FdR in combination with EV-CFL and NADH. However, 24 % 1-indenol formation is still significantly lower than the expected result of Gally et al.'s *in vivo* studies.[23] The obtained results suggest that at some point during the bioconversion enzyme inhibition occurs. H_2O_2 is a known undesired substrate analogue-dependent side product of ROs,[48,68] which was shown to irreversibly inactivate e.g. the Oxy of NDO, but upon catalase addition this inactivation could be prevented.[48] This would explain the 40-fold lower 1-indenol formation (0.6 %) without added EV-CFL compared to the reaction with EV-CFL, reported in this work. Finally, despite the lack of published literature for *in vitro* biocatalysis with the CDO, the mentioned findings of others regarding either other DOs or CDO *in vivo* studies do provide worthwhile approaches for optimization of this *in vitro* system. These include implementation of a cofactor regeneration system, addition of catalase, reducing agents, or Fe^{2+}, as well as considering different expression strains and systems that could lead to significant improvement for *in vitro* biocatalysis and would allow the determination of the actual cofactor preference of the CDO.

6 Appendix

6.1 Primers

Table 21 List of the used primers for PCRs during this thesis including the respective sequences. Primer IDs marked with "*": Gibson overhangs of the *cumA1* gene contain 16 bp not codon-optimized DNA, since the constructs were initially designed according to the *cumA1* sequence of the wild-type gene from *P. fluorescens* IP01 *in silico*.

ID	Name	Sequence (5'-3')	Description
P1	Primer1_Gibson_insert_CumA2_fw	atctagaaataattttgtttaactttaagaaggagatataccatgaccagcgcagatct	Fwd. primer: CumA2 gene without His-tag including one overhang for Gibson® assembly.
P2	Primer2=4=6_Gibson_insert_CumA2_r	gatctcagtggtggtggtggtggtgctcgagtgcggccgctcaaaaaaactggctcaga	Rev. primer: CumA2 gene with or without His-tag including an overhang for Gibson® assembly. Overhang is complementary to vector backbone of pCumA1(N-His). Used to assemble both pOxy(2His) and pOxy(1His).
P3*	Primer3_Gibson_CumA2_pET_fw	gtccgagccgagttgggacacgctaaagtcttgaatctagaaataattttgtttaac	Fwd. Primer: CumA2 gene without His-tag including two overhangs for Gibson® assembly.
P5*	P5_Gib_CumA2_N-His_fw	atgatgtccgagccgagttgggacacgctaaagtcttgactctagaaataattttgttt	Fwd. Primer: CumA2 gene with His-tag including two overhangs for Gibson® assembly.
P7	P7_CumA1_N-His_Lin_fw_pET	gcggccgcactcgagcaccac	Fwd. primer: linearized pCumA1(N-His) for Gibson® assembly.
P8*	P8_CumA1_N-His_Lin_rev_pET:	tcaagactttagcgtgtcccaactcggctc	Rev. primer: linearized pCumA1(N-His) for Gibson® assembly.
P9	T7_pET_mod	cccgcgaaattaatacgactcac	Fwd. primer: colony PCR of pOxy(2His) and pOxy(1His). Sequencing of all used pET28a constructs.
P10	T7_term	ctagttattgctcagcggt	Rev. primer: colony PCR of pOxy(2His) and pOxy(1His). Sequencing of all used pET28a constructs.
P13	Primer_FdR_rep_co_fw	ctttaccgctcagggtatctttgctcaggc	Repair of base deletion in pFdR(N-His)^x via QuikChange™ site-directed mutagenesis
P14	Primer_FdR_rep_co_rv	gtccgagcctgagcaaagataccctgagc	Repair of base deletion in pFdR(N-His)^x via QuikChange™ site-directed mutagenesis
P21	p21_gib_cuma2_pet_fw_(p3a)	gagcgaaccgagttgggataccctgaaaagctaaatctagaaataattttgtttaac	Fwd. Primer: CumA2 gene without His-tag including two overhangs for Gibson® assembly.
P22	p22_gib_cuma2_n-his_fw_(p5a)	atgatgagcgaaccgagttgggatacctgaaaagctaactctagaaataattttgttt	Fwd. Primer: CumA2 gene with His-tag including two overhangs for Gibson® assembly.
P23	p23_cuma1(co)_n-his_lin_rev_pet_(p8a)	ttagcttttcagggtatcccaactcggttcgctcatcatac	Rev. primer: linearized pCumA1(N-His) for Gibson® assembly.

6.2 PCR programs

6.2.1 Gibson® assembly: Oxy. co-expression constructs

Table 22 PCR conditions and programs used for Gibson assembly

PCR 1: pre-insert 1		PCR 1 program	temperature	time
2.5 µL	10x DreamTaq buffer	initial denaturation	95°C	5 min
2.5 µL	dNTP mix, 2 mM each			
1.25 µL	Forward primer P1 [10 µM]	30 cycles:		
1.25 µL	Reverse primer P2 [10 µM]	denaturation	95°C	1 min
x µL	pCumA2(N-His) (25 ng fin.)	annealing	53°C	30 s
0.125 µL	DreamTaq DNA Pol. (0.625 U fin.)	Extension	72°C	01:30 min
x µL	ddH$_2$O			
		final extension	72°C	2 min
25 µL	final volume	store	10°C	∞

Table 23 PCR conditions and programs used for Gibson assembly

PCR 2: insert 1		PCR 2 program	temperature	time
2.5 µL	10x DreamTaq buffer	initial denaturation	95°C	5 min
2.5 µL	dNTP mix, 2 mM each			
1.25 µL	Forward primer P23 [10 µM]	30 cycles:		
1.25 µL	Reverse primer P2 [10 µM]	denaturation	95°C	1 min
x µL	pre-insert 1 (25 ng fin.)	annealing	60°C	30 s
0.125 µL	DreamTaq DNA Pol. (0.625 U fin.)	Extension	72°C	01:30 min
x µL	ddH$_2$O			
		final extension	72°C	2 min
25 µL	final volume	store	10°C	∞

Table 24 PCR conditions and programs used for Gibson assembly

PCR 3: insert 2		PCR 3 program	temperature	time
2.5 µL	10x DreamTaq buffer	initial denaturation	95°C	5 min
2.5 µL	dNTP mix, 2 mM each			
1.25 µL	Forward primer P22 [10 µM]	30 cycles:		
1.25 µL	Reverse primer P2 [10 µM]	denaturation	95°C	1 min
x µL	pCumA2(N-His) (25 ng fin.)	annealing (gradient)	45-53°C	30 s
0.125 µL	DreamTaq DNA Pol. (0.625 U fin.)	extension	72°C	01:30 min
x µL	ddH$_2$O			
		final extension	72°C	2 min
25 µL	final volume	store	10°C	∞

Table 25 PCR conditions and programs used for Gibson assembly

PCR 3: vector backbone linerization		PCR 3 program	temperature	time
2.5 µL	10x DreamTaq buffer	initial denaturation	95°C	5 min
2.5 µL	dNTP mix, 2 mM each			
1.25 µL	Forward primer P7 [10 µM]	30 cycles:		
1.25 µL	Reverse primer P23 [10 µM]	denaturation	95°C	1 min
x µL	pCumA1(N-His) (25 ng fin.)	annealing (gradient)	66-72°C	30 s
0.75	DMSO (3 % fin.)	extension	72°C	05:30 min
0.25 µL	Phusion DNA Pol. (0.5 U fin.)			
x µL	ddH$_2$O	final extension	72°C	10 min
25 µL	final volume	store	10°C	∞

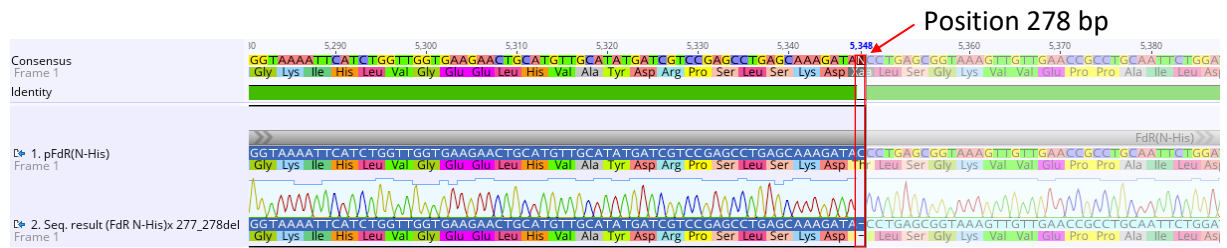## 6.3 QuikChange™ repair of pFdR(N-His)ˣ

Position 278 bp

Figure 32 Pairwise alignment of the vector construct pFdR(N-His) (top) and the sequencing result of pFdR(N-His)ˣ (bottom). Sequencing of the vector construct pFdR(N-His)ˣ revealed a base deletion at position 277 bp (277_278del) within the FdR gene, which led to a nonsense mutation and further to an incomplete translation of the FdR gene. Sanger sequencing was carried out by Microsynth AG (Balgach, Switzerland) and the illustration was created using the software Genious Prime (Biomatters Ltd.; Auckland, New Zealand).
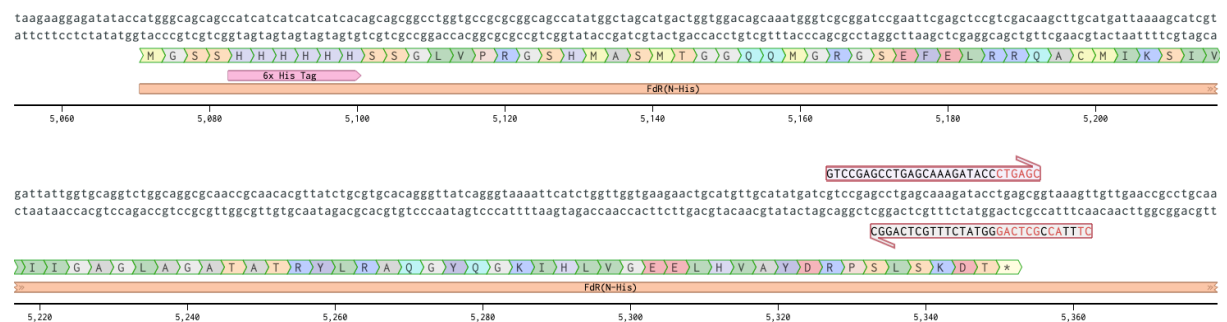

Figure 33 The sequence of the construct pFdR(N-His) (6607 bp) was used as the template for the design of a primer pair (depicted in red) for the QuikChange™ site-directed mutagenesis, in order to introduce the one single missing nucleotide (C or G), respectively, at the bp position 277 of the FdR gene in the construct pFdR(N-His)ˣ (6606 bp). The sequence of the used primers (P13 and P14) is listed in table 21. The illustration was created using the software Benchling (San Francisco, USA).
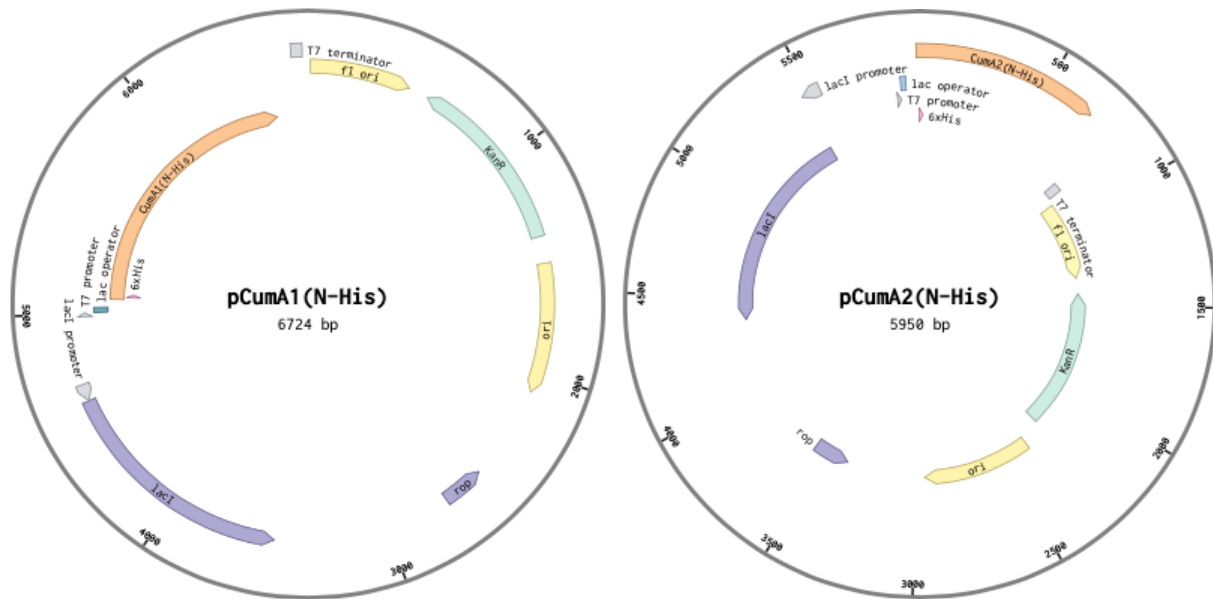
6.4 Plasmid maps

Figure 34 CDO Oxy pCumA1(N-His) (6724 bp, left) and pCumA2(N-His) (5950 bp, right). The constructs contain the for *E.coli* codon-optimized CDO genes *cumA1* or *cumA2*, both carrying N-terminal His-tags. The illustration was created using the software Benchling (San Francisco, USA).
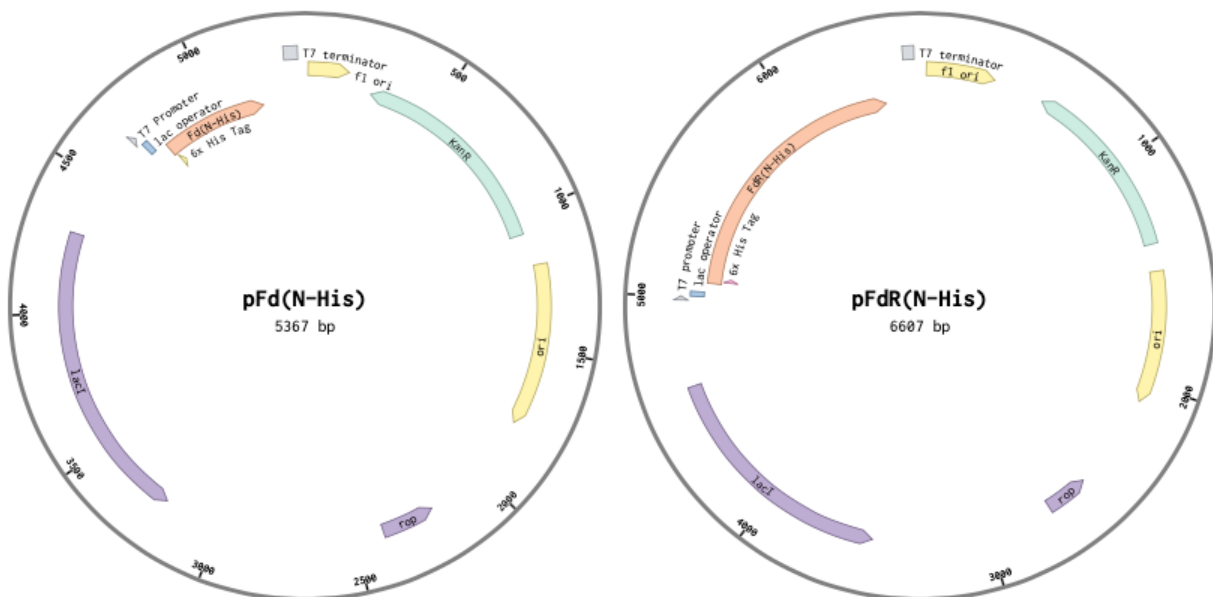

Figure 35 CDO Fd(N-His) (5367 bp, left) and FdR(N-His) (6607 bp, right). The constructs contain the for *E.coli* codon-optimized CDO genes *cumA3* or *cumA4*, both carrying N-terminal His-tags. The illustration was created using the software Benchling (San Francisco, USA).

7 References

(1)   Burton, S. G. Oxidizing Enzymes as Biocatalysts. *Trends Biotechnol.* **2003**, *21* (12), 543–549.

(2)   Ran, N.; Zhao, L.; Chen, Z.; Tao, J. Recent Applications of Biocatalysis in Developing Green Chemistry for Chemical Synthesis at the Industrial Scale. *Green Chem.* **2008**, *10* (4), 361–372.

(3)   Bezborodov, A. M.; Zagustina, N. A. Enzymatic Biocatalysis in Chemical Synthesis of Pharmaceuticals (Review). *Appl. Biochem. Microbiol.* **2016**, *52* (3), 237–249.

(4)   Porter, J. L.; Rusli, R. A.; Ollis, D. L. Directed Evolution of Enzymes for Industrial Biocatalysis. *ChemBioChem* **2016**, *17* (3), 197–203.

(5)   Anastas, P.; Eghbali, N. Green Chemistry: Principles and Practice. *Chem. Soc. Rev.* **2010**, *39* (1), 301–312.

(6)   Sellés Vidal, L.; Kelly, C. L.; Mordaka, P. M.; Heap, J. T. Review of NAD(P)H-Dependent Oxidoreductases: Properties, Engineering and Application. *Biochim. Biophys. Acta, Proteins Proteomics* **2018**, *1866* (2), 327–347.

(7)   Gamenara, D.; Seoane, G. A.; Saenz-Méndez, P.; de María, P. D. *Redox Biocatalysis*; John Wiley & Sons, Inc.: Hoboken, NJ, USA, 2012.

(8)   Faber, K. *Biotransformations in Organic Chemistry*, 7th ed.; Springer International Publishing: Berlin, Heidelberg, 2018.

(9)   Wang, Y.; Li, J.; Liu, A. Oxygen Activation by Mononuclear Nonheme Iron Dioxygenases Involved in the Degradation of Aromatics. *JBIC, J. Biol. Inorg. Chem.* **2017**, *22* (2–3), 395–405.

(10)   Barry, S. M.; Challis, G. L. Mechanism and Catalytic Diversity of Rieske Non-Heme Iron-Dependent Oxygenases. *ACS Catal.* **2013**, *3* (10), 2362–2370.

(11)   Costas, M.; Mehn, M. P.; Jensen, M. P.; Que, L. Dioxygen Activation at Mononuclear Nonheme Iron Active Sites: Enzymes, Models, and Intermediates. *Chem. Rev.* **2004**, *104* (2), 939–986.

(12)   Ferraro, D. J.; Gakhar, L.; Ramaswamy, S. Rieske Business: Structure–Function of Rieske Non-Heme Oxygenases. *Biochem. Biophys. Res. Commun.* **2005**, *338* (1), 175–190.

(13)   Wackett, L. P. Mechanism and Applications of Rieske Non-Heme Iron Dioxygenases. *Enzym. Microb. Technol.* **2002**, *31* (5), 577–587.

(14)   Özgen, F. F.; Schmidt, S. Rieske Non-Heme Iron Dioxygenases: Applications and Future Perspectives. In *Biocatalysis*; Husain, Q., Ullah, M. F., Eds.; Springer International Publishing, Cham, 2019; pp 57–82.

(15)   Catterall, F. A.; Williams, P. A. Some Properties of the Naphthalene Oxygenase from *Pseudomonas Sp.* NCIB 9816. *J. Gen. Microbiol.* **1971**, *67* (1), 117–124.

(16)   Halder, J. M.; Nestl, B. M.; Hauer, B. Semirational Engineering of the Naphthalene

Dioxygenase from *Pseudomonas Sp.* NCIB 9816-4 towards Selective Asymmetric Dihydroxylation. *ChemCatChem* **2018**, *10* (1), 178–182.

(17) Gibson, D. T.; Koch, J. R.; Kallio, R. E. Oxidative Degradation of Aromatic Hydrocarbons by Microorganisms. I. Enzymic Formation of Catechol from Benzene. *Biochemistry* **1968**, *7* (7), 2653–2662.

(18) Resnick, S. M.; Gibson, D. T. Regio- and Stereospecific Oxidation of Fluorene, Dibenzofuran, and Dibenzothiophene by Naphthalene Dioxygenase from *Pseudomonas Sp.* Strain NCIB 9816-4. *Appl. Environ. Microbiol.* **1996**, *62* (11), 4073–4080.

(19) Escalante, D. E.; Aukema, K. G.; Wackett, L. P.; Aksan, A. Simulation of the Bottleneck Controlling Access into a Rieske Active Site: Predicting Substrates of Naphthalene 1,2-Dioxygenase. *J. Chem. Inf. Model.* **2017**, *57* (3), 550–561.

(20) Chartrain, M.; Jackey, B.; Taylor, C.; Sandford, V.; Gbewonyo, K.; Lister, L.; Dimichele, L.; Hirsch, C.; Heimbuch, B.; Maxwell, C.; Pascoe, D.; Buckland, B.; Greasham, R. Bioconversion of Indene to Cis (1S,2R) Indandiol and Trans (1R,2R) Indandiol by *Rhodococcus* Species. *J. Ferment. Bioeng.* **1998**, *86* (6), 550–558.

(21) Chartrain, M.; Jackey, B. A.; Heimbuch, B.; Taylor, C. S. Conversion of Indene to (1S)-Amino-(2R)-Indanol Free of Any Steroisomer by Combination of Fermentation of *Rhodococcus Sp.* ATCC 55805 and Chemical Steps. U.S. Patent 5,871,981, August 1997.

(22) Wackett, L. P.; Kwart, L. D.; Gibson, D. T. Benzylic Monooxygenation Catalyzed by Toluene Dioxygenase from *Pseudomonas Putida. Biochemistry* **1988**, *27* (4), 1360–1367.

(23) Gally, C.; Nestl, B. M.; Hauer, B. Engineering Rieske Non-Heme Iron Oxygenases for the Asymmetric Dihydroxylation of Alkenes. *Angew. Chem., Int. Ed.* **2015**, *54*, 12952–12956.

(24) Batie, C. J.; Ballou, D. P.; Correll, C. C. Phthalate Dioxygenase Reductase and Related Flavin–Iron–Sulfur-Containing Electron Transferases. In *Chemistry and Biochemistry of Flavoenzymes*; Müller, F., Ed.; CRC Press: Boca Raton, FL, 1992; Vol. 3, pp 543–556.

(25) Gassner, G. T.; Ludwig, M. L.; Gatti, D. L.; Correll, C. C.; Ballou, D. P. Structure and Mechanism of the Iron-sulfur Flavoprotein Phthalate Dioxygenase Reductase. *FASEB J.* **1995**, *9* (14), 1411–1418.

(26) Nam, J. W.; Nojiri, H.; Yoshida, T.; Habe, H.; Yamane, H.; Omori, T. New Classification System for Oxygenase Components Involved in Ring-Hydroxylating Oxygenations. *Biosci., Biotechnol., Biochem.* **2001**, *65* (2), 254–263.

(27) Werlen, C.; Kohler, H.-P. E.; Van Der Meer, J. R. The Broad Substrate Chlorobenzene Dioxygenase and Cis-Chlorobenzene Dihydrodiol Dehydrogenase of *Pseudomonas Sp.* Strain P51 Are Linked Evolutionarily to the Enzymes for Benzene and Toluene Degradation. *J. Biol. Chem.* **1996**, *271* (8), 4009–4016.

(28) Mason, J. R.; Cammack, R. The Electron-Transport Proteins of Hydroxylating Bacterial Dioxygenases. *Annu. Rev. Microbiol.* **1992**, *46*, 277–305.

(29) Gibson, D. T.; Parales, R. E. Aromatic Hydrocarbon Dioxygenases in Environmental Biotechnology. *Curr. Opin. Biotechnol.* **2000**, *11* (3), 236–243.

(30)   Beinert, H. Iron-Sulfur Proteins: Ancient Structures, Still Full of Surprises. *JBIC, J. Biol. Inorg. Chem.* **2000**, *5*, 2–15.

(31)   Johnson, D. C.; Dean, D. R.; Smith, A. D.; Johnson, M. K. Structure, Function, and Formation of Biological Iron-Sulfur Clusters. *Annu. Rev. Biochem.* **2005**, *74*, 247–281.

(32)   Kauppi, B.; Lee, K.; Carredano, E.; Parales, R. E.; Gibson, D. T.; Eklund, H.; Ramaswamy, S. Structure of an Aromatic-Ring-Hydroxylating Dioxygenase – Naphthalene 1,2-Dioxygenase. *Structure* **1998**, *6* (5), 571–586.

(33)   Dong, X.; Fushinobu, S.; Fukuda, E.; Terada, T.; Nakamura, S.; Shimizu, K.; Nojiri, H.; Omori, T.; Shoun, H.; Wakagi, T. Crystal Structure of the Terminal Oxygenase Component of Cumene Dioxygenase from *Pseudomonas Fluorescens IP01. J. Bacteriol.* **2005**, *187* (7), 2483–2490.

(34)   Ferraro, D. J.; Okerlund, A. L.; Mowers, J. C.; Ramaswamy, S. Structural Basis for Regioselectivity and Stereoselectivity of Product Formation by Naphthalene 1,2-Dioxygenase. *J. Bacteriol.* **2006**, *188* (19), 6986–6994.

(35)   Karlsson, A.; Parales, J. V.; Parales, R. E.; Gibson, D. T.; Eklund, H.; Ramaswamy, S. Crystal Structure of Naphthalene Dioxygenase: Side-on Binding of Dioxygen to Iron. *Science.* **2003**, *299* (5609), 1039–1042.

(36)   Ohta, T.; Chakrabarty, S.; Lipscomb, J. D.; Solomon, E. I. Near-IR MCD of the Nonheme Ferrous Active Site in Naphthalene 1,2-Dioxygenase: Correlation to Crystallography and Structural Insight into the Mechanism of Rieske Dioxygenases. *J. Am. Chem. Soc.* **2008**, *130* (5), 1601–1610.

(37)   Wolfe, M. D.; Parales, J. V.; Gibson, D. T.; Lipscomb, J. D. Single Turnover Chemistry and Regulation of O2 Activation by the Oxygenase Component of Naphthalene 1,2-Dioxygenase. *J. Biol. Chem.* **2001**, *276* (3), 1945–1953.

(38)   Imlay, J. A. Iron-Sulphur Clusters and the Problem with Oxygen. *Mol. Microbiol.* **2006**, *59* (4), 1073–1082.

(39)   Johnson, P. W.; Canale-Parola, E. Properties of Rubredoxin and Ferredoxin Isolated from Spirochetes. *Arch. Mikrobiol.* **1973**, *89*, 341–353.

(40)   Tan, H. M.; Joannou, C. L.; Cooper, C. E.; Butler, C. S.; Cammack, R.; Mason, J. R. The Effect of Ferredoxin(BED) Overexpression on Benzene Dioxygenase Activity in *Pseudomonas Putida* ML2. *J. Bacteriol.* **1994**, *176* (9), 2507–2512.

(41)   Halder, J. Naphthalen Dioxygenase Aus *Pseudomonas Sp.* NCIB 9816-4: Systematische Analyse Der Aktiven Tasche. Doctoral Thesis, University of Stuttgart: Institute of Biochemistry and Technical Biochemistry, 2017.

(42)   Jouanneau, Y.; Meyer, C.; Jakoncic, J.; Stojanoff, V.; Gaillard, J. Characterization of a Naphthalene Dioxygenase Endowed with an Exceptionally Broad Substrate Specificity toward Polycyclic Aromatic Hydrocarbons. *Biochemistry* **2006**, *45* (40), 12380–12391.

(43)   Perego, C.; Amarilli, S.; Bellussi, G.; Cappellazzo, O.; Girotti, A. G. Development and Industrial Application of a New Beta Zeolite Catalyst for the Production of Cumene. In *Proceedings of the 12th International Zeolite Conference*; Baltimore, Maryland, USA,

1998; pp 575–582.

(44)   Aoki, H.; Kimura, T.; Habe, H.; Yamane, H.; Kodama, T.; Omori, T. Cloning, Nucleotide Sequence, and Characterization of the Genes Encoding Enzymes Involved in the Degradation of Cumene to 2-Hydroxy-6-Oxo-7-Methylocta-2,4-Dienoic Acid in *Pseudomonas Fluorescens* IP01. *J. Ferment. Bioeng.* **1996**, *81* (3), 187–196.

(45)   Takami, W.; Horinouchi, M.; Nojiri, H.; Yamane, H.; Omori, T. Evaluation of Trichloroethylene Degradation by E. Coli Transformed with Dimethyl Sulfide Monooxygenase Genes and/or Cumene Dioxygenase Genes. *Biotechnol. Lett.* **1999**, *21*, 259–264.

(46)   Feyza Özgen, F.; Runda, M. E.; Burek, B. O.; Wied, P.; Bloh, J. Z.; Kourist, R.; Schmidt, S. Artificial Light-Harvesting Complexes Enable Rieske Oxygenase Catalyzed Hydroxylations in Non-Photosynthetic Cells. *Angew. Chem., Int. Ed.* **2020**, *59*, 3982–3987.

(47)   Munro, A. W.; Girvan, H. M.; McLean, K. J. Cytochrome P450–Redox Partner Fusion Enzymes. *Biochim. Biophys. Acta* **2007**, *1770* (3), 345–359.

(48)   Lee, K. Benzene-Induced Uncoupling of Naphthalene Dioxygenase Activity and Enzyme Inactivation by Production of Hydrogen Peroxide. *J. Bacteriol.* **1999**, *181* (9), 2719–2725.

(49)   Wolfe, M. D.; Lipscomb, J. D. Hydrogen Peroxide-Coupled Cis-Diol Formation Catalyzed by Naphthalene 1,2-Dioxygenase. *J. Biol. Chem.* **2003**, *278* (2), 829–835.

(50)   Sutherlin, K. D.; Rivard, B. S.; Böttger, L. H.; Liu, L. V.; Rogers, M. S.; Srnec, M.; Park, K.; Yoda, Y.; Kitao, S.; Kobayashi, Y.; Saito, M.; Seto, M.; Hu, M.; Zhao, J.; Lipscomb, J. D.; Solomon, E. I. NRVS Studies of the Peroxide Shunt Intermediate in a Rieske Dioxygenase and Its Relation to the Native FeII O2 Reaction. *J. Am. Chem. Soc.* **2018**, *140*, 5544–5559.

(51)   Holtmann, D.; Hollmann, F. The Oxygen Dilemma: A Severe Challenge for the Application of Monooxygenases? *ChemBioChem* **2016**, *17*, 1391–1398.

(52)   Gibson, D. G.; Young, L.; Chuang, R.-Y.; Venter, J. C.; Hutchison, C. A.; Smith, H. O. Enzymatic Assembly of DNA Molecules up to Several Hundred Kilobases. *Nat. Methods* **2009**, *6*, 343–345.

(53)   Zhang, N.; Stewart, B. G.; Moore, J. C.; Greasham, R. L.; Robinson, D. K.; Buckland, B. C.; Lee, C. Directed Evolution of Toluene Dioxygenase from *Pseudomonas Putida* for Improved Selectivity toward Cis-Indandiol during Indene Bioconversion. *Metab. Eng.* **2000**, *2*, 339–348.

(54)   Dafoe, J. T.; Daugulis, A. J. Manipulating the Composition of Absorbent Polymers Affects Product and By-Product Concentration Profiles in the Biphasic Biotransformation of Indene to Cis-1,2-Indandiol. *Biochem. Eng. J.* **2013**, *77*, 7–14.

(55)   Briand, L.; Marcion, G.; Kriznik, A.; Heydel, J. M.; Artur, Y.; Garrido, C.; Seigneuric, R.; Neiers, F. A Self-Inducible Heterologous Protein Expression System in Escherichia Coli. *Sci. Rep.* **2016**, *6*, 33037.

(56)   Zhu, S.; Gong, C.; Ren, L.; Li, X.; Song, D.; Zheng, G. A Simple and Effective Strategy for

Solving the Problem of Inclusion Bodies in Recombinant Protein Technology: His-Tag Deletions Enhance Soluble Expression. *Appl. Microbiol. Biotechnol.* **2013**, *97*, 837–845.

(57)   Koeller, K. M.; Wong, C. H. Enzymes for Chemical Synthesis. *Nature* **2001**, *409*, 232–240.

(58)   Alissandratos, A. In Vitro Multi-Enzymatic Cascades Using Recombinant Lysates of E. Coli: An Emerging Biocatalysis Platform. *Biophys. Rev.* **2020**, *12*, 175–182.

(59)   Wied, P. Engineering Rieske Non-Heme Oxygenases for Improved Electron Transfer in Light-Driven Biocatalysis. Masters Thesis, Graz University of Technology: Institute of Molecular Biotechnology, 2018.

(60)   Gally, C. Enzymatic Asymmetric Dihydroxylation of Alkenes. Doctoral Thesis, University of Stuttgart: Institute of Technical Biochemistry, 2016.

(61)   Runda, M. Characterization and optimization of light-driven whole-cell hydroxylations catalyzed by Rieske non-heme iron oxygenases. Masters Thesis, Graz University of Technology: Institute of Molecular Biotechnology, 2019.

(62)   Jaganaman, S.; Pinto, A.; Tarasev, M.; Ballou, D. P. High Levels of Expression of the Iron-Sulfur Proteins Phthalate Dioxygenase and Phthalate Dioxygenase Reductase in *Escherichia Coli. Protein Expr. Purif.* **2007**, *52* (2), 273–279.

(63)   Guzman, L. M.; Belin, D.; Carson, M. J.; Beckwith, J. Tight Regulation, Modulation, and High-Level Expression by Vectors Containing the Arabinose P(BAD) Promoter. *J. Bacteriol.* **1995**, *177* (14), 4121–4130.

(64)   Hunold, A. On the Rieske Non-Heme Iron Oxygenases of *Phenylobacterium Immobile* Strain E. Doctoral Thesis, University of Stuttgart: Institute of Biochemistry and Technical Biochemistry, 2019.

(65)   Munk, K.; Dersch, P.; Eikmanns, B.; Eikmanns, M.; Fischer, R. *Taschenlehrbuch Biologie: Mikrobiologie*, 1st ed.; Georg Thieme Verlag KG: Stuttgart, Germany, 2018.

(66)   Wu, J. T.; Wu, L. H.; Knight, J. A. Stabilityof NADPH: Effect of Various Factors on the Kinetics of Degradation Materials and Methods. *Clin. Chem.* **1986**, *32* (2), 314–319.

(67)   Sauber, K.; Fröhner, C.; Rosenberg, G.; Eberspächer, J.; Lingens, F. Purification and Properties of Pyrazon Dioxygenase from Pyrazon-Degrading Bacteria. *Eur. J. Biochem.* **1977**, *74*, 89–97.

(68)   Imbeault, N. Y. R.; Powlowski, J. B.; Colbert, C. L.; Bolin, J. T.; Eltis, L. D. Steady-State Kinetic Characterization and Crystallization of a Polychlorinated Biphenyl-Transforming Dioxygenase. *J. Biol. Chem.* **2000**, *275* (17), 12430–12437.

(69)   Inoue, K.; Ashikawa, Y.; Umeda, T.; Abo, M.; Katsuki, J.; Usami, Y.; Noguchi, H.; Fujimoto, Z.; Terada, T.; Yamane, H.; Nojiri, H. Specific Interactions between the Ferredoxin and Terminal Oxygenase Components of a Class IIB Rieske Nonheme Iron Oxygenase, Carbazole 1,9a-Dioxygenase. *J. Mol. Biol.* **2009**, *392*, 436–451.